İSTANBUL TECHNICAL UNIVERSITY ★ GRADUATE SCHOOL OF SCIENCE ENGINEERING AND TECHNOLOGY

EXPERIMENTAL INVESTIGATION OF SINGULAR SOURCES METHOD FOR MICROWAVE IMAGING

M.Sc. THESIS

Tuğhan ÇAĞLAYAN

Department of Electronics and Communications Engineering

Telecommunications Engineering Programme

JUNE 2016

İSTANBUL TECHNICAL UNIVERSITY ★ GRADUATE SCHOOL OF SCIENCE ENGINEERING AND TECHNOLOGY

EXPERIMENTAL INVESTIGATION OF SINGULAR SOURCES METHOD FOR MICROWAVE IMAGING

M.Sc. THESIS

Tuğhan ÇAĞLAYAN
504141327

Department of Electronics and Communications Engineering

Telecommunications Engineering Programme

Thesis Advisor: Assoc. Prof. Dr. Mehmet ÇAYÖREN

JUNE 2016

İSTANBUL TEKNİK ÜNİVERSİTESİ ★ FEN BİLİMLERİ ENSTİTÜSÜ

TEKİL KAYNAKLAR YÖNTEMİYLE MİKRODALGA GÖRÜNTÜLEMENİN DENEYSEL OLARAK İNCELENMESİ

YÜKSEK LİSANS TEZİ

Tuğhan ÇAĞLAYAN
504141327

Elektronik ve Haberleşme Mühendisliği Anabilim Dalı

Telekomünikasyon Mühendisliği Programı

Tez Danışmanı: Doç. Dr. Mehmet ÇAYÖREN

HAZİRAN 2016

Tuğhan ÇAĞLAYAN, a M.Sc. student of İTU Graduate School of Science Engineering and Technology student ID 504141327, successfully defended the thesis/dissertation entitled “EXPERIMENTAL INVESTIGATION OF SINGULAR SOURCES METHOD FOR MICROWAVE IMAGING”, which he prepared after fulfilling the requirements specified in the associated legislations, before the jury whose signatures are below.

Thesis Advisor :	**Assoc. Prof. Dr. Mehmet ÇAYÖREN** İstanbul Technical University	....
Jury Members :	**Prof. Dr. İbrahim AKDUMAN** İstanbul Technical University	....
	Assoc. Prof. Dr. Fikret TOKAN Yıldız Technical University	....

Date of Submission : 02 May 2016
Date of Defense : 13 June 2016

To my beloved family,

FOREWORD

I would like to thank my thesis advisor Dr. Mehmet ÇAYÖREN for assisting and guiding me throughout the entire study and also for his contributions to this research.

Also, I would like to thank Dr. İbrahim AKDUMAN and the Istanbul Technical University Electromagnetics Research Group family for their support and giving me the opportunity to use the facility in all its capability.

Finally, I would like to express my intense gratitude to my family as they supported me for this entire time how hard the situation might be with their loving care.

June 2016

Tuğhan ÇAĞLAYAN
Electronics and Communications
Engineer

TABLE OF CONTENTS

Page

ABBREVIATIONS

SSM : Singular Sources Method
PSM : Point Source Method
MRI : Magnetic Resonance Imaging
PET : Pozitron Emission Tomography
CT : Computerized Tomography
BP : Backpropagation
MoM : Method of Moments
LSM : Linear Sampling Method
FM : Factorization Method
NRT : No-Response Test
RTM : Reverse Time Migration
CSI : Contrast Source Inversion
BIM : Born Iterative Method
DBIM : Distorted Born Iterative Method
VBA : Variational Bayesion Approximation

LIST OF FIGURES

Page

EXPERIMENTAL INVESTIGATION OF SINGULAR SOURCES METHOD FOR MICROWAVE IMAGING

SUMMARY

In last several decades, inverse scattering has gained a lot of interest with the development of high central processor systems and more sensitive and efficient sensors. According to the needs of the society, inverse scattering problems have become increasingly an attraction to academical circles as well. With more focus on the subject, astonishing discoveries have been made and many theories have been developed which effects our lives daily. For example, less than 100 years ago, it was usually not possible to diagnose most of the deadly diseases let alone imaging inside of the human body without opening it. But today, we are able to detect even milimetrical objects inside the human tissue through strong inverse scattering algorithms such as Magnetic Resonance Imaging (MRI), Computerized Tomography (CT), Pozitron Emission Tomography (PET), without even touching it. For example, to detect kidney stones, we use ultrasound imaging which is a basic scheme of acoustic imaging. Ground radar systems use inverse scattering to detect objects in the air. Similarly, a radar system which is mounted on a plane also uses inverse scattering algorithms to map Earth’s curvature and geological structures. In this study however, we tried to focus on another form of an inverse problem, an electromagnetic inverse scattering algorithm, with an intention of using it for medical imaging which has not been made successfully so far.

The main focus on this study is to solve the electromagnetic inverse scattering problem in microwave frequency region. The problem is to determine the object function which gives electrical parameters of the scattering objects or at least an indicator of it which will later be used to determine the location, shape and other differentiating parameters of the scatterer. Electromagnetic inverse scattering is a highly nonlinear problem in microwave region since both sides of the Lippmann-Schwinger equation depends continuously on total field inside the object which cannot be acquired without the shape and electrical parameters of the object. Thus, two different types of solution can be proposed, an iterative solution which updates certain parameters in the given equation to acquire object function through an optimization scheme, or a solution that solves linearized ill-posed integral equations to obtain a density function which can later be used as the indicator function to determine the shape, location and possibly boundary conditions of the scattering object(s). The first type of methodology is called quantitative, while the second one is classified as qualitative inverse scattering method. Contrast Source Inversion (CSI), Born Iterative Method (BIM), Distorted Born Iterative Method (DBIM), Variational Bayesian Approximation (VBA) can be given as examples to quantitative methods while Linear Sampling Method (LSM), Factorization Method (FM), Singular Sources Method (SSM), No-Response Test (NRT), Reverse Time Migration (RTM), Level Set

Methods are some of the qualitative methods that can be used for electromagnetic scattering.

In this study, we deal with the algorithmical implementation of Singular Source Method along with its improvement for multifrequency and scattering parameter measurement cases. First, contemporary and interesting topics on inverse scattering are introduced by providing examples on the commonly faced problems, continuing with the description of qualitative and quantitative methods and general information on the popular inverse electromagnetic scattering methods. Then, a gentle mathematical description on the scattering problem and the mathematical tools that are used in the study is provided. After that, detailed mathematical formulation of the Singular Sources Method is given with addition of simple explanation on LSM and FM which our algorithm is compared to. In the same chapter, multifrequency and scattering parameter improvements on the original SSM is given in detail with their justification. Later in the results section, two different experimental setups that are used to obtain results are explained and then imaging outcomes from the algorithm is discussed in detail. Indicator functions includes various cases such as the comparison of different scattering objects with varying shape, size, location and electrical parameters. Another comparison is made between single frequency and multiple frequency schemes. A third comparison includes two other qualitative methods, LSM and FM. In this comparison, the performance of SSM is tested against LSM and FM in terms of success of the outcome, processing time, used resources etc. All these discussions are made in detail along with the visual support with figures of results and experimental setup figures and drawings. With this study, it is observed that the outcome of the SSM is head-to-head with other qualitative methods such as LSM and FM, and even better in some cases which includes performance, processing, result quality and resolution segments. The method also responded positively to the multifrequency modification and produced consistent outcomes with the scattering parameter data. Even though a theoretical justification has not been made in this study for the scattering parameter case, the results seems to support our claim. The study is concluded with an insight of the improvements that are intended to be developed which are anticipated to improve the performance of the algorithm or even take it to the next step.

TEKİL KAYNAKLAR YÖNTEMİYLE MİKRODALGA GÖRÜNTÜLEME İÇİN DENEYSEL OLARAK İNCELENMESİ

ÖZET

Son yıllarda teknolojinin gelişmesi ve işlem gücünün artmasıyla oldukça karmaşık ters problem yapıları da çözülebilir hale gelinmiştir. Ters problem tanımının içine çıktısı belli olan ancak sorunun nedeni araştırılan her durum dahildir. Bu sebeple, ters problem ifadesi tek bir araştırma alanının alt grubuna dahil edilemeyecek kadar geniş bir konu olduğu ve her alanın kendi konuları dahilinde sorunların sebebini anlayabilmek adına ters problem çözmesinin zorunlu olduğu aşikardır. Bazı örnekler verecek olursak, radar sistemleri buna verilebilecek en güzel örneklerden birisidir. Bu yapılar hem yerde konumlandırılıp havadaki cisimleri tespit edebilmek ya da uçan bir nesneye yerleştirilip yeryüzünün haritasını çıkarmak için kullanılabilir. Radar sistemleri için yapılan çalışmalar, elektromanyetik düzenekler üzerinden gerçekleştirilir. Burada geliştirilen yöntemlere örnek olarak, gerçek açıklık radarı (RAR), sentetik açıklık radarı (SAR), ters açıklık radarı (ISAR) verilebilir.

İkinci bir örnek olarak jeoloji, jeofizik ve petrol mühendisliği alanlarında yapılan çalışmalar verilebilir. Burada, petrol yataklarının keşfedilmesi ve çıkarılması, yeraltındaki maden ve değerli minerallerin bulunması ve yeraltının genel haritasının çıkarılması gibi konularda çeşitli ters problemlerin çözümünden faydalanılır. Bu alanlarda elektromanyetik olduğu kadar, akustik görüntüleme yapan sistemler de kullanılır.

Ters saçılma problemlerinin en yoğun kullanıldığı alanlardan birisi, bizim de bu çalışmayı yaparken yönelmeyi amaçladığımız sağlık alanında yapılan çalışmalardır. Son yıllarda yapılan çalışmalarla birlikte geliştirilen yöntemler insan vücudunun haritasını çıkararak, genellikle zararlı dokuları veya anomalileri teşhis edebilmek üzerinedir. Bu yöntemler, anten, sensör, manyetik sargı vb. yapıları kullanarak oluşturulan elektromanyetik, manyetik, akustik ışımaların dokuların üstünden saçılmasıyla birlikte, yine aynı alıcılar yardımıyla toplanan sonuçların çeşitli tekniklerle işlenip doku hakkında bilgi edinilmesiyle gerçekleştirilir. Teknikler terimiyle belirtilen ise aslında bir ters saçılma problemi çözümünden başka bir şey değildir. Günümüzde en sık kullanılan medikal görüntüleme yöntemleri arasında Manyetik Rezonans Görüntüleme (MRI), Bilgisayarlı Tomografi (CT), Positron Emisyon Tomografisi (PET) gibi yöntemler bulunur. Ayrıca, Difraksiyon Tomografisi gibi geçmişte yaygın olarak kullanılmış yöntemler mevcuttur. Herbir yöntem, elde edilen sonuçları kullanarak, dokulardaki farklılığı açığa çıkarmayı sağlayacak şekilde oluşturulmuştur. Bu farklılıklar kullanılarak da dokuların sınıflandırılması ve zararlı dokuların tespiti sağlanır. Bizim odaklanacağımız elektromanyetik ters saçılma problemi ise, medikal alanda onlarca yıldır kullanılmaya çalışılsa da, kalıcı bir çözüm an itibariyle bulunamamıştır. Bunun sebeplerinden birisi ise çözülmeye çalışılan elektromanyetik ters saçılma veri ve obje denklemlerinin lineer olmayan denklemler

olmalarıdır. Lineer olmayan denklemlerin çözümü ise iki farklı şekilde gerçekleştirilebilir. Birincisi, iterasyonlar kullanılıp belirli parametreler değiştirilerek denklemin yakınsaması ve hata fonksiyonunun minimize edilmesi sağlanır. Bu yöntemlerle başarılı sonuçlar elde edilebilmesine rağmen, hem ölçüm hatalarına yüksek bağımlılıklarının oluşu, hem de uzun işlem süreleri kullanılmalarını zorlaştırmaktadır. İkinci bir yöntem ise lineer olmayan problemlerin regülarize edilerek tek bir adımda evirilmeleridir. Bu yöntemler denklemde bilgi kaybına sebep olsalar da, hızlı çözüm üretmeleri sebebiyle bazı durumlarda birinci tarz tekniklere tercih edilebilmektedir. İki farklı yöntem arasında yapılacak tercih aslında gerçekleştirmeye çalışılan uygulamadan alınması beklenen sonuca bağlıdır. Mikrodalga metodların yaygın olmayışına yönelik ayrıca, mikrodalga bölgesindeki frekanslar kullanılarak içine penetre edilen doku içerisinde yeterince çözünürlük elde etmek oldukça zor olması eklenebilir. Bu da, küçük boyutlu tümörlerin vb. yapıların dokular içinde tespitini zorlaştırmaktadır. Belirtildiği gibi iki grupta ayrılan elektromanyetik ters saçılma problemleri, niteliksel ve niceliksel olarak adlandırılır. Niceliksel yöntemler bahsedilen birinci gruba girerken bu yöntemler arasında yaygın olarak kullanılan Kontrast Kaynak İnversiyonu (CSI), Born Yaklaşıklığı, Born Iteratif Yöntemi (BIM), Distorted Born Iteratif Yöntemi, Değişken Bayes Yaklaşıklığı (VBA) gibi teknikler verilebilir. Bu yöntemler, obje fonksiyonuna ulaşabilmek adına iterasyonlar gerçekleştirerek bir ya da birden fazla parametreyi her iterasyonda değiştirip gerçek değerlere yakınsamaya çalışır ve lineer olmayan denklem çözümü kategorisinde birinci gruba dahildirler. Örneğin, BIM yöntemi sadece obje fonksiyonunu her iterasyonda güncellerken, Kontrast Kaynak İnversiyonu her iterasyonda hem obje fonksiyonunu hem de saçıcı cismin içinde indüklenen alanı güncelleyip yakınsama noktası bulmaya çalışır. Konsept olarak daha yüzeysel bir yapıda olan niteliksel yöntemler ise genellikle teorik ve matematik altyapı yönünden daha karmaşık bir yapıya sahiptirler. Bu yöntemler bahsedilen sınıflandırmada ikinci kategoriye aittirler ve ürettikleri sonuçlar bakımından niceliksel yöntemlere kıyasla genellikle daha sınırlıdırlar. Bu yöntemlere örnek olarak, Doğrusal Örnekleme Yöntemi (LSM), Faktörizasyon Yöntemi (FM) ve bu çalışmada detaylı olarak inceleyeceğimiz Tekil Kaynaklar Yöntemi (SSM) verilebilir. Örneğin, Doğrusal Örnekleme Yöntemi uzak alan verisini kullanarak bir yoğunluk fonksiyonu oluşturur ve bu fonksiyonun sadece saçıcı bir cismin içerisinde çözülebilir olduğunu kanıtlar. Faktörizasyon Yöntemi ise Doğrusal Örnekleme Yöntemi'nin bir uzantısı olup, benzer bir yoğunluk fonksiyonu yardımıyla saçıcı cismin mevcut olup olmadığını belirleyebilir. Bu ve bunun gibi daha birçok örnek vermek mümkündür. Bu çalışmada, Tekil Kaynaklar Yöntemi matematik ve teorik altyapının kurulması suretiyle temel olarak irdelenecek, yöntemi çoklu frekans ve S-parametresi ölçümlerine uyumlu hale getirecek eklentiler önerilecek, ve daha sonra yöntemin performansı ve önerilen geliştirmelerin uygunluğu geniş ölçekli bir deneysel çalışmayla denetlenecektir. Metodu matematiksel ve teorik olarak tanıtırken, daha yüzeysel bir yaklaşım izlenip, teori ve ispat yoluyla değil de, yöntemin daha çok neyi amaçladığı, bunu nasıl başardığı ve yöntemin nasıl gerçeklenebildiğinin üzerinde durulacaktır. Yönteme uygulanacak geliştirmeler verilirken de aynı şekilde eklentinin amacı ve uygulanışı öncelik taşıyacaktır. Sonuçlar kısmında yapılan her ölçüm için birden fazla durum incelenecek ve her durum da karşılaştırmalı bir şekilde yorumlanacaktır. Sonuçlar kısmı iki ana bölümden oluşmakla birlikte bu bölümler de kendi içerilerinde farklı deneysel kurulumları kapsamaktadır. İlk olarak, ters problem çözümlerinde yaygın olarak kullanılan Fresnel verileriyle elde edilen sonuçlar yorumlanacak ve her ölçüm için tek ve çok frekanstan üretilen sonuçlar karşılaştırıldığı gibi, aynı zamanda niteliksel yöntemlerin de kendi aralarında karşılaştırmalarına yer verilecektir. Daha sonra, İstanbul Teknik Üniversitesi Elektromagnetik Ölçme ve Görüntüleme Laboratuvarı'nın elektromanyetik yalıtımlı odasında kurulan ölçüm sisteminden elde edilen S-parametresi ölçümlerinin sonuçları üretilecek ve sonuçları değerlendirilecektir. Burada, önceki bölüme ek olarak, yüksek ve düşük frekansta elde edilecek sonuçların karşılaştırmasının yanında, Tekil Kaynaklar Yöntemi'ne eklenti olarak önerilen çoklu frekansta çözümün elde edilmesinin üç farklı yoluna dair de sonuçlar paylaşılacak ve yorumlanacaktır.

Sonuç kısmında ise yöntemin performans değerlendirmesi genellenip, ileride çalışmada yapılabilecek değişiklikler ve eklenebilecek adımlar tartışılacaktır. Değerlendirme yapılırken, yöntemin sonuç üretmedeki verimliliği sonuçların çözünürlük ve kalite açısından ele alındığı gibi, sonuçlar kısmının sonunda tartışılan işlemci süresi ve kullanılan bellek miktarı gibi sistemsel performans verileri de değerlendirmeye katılacaktır.

1. INTRODUCTION

In latter years, inverse problems has become a research that the academic circles have an inclination to study due to its potential and necessity in research areas such as medical, defensive, archaeological, geological, signal processing etc. For example, in medical imaging and nondestructive testing cases, inverse problems has become undoubtedly the main topic that all the researchers should focus. In medical imaging, various imaging methods have been developed to assist the diagnosis of the diseases. Magnetic Resonance Imaging (MRI) [1-2], Diffraction Tomography [3], Computerized Tomography (CT) [4-5], Positron Emission Tomography (PET) [6-7] can be given as examples to the most popular medical imaging methods that are commonly used in hospitals and research facilities for decades. MRI uses strong magnetic fields to exploit the spinning property of atoms inside the biological structures which is then used to map the tissue. CT scan is a computerized X-ray tomography where the two dimensional X-ray images of the interested body in many axial rotations are combined through a computer process to see the tissues without cutting. PET scan is a form of CT scan where a organic tracer is used to detect the biological processes occured inside the investigated body. Diffraction Tomography is a relatively primitve method that uses the probing waves and their reflections to determine the locations and shapes of the objects.

In military cases, detection of land mines are realized through metal detectors which excites magnetic fields beneath itself and then collects the returned field to determine whether a metal object is located beneath the soil. With the technological advances, these devices can be found everywhere and not just used by military. As another topic, more complex inverse scattering methods are also used to detect buried objects beneath the soil which is important in terms of the localization and classification of the precious minerals and elements that is hidden according to their distinctive properties. In that way, scientists are mapping planet Earth’s soil for the detection of mines. In the case of signal processing, a simple example might be sound processing. Determining the true source of the collected sound is realized through solving an inverse problem with sound and pressure waves. There are many more methods that is not mentioned in here. In fact, any problem that produces an outcome in which its cause needs to be determined, an inverse problem should be solved to obtain this cause. Thus, solving an inverse problem is a standard daily procedure today with the improvement of the technology and tools that are developed and enhanced everyday. In the case of electromagnetic inverse scattering, which is the focused subject in this study, there are a lot of studies that needs to be examined before we begin to focus on our methodology. There are two main topics that the inverse scattering methods can be classified which are qualitative and quantitative inverse scattering methods. These subjects differ in what they are trying achieve as a result. Quantitative methods are directly try to solve the object function which contains the sigma and epsilon parameters of the scattering object(s) and classifies them according to their electrical parameters. On the other hand, qualitative methods does not try solve the object function itself, yet they construct a density function as an indicator function which can be used to locate the scattering object(s) and their shape. As examples of quantitative methods, Contrast Source Imaging (CSI) [8-10] is a highly anticipated method for inverse electromagnetic scattering which is an extension of the Newton's Method [11-12]. It uses conjugate-gradient optimization scheme to solve the cost equation

$$F(\chi, w_j) = \frac{\sum_j \| f_j - M^S\{L_b[w_j]\} \|_S^2}{\sum_j \| f_j \|_S^2} + \frac{\sum_j \left\| \chi u_j^{inc} - w_j + \chi M^D\{L_b[w_j]\} \right\|_D^2}{\sum_j \left\| \chi u_j^{inc} \right\|_D^2} \tag{1.1}$$

To minimize the error for induced field $w(r)$ and object function $\chi(r)$. The Newton's method is a similar method, except it uses the classical Newton optimization scheme. Also, there are other methods which are in the same category with CSI such as Born Approximation [13]. Born Approximation depends on the most simple approximation on the Lippman-Schwinger equation. It approximates the total field with incident field and modifies the function as

$$E(r) = E^{inc}(r) + \int_D G(r, r')\, \chi(r') E^{inc}(r') dr' \tag{1.2}$$

Which works quite well with the low contrast objects. However, for higher contrast objects, a significant portion of the incident field scatter, so the field inside the object cannot be approximated by the incident field. To tackle this problem, Born Iterative Method (BIM) [14] is proposed, and then improved with Distorted Born Iterative Method (DBIM) [15]. BIM initially uses the same approximation with Born Approximation, but then updates the object function in each iteration until the result converges. DBIM on the other hand updates the equation both for the object function and the induced field to achieve higher and faster convergence. These are a fraction of the quantitative inverse scattering methods that can fully reconstruct the electrical parameters of the scattering objects under certain conditions.

In this study however, we will deal with a method that falls under the category of qualitative inverse scattering methods, Singular Sources Method (SSM). Qualitative inverse scattering methods deals with the detection of a discontinuity in a specific search area, through solving linearized equation systems using reciprocity and analytical continuation identities. They usually produce results faster compared to quantitative methods but they are also restricted in terms of obtained result. The imaging result obtained through qualitative methods are usually only numerical values that can be used to discriminate the scattering objects from each other but include no physical meaning in terms of electrical or acoustic parameters of the objects. Instead, they use properties of the wave structures to obtain the outer shapes and locations of these objects. This result may not be enough for certain applications, such as imaging of highly inhomogeneous areas, but even in this case it can be used as a basis for more complex algorithms such as CSI as we are intended. To be more specific, a qualitative inverse scattering method usually solves an ill-posed integral equation for a density function which is later used as an indicator function or as a base for an indicator function. By ill-posed, we mean that the problem itself cannot be classified in the sense of Hadamard [16], which proposes three requirements for a problem to be well-posed:

1- A solution exists,

2- The solution is unique,

3- The solution's behavior changes continuously with the initial conditions.

All the problems that satisfy these three conditions above are classified as well-posed. However, it is usually not the case for an inverse problem. In fact, there is hardly any well-posed inverse problem exists, if there is any. And for an ill-posed problem to be solved, a regularization scheme must be applied to it. Regularizations make modifications to the equations so that they become directly solvable. Common regularization schemes are Singular Value Decomposition [17], Tikhonov Regularization [18-19], Linear Regression [20], Least Squares [21] etc. With a regularization scheme applied, these inverse scattering algorithms can be directly solved to obtain the indicator function. Each method has a different indicator function which is obtained using steps that varies for each scenario. For example, Linear Sampling Method (LSM) [22-25] uses the integral equation

$$(Fg)(\hat{x}) = \int_{\Omega} u^{\infty}\,(\hat{x}, d) g(d) ds(d) \tag{1.3}$$

which is equivalent to

$$(Fg_z)(\hat{x}) = \Phi^{\infty}(\hat{x}, z) \tag{1.4}$$

to obtain kernel g which has no physical meaning but it can be used to determine the shape and the location of the scatterer(s) D. The Factorization Method (FM) [26-27] is quite similar to the LSM which uses

$$(F^{*}F)^{1/4} g = \Phi^{\infty}(.,z) \tag{1.5}$$

As the integral equation and g as the imaging functional. The Reverse Time Migration (RTM) [28] method uses the cross-correlation of the back-propagated scattered field with the incident field as

$$I(z) = -k^2 Im\left\{\frac{1}{N_s N_r}\sum_{i=1}^{N_s}\sum_{i=1}^{N_r} g(z, x_s)|\Delta(x_r)||\Delta(x_s)|\,.\,G(z, x_r)\,\overline{E^s(x_r, x_s)}\right\} \tag{1.6}$$

to obtain an indicator function I which also have no physical meaning. There are also methods that are similar to Singular Sources Method which we will be explaining thoroughly, such as No Response Test [29-30], Probe Method [31-32] etc. These methods uses the kernel which is obtained with the Point Source Method (PSM) [33-34] to reconstruct the incident and scattered field at desired points to obtain an imaging functional. PSM will be explained in the section with the SSM.

In this study, Singular Sources Method (SSM) is algorithmically constructed, and tested against various experimental setups under different conditions. In SSM, which we will focus on, along with a small comparison of results with LSM and FM, the main purpose is to reconstruct the scattered field from a point source at its source point. When this point becomes close to the discontinuity, this reconstructed field will be higher than some predetermined constant which is otherwise lower. In this way, it is possible to determine where are the boundaries of the scattering object(s). The limitation of the qualitative inverse scattering methods is when there is an inhomogeneity inside the outer boundary, these methods are not able to reconstruct it accurately since they are designed to find only single boundary for all the objects in the domain through solving linearized integral equations. We will show experimentally and explain that all three methods are incapable of producing viable reconstructions for such a problem. These SSM is one of the popular qualitative inverse scattering methods found in 99 [35-38] as an extension to Point Source Method (PSM) [33] by Roland Potthast. The method basically exploits the behaviour of point sources at their source points and reconstructs the scattered field from a point source at its source point using analytical continuation and reciprocity techniques. Method of Moments (MoM) is used while solving the problem with discretization for the computer algorithm.

Scattering data that is used in this thesis is obtained from two different sources. First source is the Fresnel data, which are the most widely used experimental results so far in electromagnetic scattering studies as a ground point. Because of the prevalence of the Fresnel data, we also have decided to test our algorithm against it to verify its accuracy. Various situations tested with Fresnel data including the reaction of the method to different frequency, size, location and electrical parameters from the electric field values obtained by horn type antennas. After the correctness and efficiency of the algorithm is verified, a second source is used as a scattering data, which is bistatic scattering parameter measurement contucted in our laboratory environment using a Vector Network Analyzer, two antennas and various scattering objects with different electrical parameters. Some of the measured situations can be given as: a single off-centered conductor, multiple off-centered conductors, multiple off-centered dielectrics to observe the effects of the contrast to the algorithm results. All these measurements are made within a frequency band at discrete points so that it would also be possible to observe the results in terms of frequency. The method is realized using MATLAB codes which are constructed based on the mathematical formulation we will explain in detail, along with the discretization scheme that will be used for numerical scenarios. Finally, by applying all the measured data to the codes written, imaging functionals are obtained for all the scenarios.

The workflow of the study will be as follows; first, we will gently give a mathematical insight on the scattering problem and the operators that we will later use while formulating SSM. After that, in the third chapter, we will develop and explain the main components of the SSM along with its implementation algorithm for which is followed by the experimental results section in the fourth chapter. In this section, we provide various results for the cases in two different experimental setups. First, the results obtained from Fresnel Data for inverse problem will be discussed for several objects, different kinds of materials, various number of measurement points with variable frequency ranges. We also give a basic comparison between LSM, FM and SSM for these data. Later, we will explain the structure of our measurement system and repeat all the cases that we covered for the earlier data. And finally, a conclusion is made that summarizes all the results obtained throughout the study.

2. ELECTROMAGNETIC SCATTERING PROBLEM

2.1 Electromagnetic Scattering Formulation

In terms of constructing and formulating the inverse scattering algorithm that we will use, understanding the basic concept that lies beneath the inverse scattering theory is necessary. Because of this reason, we should give the basic concepts of the forward problem. Since we will only focus on the electromagnetic inverse scattering in this study, it would be appropriate to give the basic concepts of the forward problem in electromagnetic notation. Note that the scalar notation will be used to develop the formulation in the entire study since it is easier to understand for the non-academic reader and also more compatible with the experimental results that will be obtained in the results section.

Both electromagnetic and acoustic fields satisfy the Helmholtz equation

$$\Delta E(r) + k^2 E(r) = 0 \tag{2.1}$$

Here, E refers to the total field outside the scattering object and k is the wavenumber given as

$$k = \omega^2 \mu \varepsilon + j\omega\mu\sigma \tag{2.2}$$

It is also known that the total field consist of the summation of incident and scattered field written by

$$E(r) = E^{inc}(r) + E^{s}(r) \tag{2.3}$$

Here, the incident field can also be identified as the total field when there is no scattering object, and the scattered field as the effect of the scattering object to the total field. Incident field satisfies the Helmholtz equation with the wavenumber of the background (which is usually air) given as

$$\Delta E^{inc}(r) + k_0^2 E^{inc}(r) = 0 \tag{2.4}$$

Thus, if we extract the incident field from the total field in the Helmholtz equation, we get

$$\Delta E^s(r) + k_0^2 E^s(r) = -(k^2 - k_0^2)E(r) \tag{2.5}$$

Here, it can be seen that the total field acts as a source inside the scattering object and induces the scattered field that radiates outside of the object. Note that, this cause a high level of nonlinearity of the equation system and makes the solution of this system much more difficult.

As a mathematical constraint, the Sommerfeld Radiation Condition is satisfied as the scattered field goes to infinity which is given by

$$r^{\frac{m-1}{2}}\left(\frac{\partial}{\partial r} - jk\right)E^s(x) \rightarrow 0, \;\; as\, r = \;|x| \rightarrow \infty \tag{2.6}$$

This states that the scattered field is outgoing and vanishes as x goes to infinity. This condition acts as another equation in the system and reduces the number of variables by one.

The total field can also be given in the integral form which is also known as Lippman-Schwinger Equation by

$$E(r) = E^{inc}(r) + \int_D G(r,r')\,\chi(r')E^{inc}(r')dr' \tag{2.7}$$

Where $G(r,r')$ is the Green's function and $\chi(r')$ is the object function that contains the electrical parameters of the scattering object. Green's function is the fundamental solution of the Helmholtz Equation for a point source given as

$$\Phi(r,r') = G(r,r') = \begin{cases} \frac{j}{4}H_0^{(1)}(k|r-r'|), \; m = 2 \\ \dfrac{e^{jk|r-r'|}}{4\pi|r-r'|} \qquad\quad , \; m = 3 \end{cases} \tag{2.8}$$

Here, the variable m is the dimension of the space $\mathbb{R}^m$. The parameter $\chi(r)$ is given as

$$\chi(r) = \left(\delta\varepsilon(r) + \frac{j\delta\sigma(r)}{\varepsilon_b\omega}\right) \tag{2.9}$$

This parameter constitutes the main unknown of the inverse problem. The objective of the inverse problem is basically learning this parameter, or at least a form of it that could serve as a discriminator using the scattered field data obtained through measurements. The aim of the forward problem however, is to obtain the scattered field from the knowledge of the scattering object and the excitation that induces field inside and outside of the scatterer. Detailed information on forward and inverse problem can be found in [39-44].

There is also another concept that we will use in the entire study which is called far-field pattern. Far field pattern can be considered as the angular components of the field stripped off from the components dependent on the distance. For a given scattered field E^s, its far-field pattern can be written as

$$E^s(r) = \frac{e^{jk|r|}}{|r|^{(m-1)/2}}\left\{E^\infty(\hat{r}, d) + O\left(\frac{1}{|r|}\right)\right\} \tag{2.10}$$

Notation given above is vital in understanding the rest of the study. Here, for an acoustic or electromagnetic wave in time harmonic case, the angular and distance components can be separated as above. This simplifies the notation of the inverse scattering algorithm because one of the variables is reduced from the obtained data as the far-field pattern includes only the angular variables. More information on the far-field pattern is given in the [39-44].

In this section, we have given the basic utilities and equations of the electromagnetic scattering problem. We will continue with the integral equations and layer potentials that will be used in the formulation of the SSM.

2.2 Boundary Conditions, Layer Potentials and Space Operators

Since an introduction for the scattering problem has been made, it is now appropriate to mention the boundary conditions that the scattering problems is constructed upon, layer potential tools to represent and solve these problems and different space operators that forms a basis in representing the various scattering cases under mathematical terms, along with giving an insight on their physical meaning. All these preliminary subjects are critical since they will form a basis in our theoretical discussion for SSM.

First, the space term should be made clear in mathematical aspects so that no confussion occur when these terms are mentioned later in the thesis. As someone could easily find with enough research that a space in mathematics is basically a set that contains properties. These properties are the discriminators of the spaces. For example, if a space (set) contains the norm property, this space can be classified as a normed space. Another example is that when the inner product can be defined in a space, that space is a Hilbert space. There are uncountable number of spaces that contains different properties in themselves, so it would be unwise to try to explain all the spaces that exists. Rather, we will only give a simple explanation to the space types and some terms related to them that is used in this study.

Let us begin with some terms related to functional analysis. Assuming that all the readers are familiar with the concept of metric, a set can be defined with correct elements to satisfy some requirements. The completeness refers to the containment of the space in itself. More clearly, a space is complete if it contains all the points in itself and its limits or its closure. For example, a space is not complete if a set inside this space converges to a point which is outside of the given space. Most used space types in our study is Hilbert Spaces which are inner product spaces, Banach spaces and Lebesgue spaces. As we mentioned earlier, Hilbert spaces are the sets that an inner product can be defined within. For example, two and three dimensional Euclidian spaces which forms the Cartesian coordinates are included in the Hilbert spaces. An inner product operation between two functions f and g between interval [a,b] can be written for the general case as

$$\langle f, g \rangle = \int_a^b f(x)g(x)dx \tag{2.11}$$

The notation for the Hilbert spaces throughout the study is $H(.)$. Next, Banach spaces are the complete, normed vector spaces that has a metric deined on them. Banach spaces is formed with most general properties, norm and vector, so they contain lots of more specific spaces that contain also these two property, such as Lebesgue spaces, Sobolev spaces, Hardy spaces etc. Even Hilbert spaces are classified under Banach spaces. A space should satisfy three requirements to be considered as a normed vector space:

1- Every vector defined inside has a length equal to or higher than 0,

2- Multiplying the vector by a constant does not change its direction,

3- The triangle inequality holds which is given as

$$\|x + y\| \leq \|x\| + \|y\| \tag{2.12}$$

For any vectors x and y. These are requirements that every normed vector space should satisfy. Addition to being a normed vector space, A Lebesgue space, or $L^p(.)$ space in mathematical notation also contains the p-integrability property inside of it. This space type is important because most of the wave equations falls under this category, especially the $L^2(.)$, which is square integrable Lebesgue space, thus it is used in the scattering formulations quite frequently. To be more specific, the p-integrability property is given as

$$\|f\|_p \equiv \left(\int_S |f|^p dx\right)^{\frac{1}{p}} < \infty \tag{2.13}$$

Second, the layer potentials should be provided so that some of the cumbersome scattering formulations can be simplified with elegance. First of our layer potential is the single layer potential given as

$$(S\varphi)(r) \coloneqq 2\int_{\partial D} \Phi(r,r')\varphi(r')ds(r') \tag{2.14}$$

This corresponds to the field that is induced from a point source one the boundary ∂D of the object. The second potential is the double layer potential which is written below as

$$(K\varphi)(r) \coloneqq 2\int_{\partial D} \frac{\partial\Phi(r,r')}{\partial v(r')}\varphi(r')ds(r') \tag{2.15}$$

Similar to single layer potential, double layer potential represents the field induced from the boundary ∂D, but this time, the source is a dipole. The other layer potentials are derived from these two potentials to serve a variety of purposes. One of them is adjoint of the double layer potential

$$(K'\varphi)(r) \coloneqq 2\int_{\partial D} \frac{\partial\Phi(r,r')}{\partial v(r)}\varphi(r')ds(r') \tag{2.16}$$

Another potential is given by

$$(T\varphi)(r) \coloneqq 2\frac{\partial}{\partial v(r)}\int_{\partial D} \frac{\partial\Phi(r,r')}{\partial v(r')}\varphi(r')ds(r') \tag{2.17}$$

And another one is

$$(T'\varphi)(r) \coloneqq 2\frac{\partial}{\partial v(r')}\int_{\partial D} \frac{\partial\Phi(r,r')}{\partial v(r)}\varphi(r')ds(r') \tag{2.18}$$

These potentials are quite useful in understanding and simplifying the scattering notations with a single terms that represents an integral equation that each serves a specific purpose and have a different physical meaning.

In scattering problems, we also classify the scattering objects according to the type of their boundaries. There are three different boundary types in which each of them represent a different scattering problem, given as Dirichlet, Neumann and Impedance (Robin) boundary conditions. Dirichlet boundary condition can be given as

$$E|_{\partial D} = 0 \tag{2.19}$$

This condition physically means that the field value at the boundary and inside the scatterer is zero that points to a perfect conductor in which no field can be induced inside the object. Using the Green's theorem, the scattered field at point x induced by the sources at the boundary of the scattering object can be written by an integration at the boundary ∂D as

$$E^s(r) = \int_{\partial D} \left(\frac{\partial \Phi(r, r')}{\partial v(r')} - j\eta \Phi(r, r') \right) \varphi(r') ds(r') \tag{2.20}$$

In terms of layer operators,

$$\varphi + K\varphi - j\eta S\varphi = -2E^{inc} \tag{2.21}$$

As it can be seen, the layer operators simplifies the notation and the understanding of the complex equations for the ones who are familiar with the use and the meaning of them. Neumann condition is written as

$$\left. \frac{\partial E}{\partial v} \right|_{\partial D} = 0 \tag{2.22}$$

Physical meaning of this condition is that there is no change in the normal component of the field inner or outer limits of the boundary. This generally occurs when the object is an insulator and the scattered field induced from this type of boundary can be written as

$$E^s(r) = \int_{\partial D} \left(\Phi(r, r') + j\eta \frac{\partial \Phi(r, r')}{\partial v(r')} S_0^2 \right) \varphi(r') ds(r') \tag{2.23}$$

In terms of layer operators,

$$\varphi - K\varphi - j\eta T S_0^2 \varphi = 2 \frac{\partial E^{inc}}{\partial v} \tag{2.24}$$

Finally, the impedance boundary condition can be given as a combination of the Dirichlet and Neumann boundary conditions by

$$\left. \frac{\partial E}{\partial v} \right|_{\partial D} + \lambda E|_{\partial D} = 0 \tag{2.25}$$

Here, λ is the impedance value of the boundary and contains information about electrical parameters of the scatterer. Most of the materials are evaluated under this boundary condition as they can be classified neither as a perfect conductor nor a perfect insulator. The integral equation that represents the scattered field is more complex compared to latter two cases which is written according to Green's Theorem as,

$$E^s(r) = \int_{\partial D} \left(\Phi(r, r')(1 - j\eta\lambda) + \frac{\partial \Phi(r, r')}{\partial v(r')} (j\eta S_0^2 + \lambda) \right) \varphi(r') ds(r') \qquad (2.26)$$

Which should be simplified in terms of layer potentials as,

$$[I - K' - j\eta T S_0^2 - \lambda S - j\eta\lambda(I + K)S_0^2]\varphi = -2E^s = 2\frac{\partial E^{inc}}{\partial v} + 2\lambda E^{inc} \qquad (2.27)$$

This should be the case where a general inverse scattering algorithm covers or forms a beginnning point Since it includes both the Dirichlet and the Neumann conditions in itself. To obtain more detailed information on the concepts of this section, refer to [39-44].

This concludes our discussion about the general concepts of the scattering problem. Since the walkthrough of the basic concepts that will be used in SSM, we are now ready to begin with the formulation of SSM algorithm along with other inverse scattering we will use. While doing that, we will also give simple explanations of the other methods LSM and FM .

3. QUALITATIVE INVERSE SCATTERING AND SINGULAR SOURCES METHOD

In this chapter, we will focus on our main subject, SSM. First, the basic information about the qualitative inverse scattering methods and a few mathematical notion on the subjects of LSM and FM since a comparison will be made in the results section. Secondly, a detailed explanation of the SSM is given without proofs of theorems related to it since it is unnecessary to go through all the mathematical details that has been done earlier. Instead, we will refer the readers to appropriate articles that should be examined to understand the concept of the method thoroughly.

3.1 Summary and Methodology of Qualitative Inverse Scattering Methods

All the qualitative methods search for an indicator to identify the target from the suspect domain. To achieve this goal, most of these methods use integral equations with unknown kernel or a denstiy function to point out the target itself. Unlike the quantitative methods, these processes are not solved to obtain a parameter that contains physical meaning, but rather a variable that can be interpreted to have a physical meaning. They usually solved through linearized equations with regularization and without iterations (which can be added to improve the results but not initially required), so they produce much faster results than quantitative methods.

In LSM, the goal is to obtain a kernel $g(r)$ by solving far-field operator F for excitation E^{inc} using regularization. It is shown that the inverse of the kernel g blows up when it reaches to a boundary inside investigation domain. The far field operator is given by

$$Fg = E^{inc} \tag{3.1}$$

Here, the source is assumed to be a plane wave and solved accordingly. In [24], it is proven that the density function $g(r)$ is only solveable when the point is inside the scatterer. Otherwise, it blows up. This means that the inverse of this density function can be used to determine whether a selected point inside the investigation domain is inside or outside the scattering object. The method is fairly simple in computation and produces strong outcomes compared to its complexity. The downside of the LSM however is that it needs to be regularized thoroughly to produce meaningful results since the far-field operator itself is highly ill-posed and its solution is directly depends on the level of noise of the far-field data. Thus, we use Tikhonov’s Regularization along with Morozov Discrepancy to correctly estimate the penalty term for the accurate solution. This increases the computing time of the method significantly and more importantly, this disadvantage effects the results completely when the estimate of the error is not accurate. For more information on Tikhonov’s Regularization and Morozov’s Discrepancy, see [45].

FM is just an extension to LSM that shows a factorization of the far-field operator is in the same range with the far-field operator itself thus can be used for imaging with same conditions. To be more specific, the far-field operator F of LSM is factorized as

$$F = H^{*}TH \tag{3.2}$$

It is proven by Kirsch that the operator $(F^{*}F)^{1/4}$ is in the same range with F as given by

$$(F^{*}F)^{1/4}g = E^{inc} \tag{3.3}$$

Which means that it has the same property that the far-field operator has thus it is only solveable inside the scattering object. The advantage of this modification is that it eliminates the need for estimating the error level in the measurement which is needed for Morozov’s discrepancy to work. This brings much faster processing time compared to the LSM algorithm. The imaging functional of FM can be calculated using Singular Value Decomposition of the equation system which is given by

$$w(r) = \left[\sum_{j=1}^{N} \frac{\left|\langle \phi_r, \psi_j \rangle_{L^2}\right|^2}{|\lambda_j|}\right]^{-1} > 0 \tag{3.4}$$

Here, we have given the basic concepts of LSM and FM so that there is no confusion when these methods are compared with the SSM. This section is not sufficient for one to understand the methodology of LSM and FM, its just a description of the processes of these methods. For more information on LSM and FM, see [22-27]. We will now continue with a theoretical discussion about our main focus, SSM.

3.2 Singular Sources Method

As it is introduced before, main idea of Singular Sources Method is to construct the scattered field E^s due to an incident point source, from the knowledge of the far-field pattern E^∞, for all points in the investigation domain, using the full aperture, or all $d \in \mathbb{S}^2$. The case of limited aperture can be handled in another study, please refer to [46] for a similar investigation. A visualization of the method is shown in Figure 3.1. In this figure, the investigation domain is denoted with Λ, the scattering object by D and its boundary as ∂D, an exemplary approximation domain and its boundary by G and ∂G, respectively. Also, in the figure, the unit circle for the determination of the far-field angles is given by the red dashed circle and the excitation and observation points are shown at the black dashed circle. Then we will show that the constructed scattered field only blows up when it reaches to a boundary and becomes singular.

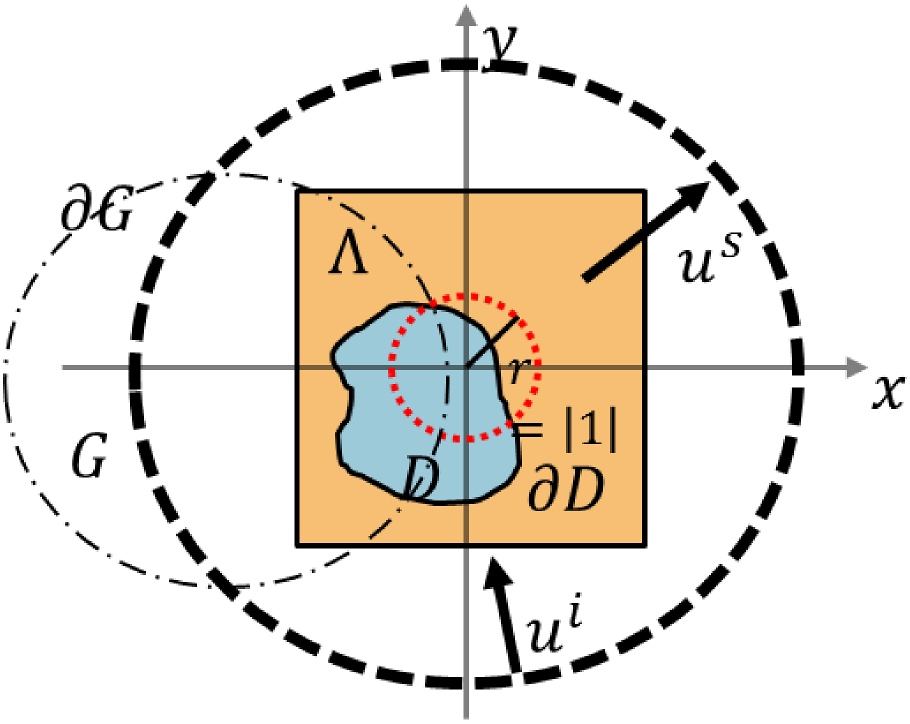

Figure 3.1 A visualization of the investigation domain and tools of SSM.

Theorem 2.1.15 of [35] shows that the scattered field from a point source in its source point contained within the limits

$$\frac{c}{|d(r,D)|} \leq |\Phi^s(r,r)| \leq \frac{C}{|d(r,D)|} \tag{3.5}$$

Where the distance metric (Hausdorf distance) on the space can be defined as

$$d(r,D) \coloneqq inf\{|r-y| : y \in D\} \tag{3.6}$$

Unless the point r is sufficiently close to boundary ∂D. In this case, the scattererd field is not bounded by the constants c and C.

To achieve this result, we should begin with writing the scattered field in terms layer potentials as earlier. Using the relation between the plane waves and point sources, we can write Φ^s as

$$(P\varphi)(r) = \int_{\partial D} \left(\Phi(r,r') + j\eta \frac{\partial\Phi(r,r')}{\partial v(r')} S_0^2\right) \varphi(r') ds(r') \tag{3.7}$$

Here P is the modified layer potential which is analogous to scattered field for Dirichlet problem, given as

$$\Phi^s(.,r) = 2P[I - K' - j\eta T S_0^2 - \lambda S - j\eta\lambda(I+K)S_0^2]^{-1} \left(\frac{\partial\Phi(.,r)}{\partial v} + \lambda\Phi(.,r)\right) \tag{3.8}$$

Using several mathematical procedures and steps, which is given in Theorem 2.1.15. in [35], we see that the scattered field really is confined within some limits as given in (3.5). This theorem proves that the function

$$I(r) \coloneqq |\Phi^s(r,r)|, \quad r \in B\backslash\overline{D} \tag{3.9}$$

is bounded in every set $B_\tau \coloneqq \{r \in B\backslash\overline{D} : d(r,D) > \tau > 0\}$, but unbounded when r tends to the boundary of the obstacle, i.e.

$$\lim_{r\to\partial D} I(r) = \infty \tag{3.10}$$

holds. Thus, the function $I(r)$ may serve as an indicator function for the reconstruction of the obstacle D. Clearly, without the knowledge of the obstacle D and the boundary condition on ∂D, we cannot calculate the indicator function $I(r) \coloneqq |\Phi^s(r,r)|$ directly. However, we will show how to calculate an approximation of the scattered field $\Phi^s(.,r)$ in the source point $r \in B\backslash\overline{D}$ from the far-field pattern $E^\infty(.,.)$ based on ideas from the point source method.

The point source method is introduced by Potthast (1998) [33]. It provides a reconstruction of a scattered field by the knowledge of its far-field pattern that neither depends on the type of the incident field nor on the type of the boundary condition on

∂D. Hence, an application of the point source method in the multiwave setting, to the far-field patterns $E^{\infty}(.,.)$, $d \in \mathbb{S}^2$ is justified. This yields approximations of the scattered fields $E^s(.,d)$ for all incident directions $d \in \mathbb{S}^2$ of the incident plane waves $E^{inc}(.,d)$.

Consider a set of sampling domains $G(x)$ parametrized by $x \in \mathbb{R}^m$, such that $x \notin \overline{G(x)}$ and $G(x)$ is large enough to contain the closure of the unknown scatterer D in its interior. We define an admissibility region $\mathcal{A}$ as

$$\mathcal{A} \coloneqq \{x \in \mathbb{R}^m : \ \overline{D} \subset G(x)\} \tag{3.11}$$

Furthermore, we call any compact subset Ɛ on an $\mathcal{A}$ 'illuminated area'. The key of the point source method is the construction of a density $g_{x,\varepsilon}$ such that the superposition of plane waves v defined by

$$v[g](y) \coloneqq \int_{\mathbb{S}^2} e^{jky.d} g(d)ds(d), \quad y \in \overline{G(x)} \tag{3.12}$$

Approximates the point source $\Phi(.,x)$ in the sense

$$\left\| v\left[g_{x,\varepsilon}\right] - \Phi(x,.)\right\|_{C^2(M_0)} \leq c\varepsilon \tag{3.13}$$

Where M_0 is a compact subset of $G(x)$ and the constant $c = c(M_0)$ is depending on M_0. To compute the density $g_{x,\varepsilon}$, we introduce the Herglotz wave operator $H: L^2(\mathbb{S}^2) \to L^2(\partial G(x))$ defined by

$$(Hg)(y) \coloneqq \int_{\mathbb{S}^2} e^{jky.d} g(d)ds(d), \quad y \in \partial G \tag{3.14}$$

And we solve the integral equation using Tikhonov Regularization as

$$(\alpha I + H^* H)g = H^* \Phi(x,.) \tag{3.15}$$

For $g = g_{x,\alpha} \in L^2(\mathbb{S}^2)$, with a small regularization parameter $\alpha = \alpha(\varepsilon) > 0$ such that

$$\left\| H\left[g_{x,\alpha}\right] - \Phi(x,.)\right\|_{L^2(\partial G)} \leq \varepsilon \tag{3.16}$$

The density operator is found in such a way that it satisfies (3.16). This can also be seen in [35].

We are now ready to construct an approximation to the indicator function $\Phi^s(r,r)$, which can be used to reconstruct the obstacle.

From the data $E^{\infty}(\hat{x},d)$, first we use the point source method to reconstruct the $E^s(r,d)$ for some point r and all $d \in \mathbb{S}^2$. The mixed reciprocity relation

$$\Phi^{\infty}(\hat{x},d)=\frac{1}{4\pi}E^{s}(r,d), \qquad r\in\mathbb{R}^{m}\backslash\overline{D}, d\in\mathbb{S}^{2} \tag{3.17}$$

Sets up a correspondence between the values of the scattered fields $E^{s}(r,.)$ and the far-field pattern $\Phi^{\infty}(.,r)$ of the scattered point source $\Phi(.,r)$. Note that the observation direction of the far-field pattern is the exact opposite of the incident direction of the corresponding plane wave. When we calculate $E^{s}(r,d)$ through (3.12), the far-field pattern of the scattered field from the point source is automatically calculated in accordance with the mixed reciprocity relation. Then, it is possible to approximately construct $\Phi^{s}(.,r)$ using a second step of application of the one wave PSM to $\Phi^{\infty}(.,r)$. This total application can be given by

$$\Phi^{s}(x,r)\approx\iint_{\mathbb{S}^{2}}u^{\infty}(\hat{x},d)g_{r,\tilde{\varepsilon}}(d)\, g_{x,\varepsilon}(\hat{x})ds(d)ds(\hat{x}) \tag{3.18}$$

Which completes the basic calculation steps of the method. Since it is still seems to be vague in concept whether this steps actually lead to an indicator that is bounded under specific conditions, it is appropriate to give the estimates of the operations used by the method itself. In the following steps, the basic idea is worked out in detailed estimates.

3.3 Stability Estimates of SSM

For $r\in B\backslash\overline{D}$, we choose an approximation domain G with $r\notin G$ which is large enough to contain the closure of the unknown scatterer D.

1. Then, we construct a density $g_{r,\tilde{\varepsilon}}$ such that the superposition of plane waves given in (3.12) approximates the point source $\Phi(.,r)$ on G within the limits of the estimate of (3.13). Since this is an ill-posed step of calculation, this approximation can be obtained through some regularization as in the (3.15). Thus, by staying within the limits of the earlier estimate (3.16), we can approximate the $\Phi^{s}(.,r)$ with

   $$\left|\Phi^{s}(x,r)-4\pi\int_{\mathbb{S}^{2}}\Phi^{\infty}(-\hat{x},r)g_{x,\varepsilon}(\hat{x})ds(\hat{x})\right|\leq\varepsilon \tag{3.19}$$

   For all z in an illuminated area Ɛ.

2. From here, using the mixed reciprocity relation in (3.17), we obtain

   $$\left|\Phi^{s}(x,r)-\int_{\mathbb{S}^{2}}E^{s}(r,\hat{x})g_{x,\varepsilon}(\hat{x})ds(\hat{x})\right|\leq\varepsilon \tag{3.20}$$

   For all $x\in$ Ɛ.

3. In the earlier step, for any given $\tilde{\varepsilon} > 0$, the PSM approximates scattered field from a plane wave and constructs densities $g_{r,\tilde{\varepsilon}}$ such that

$$\sup_{\mathrm{x}\in\mathbb{S}^2}\left|\mathrm{E}^s(r,\hat{x}) - 4\pi\int_{\mathbb{S}^2} E^\infty(-d,\hat{x})g_{r,\tilde{\varepsilon}}(d)ds(d)\right| \leq \varepsilon \qquad (3.21)$$

For all $r \in \mathcal{E}$.

4. Finally, if we apply triangle inequality using (3.20) and (3.21) to obtain the estimate

$$\left|\Phi^s(x,r) - \int_{\mathbb{S}^2}\left(4\pi\int_{\mathbb{S}^2} E^\infty(-d,\hat{x})g_{r,\tilde{\varepsilon}}(d)ds(d)\right)g_{r,\varepsilon}(\hat{x})ds(\hat{x})\right|$$

$$\leq \left|\Phi^s(x,r) - \int_{\mathbb{S}^2} E^s(r,\hat{x})g_{x,\varepsilon}(\hat{x})ds(\hat{x})\right|$$

$$+\left|\int_{\mathbb{S}^2}\left(\mathrm{E}^s(r,\hat{x}) - 4\pi\int_{\mathbb{S}^2} E^\infty(-d,\hat{x})g_{r,\tilde{\varepsilon}}(d)ds(d)\right)g_{x,\varepsilon}(\hat{x})ds(\hat{x})\right|$$

$$\leq c_1\varepsilon + c_2\tilde{\varepsilon}\left\|g_{x,\varepsilon}\right\|_{L^2(\mathbb{S}^2)} \qquad (3.22)$$

With constants $c_1, c_2 > 0$.

This concludes the theoretical discussion about the original methodology of the SSM. We are now ready to give the discretization scheme of the method to make it applicable to a countable number of measurements.

3.4 Numerical Application of the Original SSM

As given in (3.14), we use Herglotz wave operator with any incident field to compute the densities $g_{x,\varepsilon}, g_{r,\tilde{\varepsilon}}$. Here, we discretize the equation such that

$$(Hg)(r,x) = \int_{S^{m-1}} e^{ikx.r}\, g(r,d)ds(d)\,,\ x \in \partial G \qquad (3.23)$$

Here, the number N represents the the count of far-field points that the measurement has been obtained. By assuming the incident field is a point source which is excited at point set x, the summation in (3.23) can be written as a linear equation system as

$$(Hg)(r,x) = \Phi(x,r) \qquad (3.24)$$

This equation can be solved with Tikhonov Regularization to obtain the initial density function g_0

$$g_0 = (\alpha I + H^*H)^{-1}H^*\Phi(.,0) \tag{3.25}$$

That gives the g_0 function with penalty term α. The discretized version of the equation (3.24) with source point at origin can be given as

$$\begin{bmatrix} e^{ikx_1.\theta_1} & \cdots & e^{kx_1.\theta_n} \\ \vdots & \ddots & \vdots \\ e^{kx_n.\theta_1} & \cdots & e^{kx_n.\theta_n} \end{bmatrix} \begin{bmatrix} g_0 \\ \vdots \\ g_0 \end{bmatrix} = \begin{bmatrix} \Phi(x_1,0) \\ \vdots \\ \Phi(x_n,0) \end{bmatrix} \tag{3.26}$$

After the kernel g_0 is obtained, we need to find the kernel for all the points inside the investigation domain. Using the relations of scattered field and its far-field pattern we can reconstruct the scattered field at any z point as

$$E^s(r,\theta) = 4\pi \int_S E^\infty(-\hat{x},\theta)\, g_{r,\varepsilon}(\hat{x})ds(\hat{x}) \tag{3.27}$$

Its dicretized version can be given as

$$\mathrm{E}^s\,(r,\theta) = \sum_{i=0}^{N-1} E^\infty(-\widehat{x_\imath},\theta) g_{r,\varepsilon}(\hat{x}_i)\,\frac{2\pi}{N} \tag{3.28}$$

And can be written in terms of linear equation system as

$$\begin{bmatrix} \mathrm{E}^s\,(r,\theta) \\ \vdots \\ \mathrm{E}^s\,(r,\theta) \end{bmatrix} = \begin{bmatrix} E^\infty(-\widehat{x_\imath},\theta) \\ \vdots \\ E^\infty(-\widehat{x_\imath},\theta) \end{bmatrix} . \begin{bmatrix} g_{r,\varepsilon}(\hat{x}_i) \\ \vdots \\ g_{r,\varepsilon}(\hat{x}_i) \end{bmatrix} \tag{3.29}$$

Here, g_z is the density function from PSM with different source points which can be obtained easily using the equation

$$g_r(\theta_k) = e^{-ikr.\theta_k} g_0(\theta_k) \tag{3.30}$$

The density function can also be obtained by solving the inverse linear matrix system (3.26) for all z points but this increases the computational burden. Thus, the equation (3.30) is a much more effective way to obtain these kernels. It should also be mentioned that the operation $r.\theta_k$ is a pointwise multiplication given as

$$z.\theta_k = z_x\theta_{k,x} + z_y\theta_{k,y} \tag{3.31}$$

$\theta_{k,x}$ and $\theta_{k,y}$ denotes the x and y components of the far-field points.

Using these information, and the relation between the scattered field and the fundamental solution, the indicator function can be formulated as

$$\Phi^s\,(r,r) = \int_S E^s(r,\theta)\, g_{r,\varepsilon}(\theta)ds(\theta) \tag{3.32}$$

Its discretized version is given as

$$\Phi^s\,(r,r) = \sum_{k=0}^{P-1} E^s(r,\theta_k) g_{r,\varepsilon}(\theta_k)\,\frac{2\pi}{P} \tag{3.33}$$

Where $\frac{2\pi}{P}$ is the step size for the receiver antennas.

And finally, as a linear equation system, (3.32) can be written as

$$\begin{bmatrix}\Phi^{s}\ (r,r)\\ \vdots \\ \Phi^{s}\ (r,r)\end{bmatrix} = \begin{bmatrix}E^{s}(r,\theta_k)\\ \vdots \\ E^{s}(r,\theta_k)\end{bmatrix} . \begin{bmatrix}g_{r,\varepsilon}(\theta_k)\\ \vdots \\ g_{r,\varepsilon}(\theta_k)\end{bmatrix} \tag{3.34}$$

And this concludes the realization of the original SSM.

With the discretization scheme provided, the discussion on the original SSM is completed. Next section describes the additions to the original method which is provided in this study to improve the reconstructions.

3.5 Frequency Correlation and S-parameter Modification for the SSM

As anticipated earlier, we propose two simple additions to the original formulation. First one is a multifrequency scheme that is obtained to enhance the quality of the results. The second is a scattering parameter modification to the original method to make it applicable to the measurement scenarios that we have conducted. Both of the additions has been made heuristically but we will also give our justifications for these modifications.

The multifrequency approach has been introduced to enhance the imaging aspects of each of the frequencies. Since both the Fresnel data and our measurement data has been obtained for multiple frequencies within a range, we had the chance to observe the results for each frequency independently. During this observation, we have come to a conclusion that the lower frequencies are better at estimating the shape and location of the scatterer roughly since higher penetration can be achieved in these frequencies and the signal power can be preserved more compared to higher frequencies, but they smooth out the corners and wedges of the target scatterer which causes loss of information. On the other hand, since the corners and wedges scatter the incident field much more than the smooth surfaces, the higher frequencies show better resolution at corners while the smooth boundaries fade away or becomes inaccurate because of the error in the measurement inevitably. After these observations, we had decided to combine the better aspects of the frequencies to achieve more resolution at the end. We have realized three different schemes for this purpose. First, a plain addition is made on the results of each frequency which is given by

$$I(r) = \sum_{i=1}^{N} I_i^{f}(r) \tag{3.35}$$

Where $I(r)$ is the imaging functional of SSM. Secondly, all results is added to each other through a scheme of normalization which is given by

$$I(r) = \sum_{i=1}^{N} \frac{I_i^f(r)}{\left|I_i^f(r)\right|} \tag{3.36}$$

Finally, we have used a probabilistic approach to correlate each of the frequency together. First, we have determined the success of each frequency through bitwise comparison of normalized results and the actual object information for several cases and then weight each frequency accordingly. Then, this weighted results can be added to each other in the classical sense. In a mathematical sense, the algorithm looks like,

$$I(r) = \sum_{i=1}^{N} a_i I_i^f(r) \tag{3.37}$$

Where a_i are the weight constants for each frequency. Another possible scheme includes eliminating the single pixel scatterers to form better results using neighborhood of each pixel but this method requires the use of a general cut-off value for the imaging functional which we were not able to find yet, thus it is not feasible to realize this method at this point.

All the three approaches are impelemented in the algorithm, tested against various measurement scenarios which is given in the results section.

Now, we will explain the modification that is made for the method to be feasible for scattering parameter measurements. This modification actually involves two steps and is influenced by a study made by M. Haynes [47]. First step is the determination of the near-field counterpart of far-field pattern. Then, it is possible to convert the near-field measurements into scattering parameters using the published study.

In [47-49], a relationship between the scattered field and S-parameters is given using a field modeling around the transmitter and recevier antennas. Using this property and the relation between scattered field from a plane wave and its far-field pattern that we are supposed to use as measurement data, we can interreleate these parameters and use S-parameters instead of far-field pattern when required. Note that we will not prove these concepts. We merely give our justification to apply these modifications by attaching simple mathematical operations to them.

First, we start with giving the relation between the far-field pattern and near-field measurement of scattered field. Since we know that any far-field pattern can be written as

$$E^s(r,d) = \frac{e^{jk|r|}}{|r|^{(m-1)/2}} \left\{E^{\infty}(\hat{r},d) + O\left(\frac{1}{|r|}\right)\right\} \tag{3.38}$$

We can infer that $\Phi^s\ (r, d)$ can be written as

$$\Phi^s(r, d) = \frac{e^{jk|r|}}{|r|^{(m-1)/2}}\left\{\Phi^\infty(\hat{r}, d) + O(\frac{1}{|r|})\right\} \tag{3.39}$$

Secondly, in [36], it is given with the formula

$$S_{ki} = \frac{jZ_0^k}{2\omega\mu}\int_D E_k^{inc}\,(r')\chi(r')E_i(r')dr' \tag{3.40}$$

The measured scattered field at some point z is directly related to measured S-parameter S_{ki} by a simple constant which is dependent on average signal power P_{ave} generated by the source and characteristic impedance Z_0 of the antenna port, and angular frequency of the monochromatic wave that is generated by the transmitter. According to this relation, we can conclude that, by replacing the variables total field and the object function by denstiy functions, the scattered field can possibly be related to its far-field pattern by

$$\Phi^s(r, r) = \frac{jZ_0^k}{2\omega\mu}\sum_i S_{ki}\, g_{r,\varepsilon}g_{r,\varepsilon} \tag{3.41}$$

This finalizes the basic steps of configuration for the modification of the SSM for scattering parameter measurements.

In this chapter, a detailed mathematical description of the SSM is given along with the additions to the method which are designed by us and the basic explanation of the two other qualitative inverse scattering methods, LSM and FM, with which the success of the algorithm will be compared to. There are studies where the S-parameter measurements have been used for qualitative methods instead of far-field measurements and produce succesful outcomes, see [54-55]. In the next chapter, success of the method is tested against all the scenarios that is mentioned before, for both of the measurement setups along with detailed explanation of each of them.

4. EXPERIMENTAL VERIFICATION

4.1 Fresnel Database Results

In this section, we will show experimental results obtained using SSM in two different setup. First, we used Fresnel Institute Opus1 and Opus2 database to determine the efficiency of the algorithm. Opus1 is made for simple objects and Opus2 is made for more complex cases. We will mostly use Opus1 for our study, as an efficiency test for the SSM. The Fresnel Institute setup and its graphical explanation can be seen in Figure 4.1.

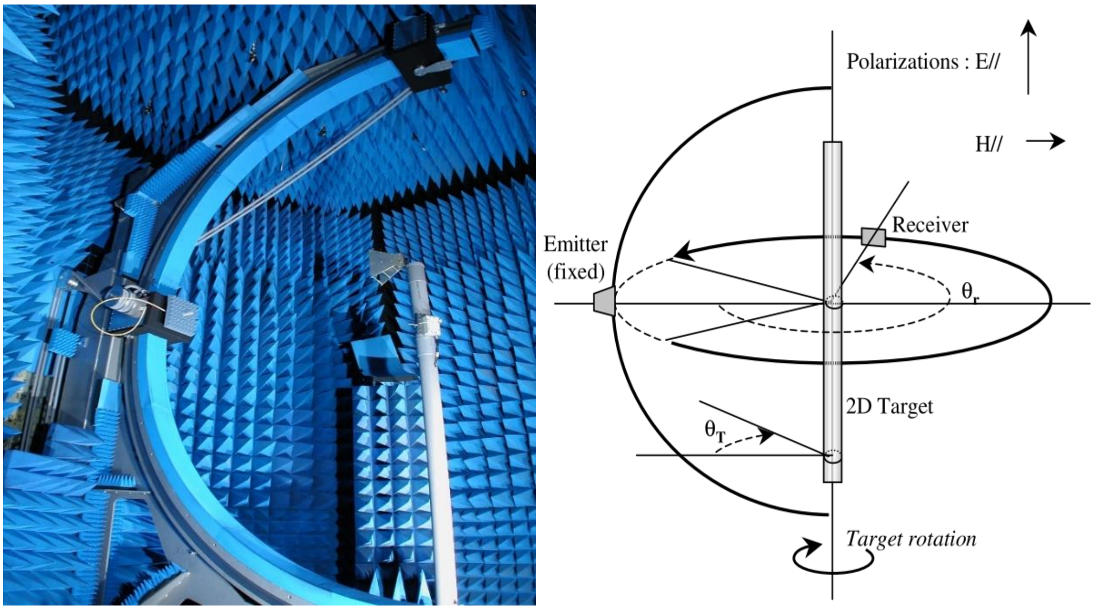

a) b)

Figure 4.1 Fresnel Institute a) Anechoic Chamber, b) Measurement setup with rotations and orientations

More information about this setup and measured objects can be found in [50-52]. Opus1 data consists of 72 receiver points and 36 transmitter points. On the other hand, Opus2 includes 360 receiver points and 8 transmitter points which are equally apart from each other. The results obtained for various cases are tested and presented to the reader in the next pages.

In the first setup, a dielectric cylindrical object is placed off-centered with a center (0,3) cm. The measurements are made at frequencies 4 GHz, 8 GHz, 12 GHz and 16 GHz. In Figure 4.2, single frequency results of this setup is shown at 4 GHz, 8 GHz, 12 GHz and 16 GHz along with the original location of the scatterer shown with a dashed line. According to the these figures, all the frequencies successfully recover the shape and location of the object.

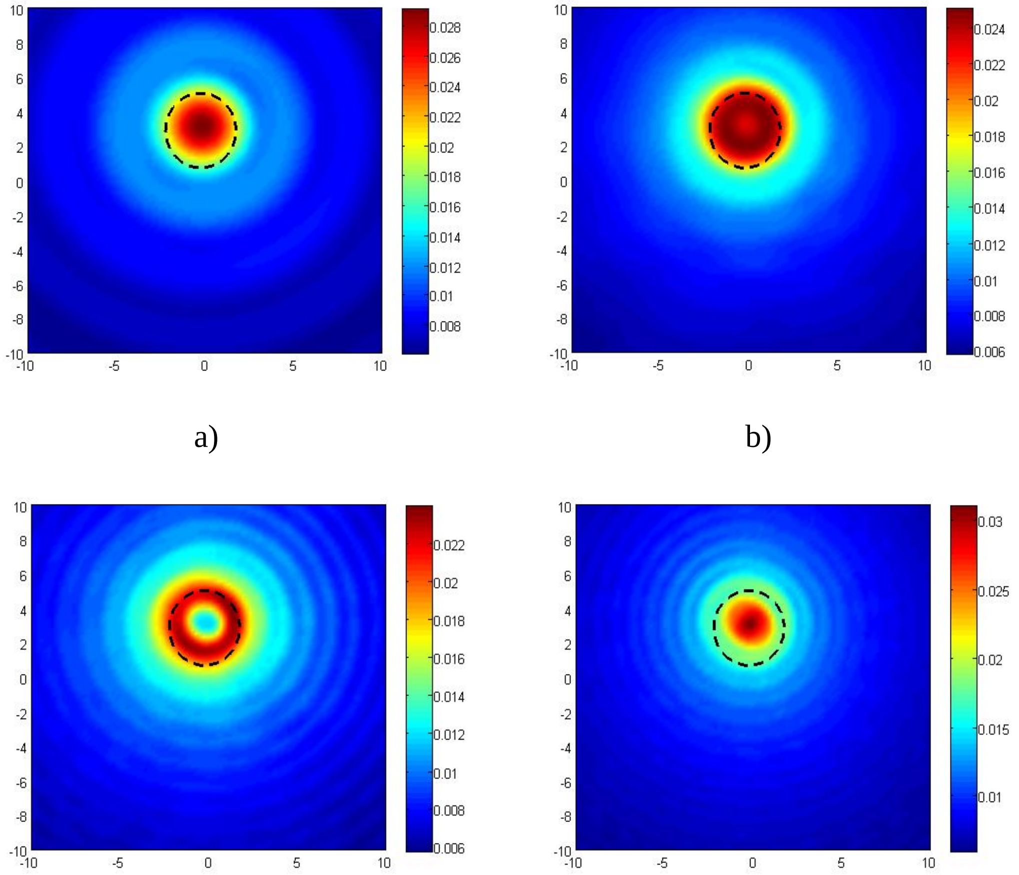

a) b)

c) d)

Figure 4.2 Single frequency reconstructions of an off-centered, cylindrical dielectric object excited with TM polarized incident field at a) 4 GHz, b) 8 GHz, c) 12 GHz, d) 16 GHz

Second result of this setup is formed for the comparison of multiple frequency cases. In Figure 4.3. same scattering object is reconstructed with the multiple frequency scheme with the combination of 4 to 8 GHz, 4 to 12 GHz and 4 to 16 GHz, respectively.

Similar results are observed with the single frequency cases and a discrimination cannot be made at this point.

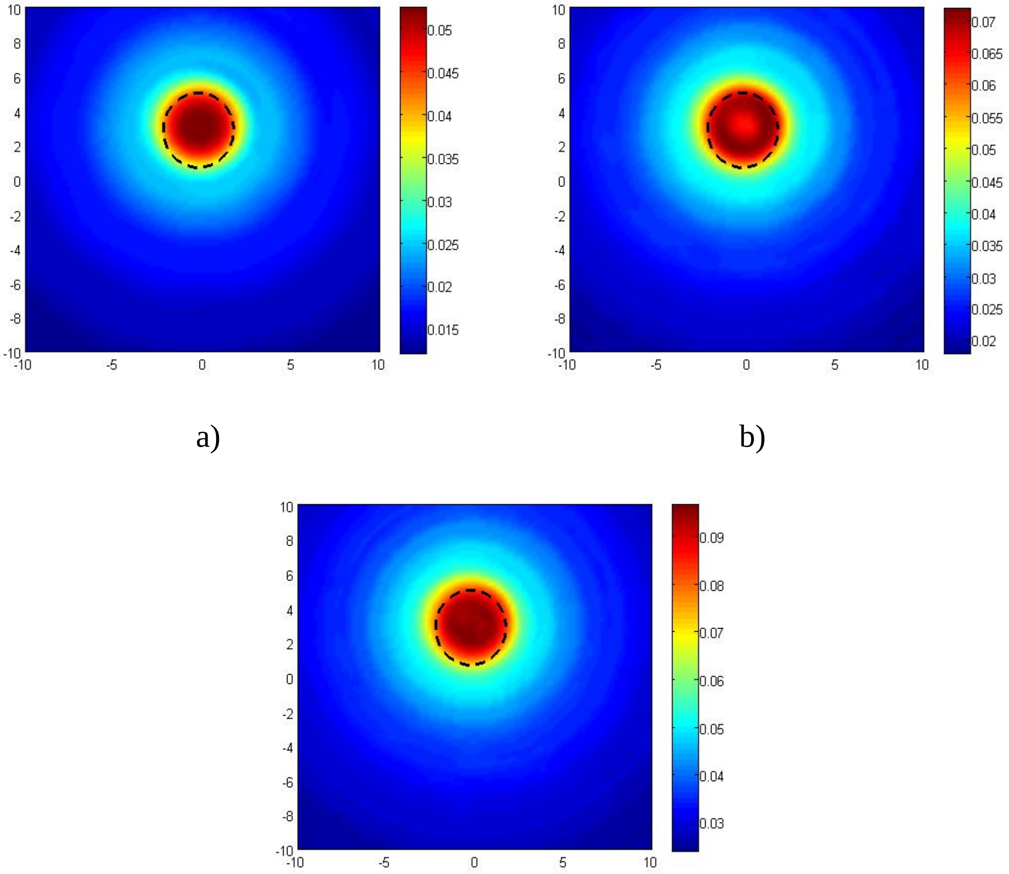

a)

b)

c)

Figure 4.3 Multiple frequency reconstructions of an off-centered, cylindrical dielectric object excited with TM polarized incident field between a) 4 and 8 GHz, b) 4 and 12 GHz, c) 4 and 16 GHz

In Figure 4.4, as a third comparison for the effectiveness of the algorithm, we give the results for three different methods, namely SSM, LSM and FM which are obtained with multiple frequency scheme between 4 and 16 GHz. As it can be said that all methods accurately reconstructs the object, the result of FM has a margin compared to the other methods. LSM seems to diminish the scattering object along with the noise, while SSM is a bit prone to the measurement error since no denoising algorithm is used and the penalty term in regularization is selected arbitrarily.

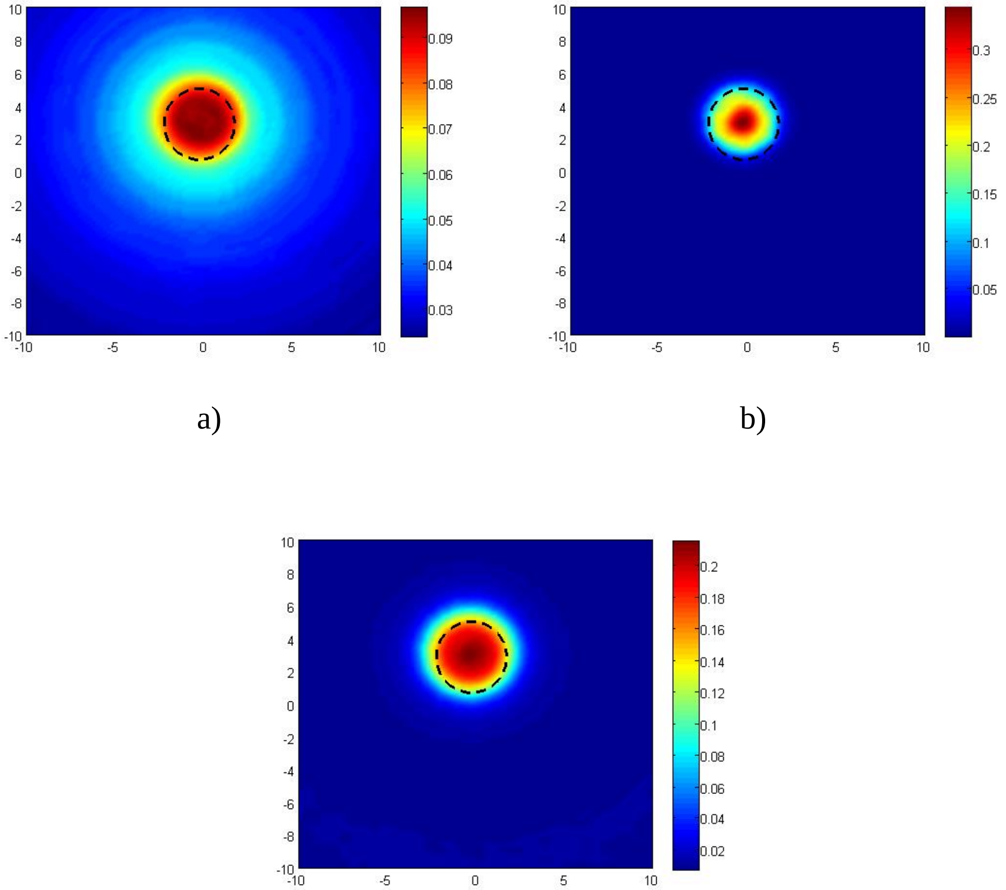

a) b)

c)

Figure 4.4 Multiple frequency reconstructions of an off-centered, cylindrical dielectric object excited with TM polarized incident field using different qualitative methods a) SSM, b) LSM, c) FM

Second setup is similar to the first one as it differs only in the frequencies that the measurements are conducted. The frequencies are selected between 1 and 8 GHz with 1 GHz interval. Results in Figure 4.5 are obtained using single frequencies at 1 GHz, 3 GHz, 5 GHz, 7 GHz, 8 GHz. The reconstructions are successful except for the 1 GHz frequency case. In that frequency, it can be observed that the reconstructed object is quite larger than the original object which might indicate an antenna inefficiency at that frequency since the result absurdly differs from the other frequencies unlike the first setup.

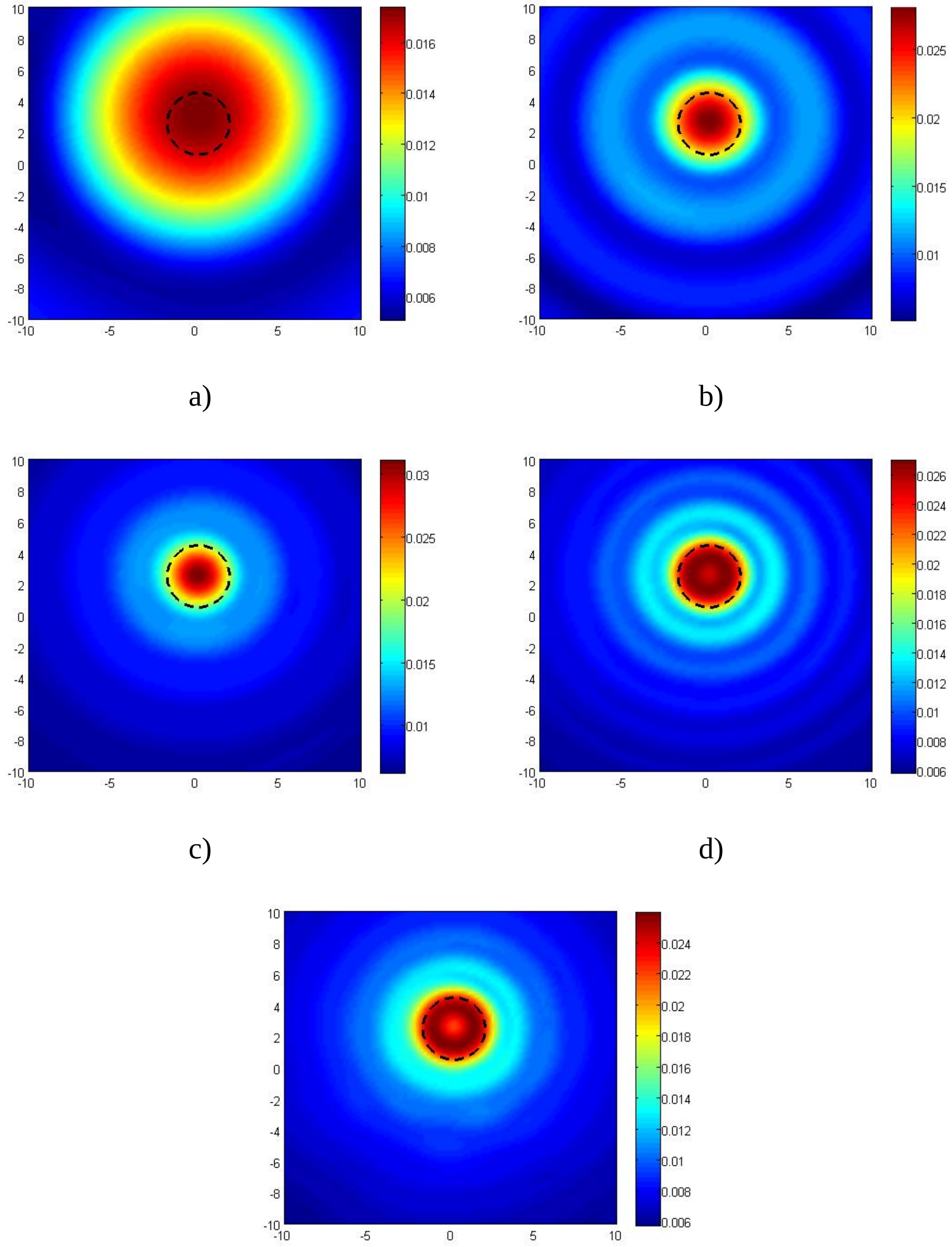

a) b)

c) d)

e)

Figure 4.5 Single frequency reconstructions of an off-centered, cylindrical dielectric object excited with TM polarized incident field at a) 1 GHz, b) 3 GHz, c) 5 GHz, d) 7 GHz, e) 8 GHz

As in the first setup, we compare multiple frequency reconstructions to determine the extension of the original algorithm. In Figure 4.6, results are obtained for 1 to 4 GHz, 5 to 8 GHz and 1 to 8 Ghz all with 1 GHz intervals. It can be observed that the results are equally succesful in all the cases and multiple frequency scheme seems to suppress the inaccurate reconstruction at 1 GHz as combined with the other frequencies. This shows a promising sign for the study as we progress to the more complex situations. This result is also confirmed at the comparison of LSM, SSM and FM given in Figure 4.7.

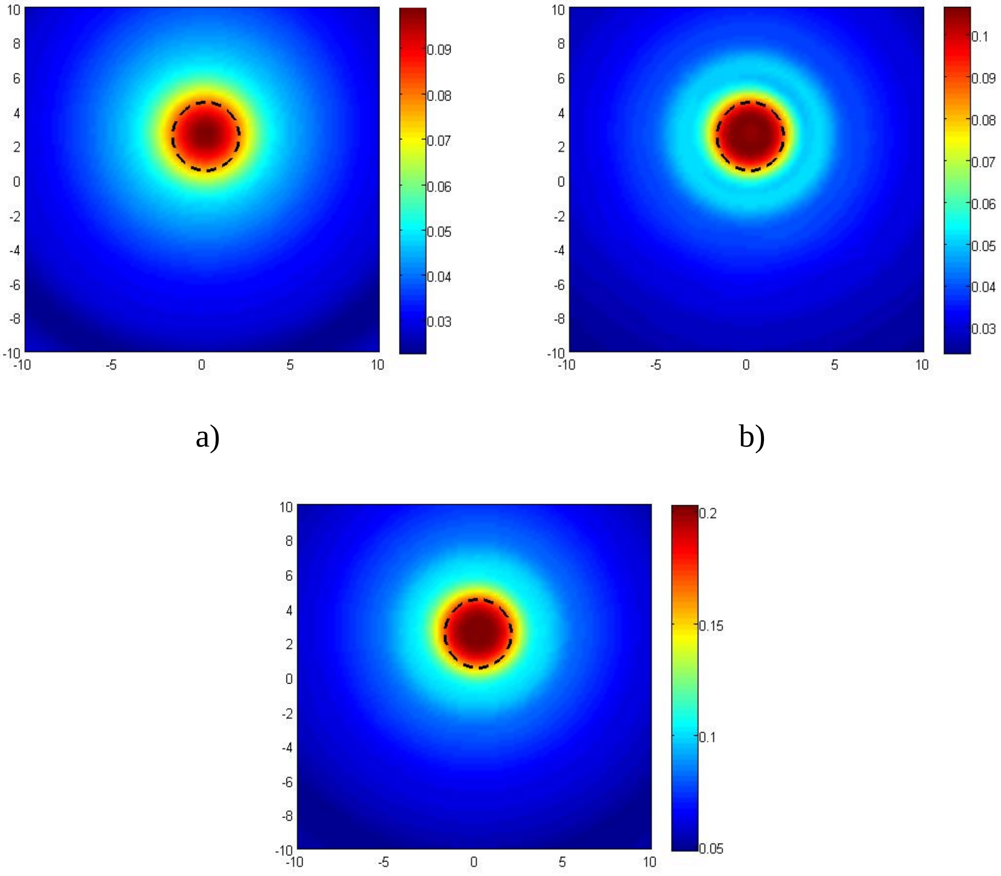

a) b)

c)

Figure 4.6 Multiple frequency reconstructions of an off-centered, cylindrical dielectric object excited with TM polarized incident field between a) 1 and 5 GHz, b) 5 and 8 GHz, c) 1 and 8 GHz

Third comparison is made between the qualitative methods same as the first setup. Results are obtained for the multi-frequency case including all the frequencies. Similar outcome can be inferred as the earlier case.

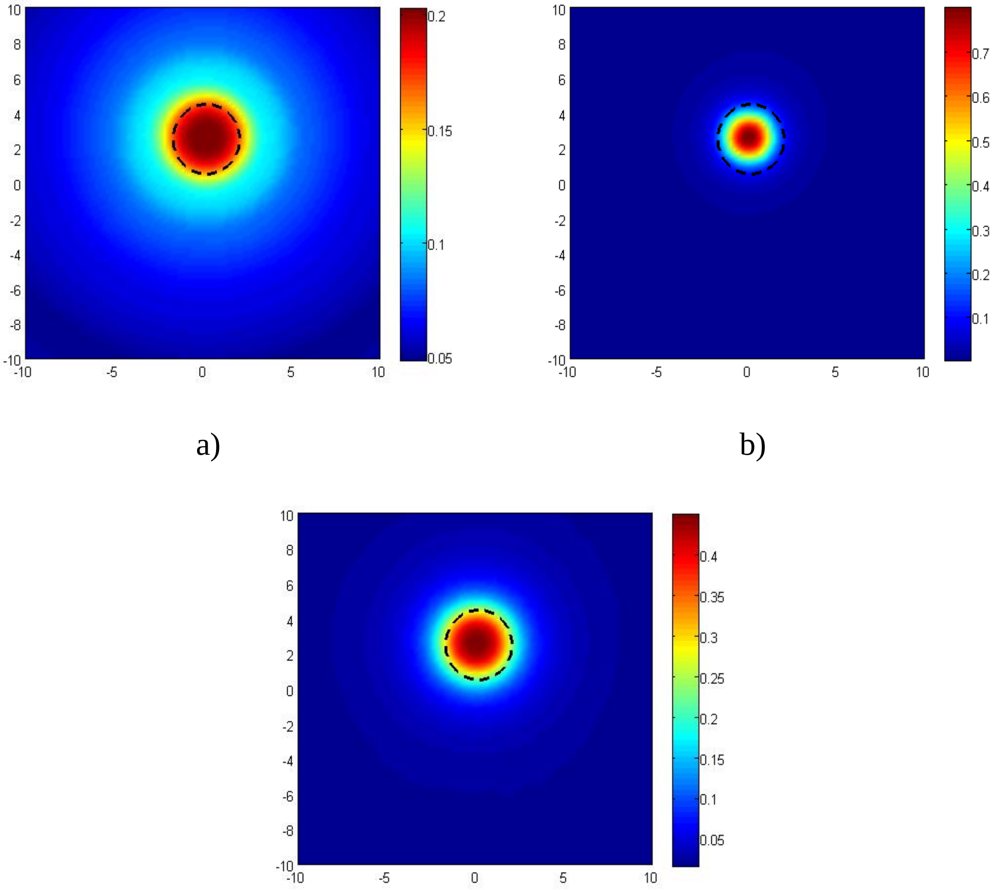

a) b)

c)

Figure 4.7 Multiple frequency reconstructions of an off-centered, cylindrical dielectric object excited with TM polarized incident field, measured between 1 and 8 GHz and solved using different qualitative methods a) SSM, b) LSM, c) FM

Next setup is made with a rectangular metallic object with size (24.5,12.7) mm centered to the investigation domain and 4 frequencies are used between 4 and 16 GHz with 4 GHz interval. Figure 4.8 shows the single frequency results obtained at frequencies 4 GHz, 8 GHz, 12 GHz and 16 GHz. As one can observe that the results are accurate, the wave structure of the scattering field is also seems to appear clearly in the reconstructions. In addition to the accuracy of the reconstructions, lower frequency results tend to smooth out the sharpness of the scattering object but this effect is minor in this case.

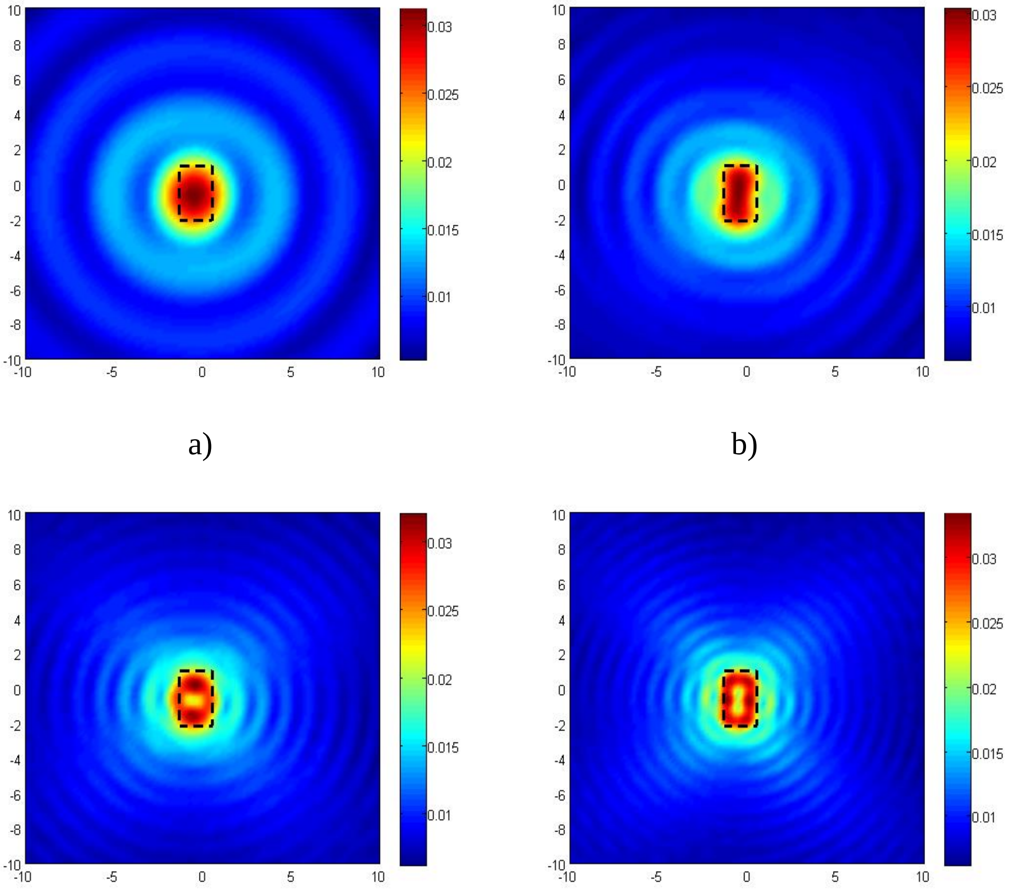

a) b)

c) d)

Figure 4.8 Single frequency reconstructions of a centered, rectangular conducting object excited with TM polarized incident field at a) 4 GHz, b) 8 GHz, c) 12 GHz, d) 16 GHz

Figure 4.9 shows the multi-frequency results for the third setup. These reconstructions are indifferent from each other in terms of quality and accuracy except for the smoothing effect of the lower frequencies as mentioned earlier. Figure 4.10 is a result of the method based comparison between the same three qualitative methods and they all successfully recover both shape and location of the object. Here, it is possible the observe the power of the denoising in LSM due to Morozov’s Discrepancy. Also, the wave structures seems to disappear in multiple frequency reconstructions as the summation tends to intertwine all the different wave structures in various frequencies altogether.

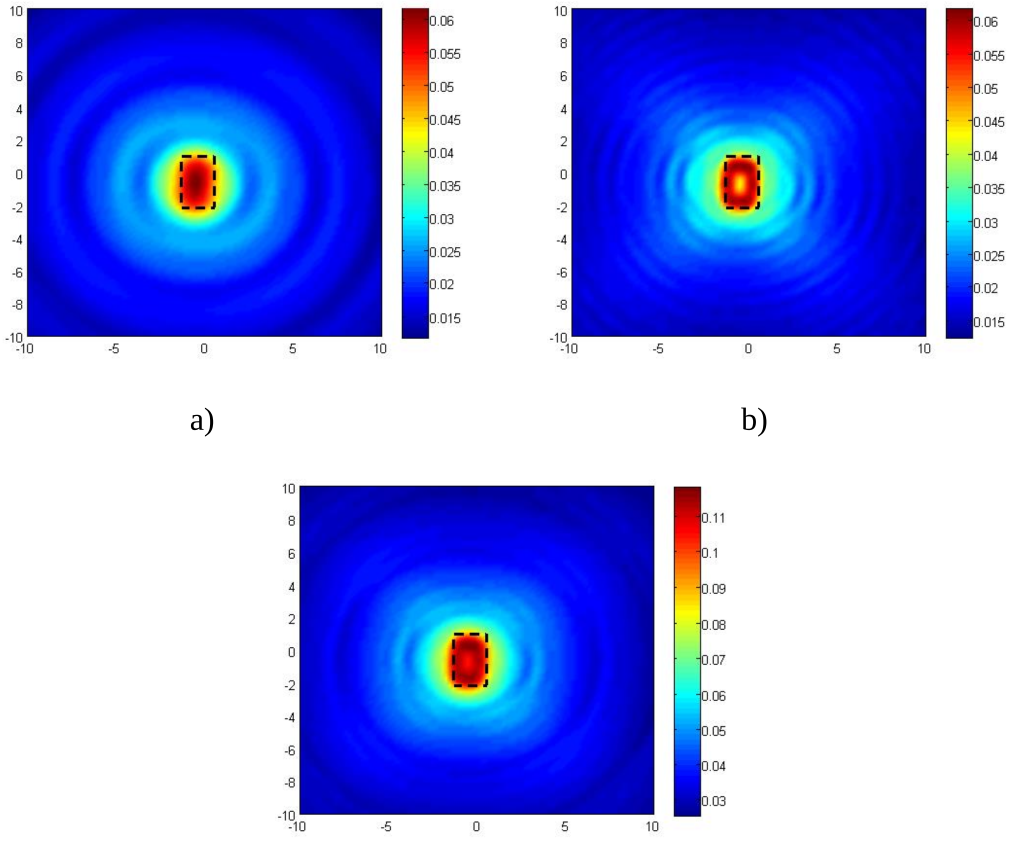

a) b)

c)

Figure 4.9 Multiple frequency reconstructions of a centered, rectangular conducting object excited with TM polarized incident field between a) 4 and 8 GHz, b) 12 and 16 GHz, c) 4 and 16 GHz

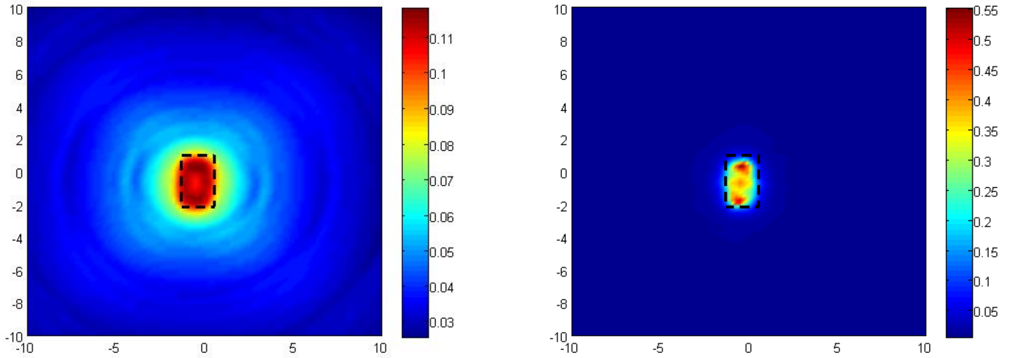

a) b)

Figure 4.10 Multiple frequency reconstructions of a centered, rectangular conducting object excited with TM polarized incident field and solved using different qualitative methods a) SSM, b) LSM, c) FM

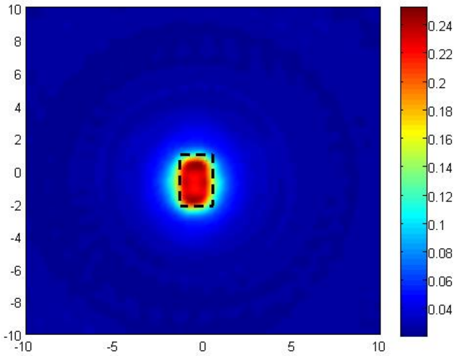

c)

Figure 4.10 (continuous) Multiple frequency reconstructions of a centered, rectangular conducting object excited with TM polarized incident field and solved using different qualitative methods a) SSM, b) LSM, c) FM

This time, same rectangular object is used as a scattering object but as a difference, it is placed off-centered with center (0,3) cm. The frequencies used in this measurement are 2 to 16 GHz with 2 GHz interval. Figure 4.11 shows the single frequency results obtained in this case. In this setup, the smoothing effect of the lower frequencies are more observable, especially at 2 GHz. Other than that, there are no distinguishable features that different frequencies can offer compared to others.

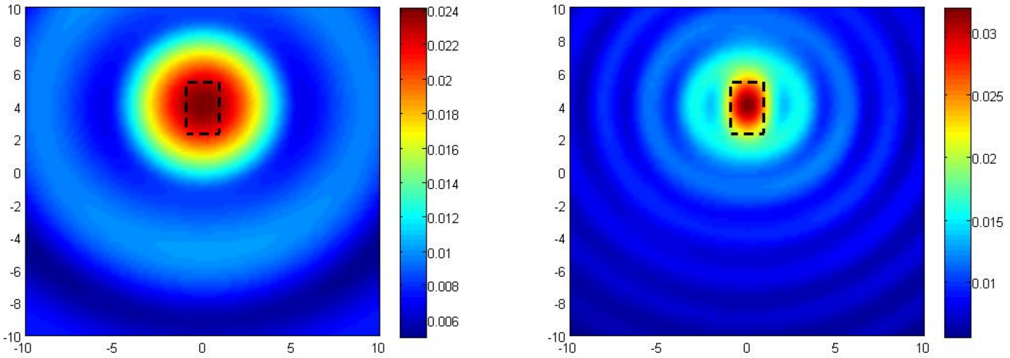

a) b)

Figure 4.11 Single frequency reconstructions of an off-centered, rectangular conducting object excited with TM polarized incident field at a) 2 GHz, b) 6 GHz, c) 10 GHz, d) 14 GHz, e) 16 GHz

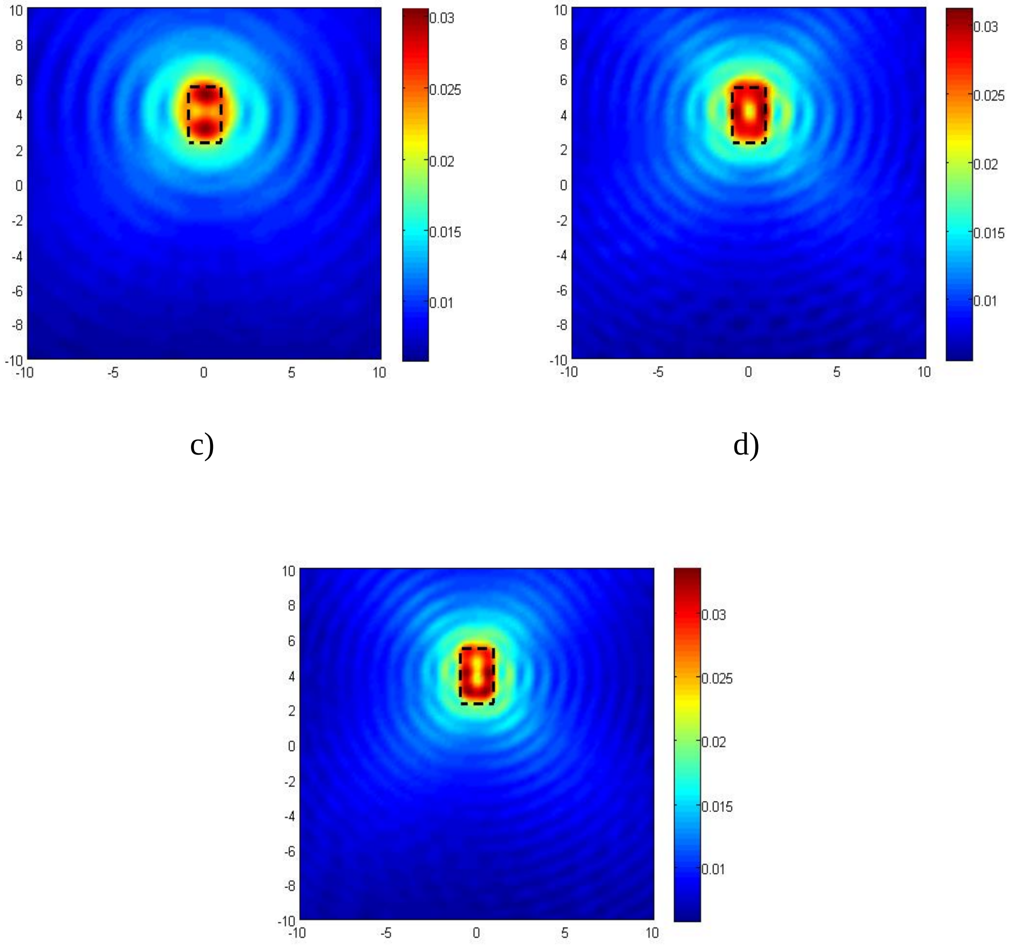

c) d)

e)

Figure 4.11 (continuous) Single frequency reconstructions of an off-centered, rectangular conducting object excited with TM polarized incident field at a) 2 GHz, b) 6 GHz, c) 10 GHz, d) 14 GHz, e) 16 GHz

Same multi-frequency summation is applied to this setup which is given in Figure 4.12 The results shows the success of the lower frequencies to determine the shape and location of the scatterer roughly, while the higher frequencies tend give more detail about the edges. This justifies our initiatives as the result of the summation supplies both the shape and the sharpness to the original reconstructions. On the other hand, as we are going to see in the latter cases, there is no certainty that the higher frequency results are more accurate than the lower ones. This depends also on the experimental system that is used. Only certainty is that the higher frequencies tend to provide sharper edges than the lower ones.

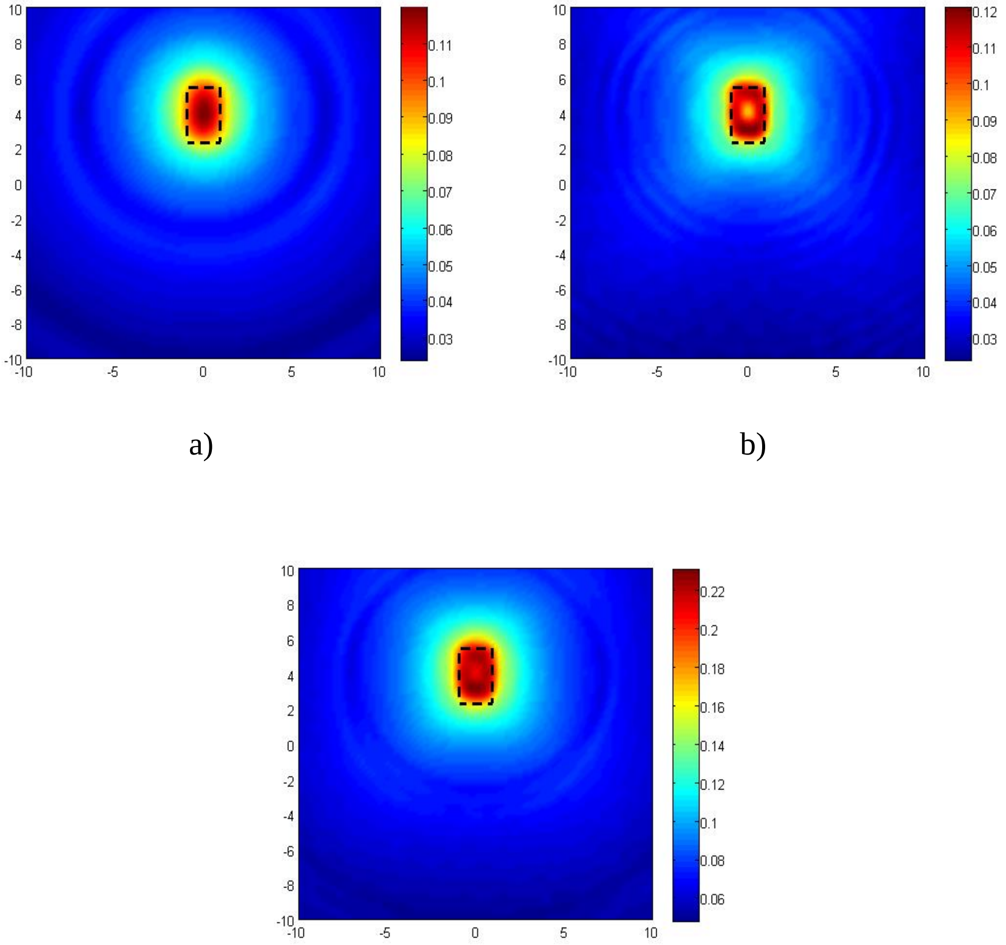

a)

b)

c)

Figure 4.12 Multiple frequency reconstructions of an off-centered, rectangular conducting object excited with TM polarized incident field between a) 2 and 8 GHz, b) 10 and 16 GHz, c) 2 and 16 GHz

The comparison of the SSM, LSM and FM are given in Figure 4.13. In this figure, it is obvious that SSM algorithm produces some significant noise around the object. In the initial formulation of the method, there is a cut-off value that should be determined for SSM after calculating the imaging functional $I(z)$, which is supposed to eliminate this generated noise, but our intention is to show the results as it is. So, we haven't used a cut-off value anywhere in this study, although it is quite possible to determine this parameter to enhance the results as the calculated values are not indicator to the electrical parameters in this method.

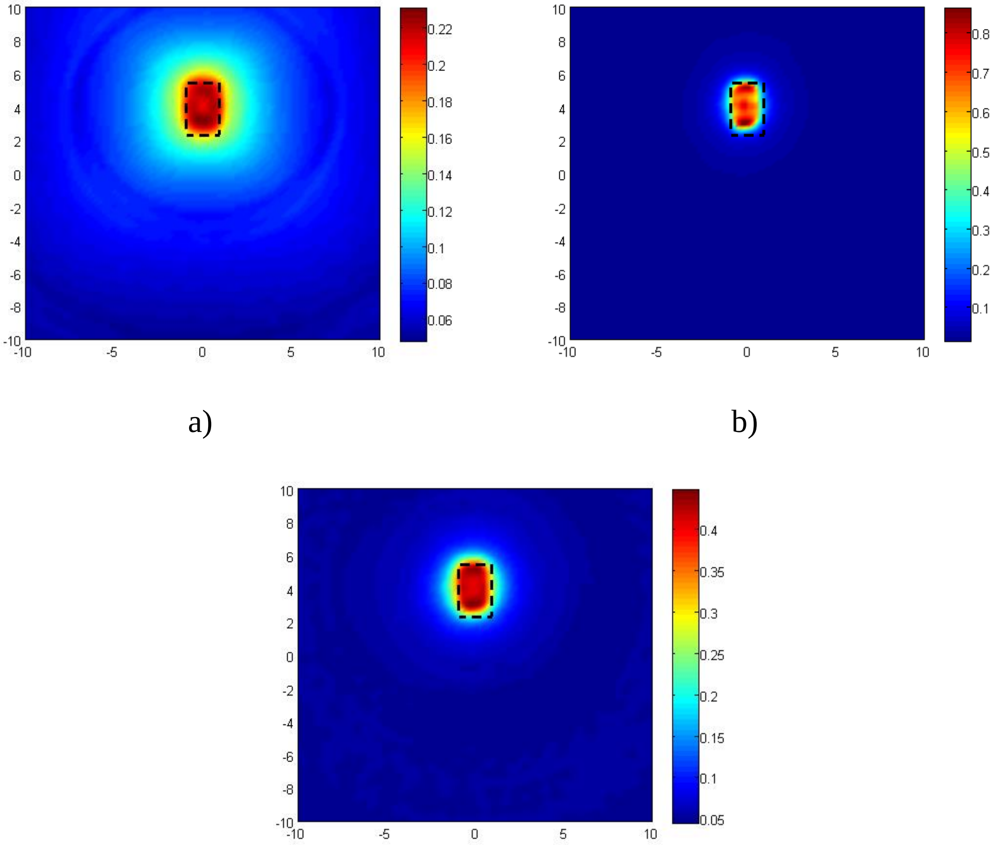

a)

b)

c)

Figure 4.13 Multiple frequency reconstructions of a centered, rectangular conducting object excited with TM polarized incident field, measured between 2 and 16 GHz and solved using different qualitative methods a) SSM, b) LSM, c) FM

Next object is a metallic U-shaped object which is obviously more complex than the ones in the earlier cases, thus it is a proper object to test the effectiveness of the SSM even further. The object is centered to the investigation domain and its dimensions are (80,50) mm. Since it is a concave shaped metallic object, we expect some multiscattering effect inside it. In Figure 4.14 single frequency results of the experiment is given for 2 GHz, 6 GHz, 10 GHz, 14 GHz and 16 GHz. Here, we observe that it is not possible to obtain a detailed information about the actual shape of the object at lower frequencies, namely 2 GHz. Beginning with 6 GHz, we start to obtain some details about the shape as the detail increases while increasing the frequency. It is possible to say in this setup that the higher frequencies are much more promising in reconstructing the scatterer in its whole detail.

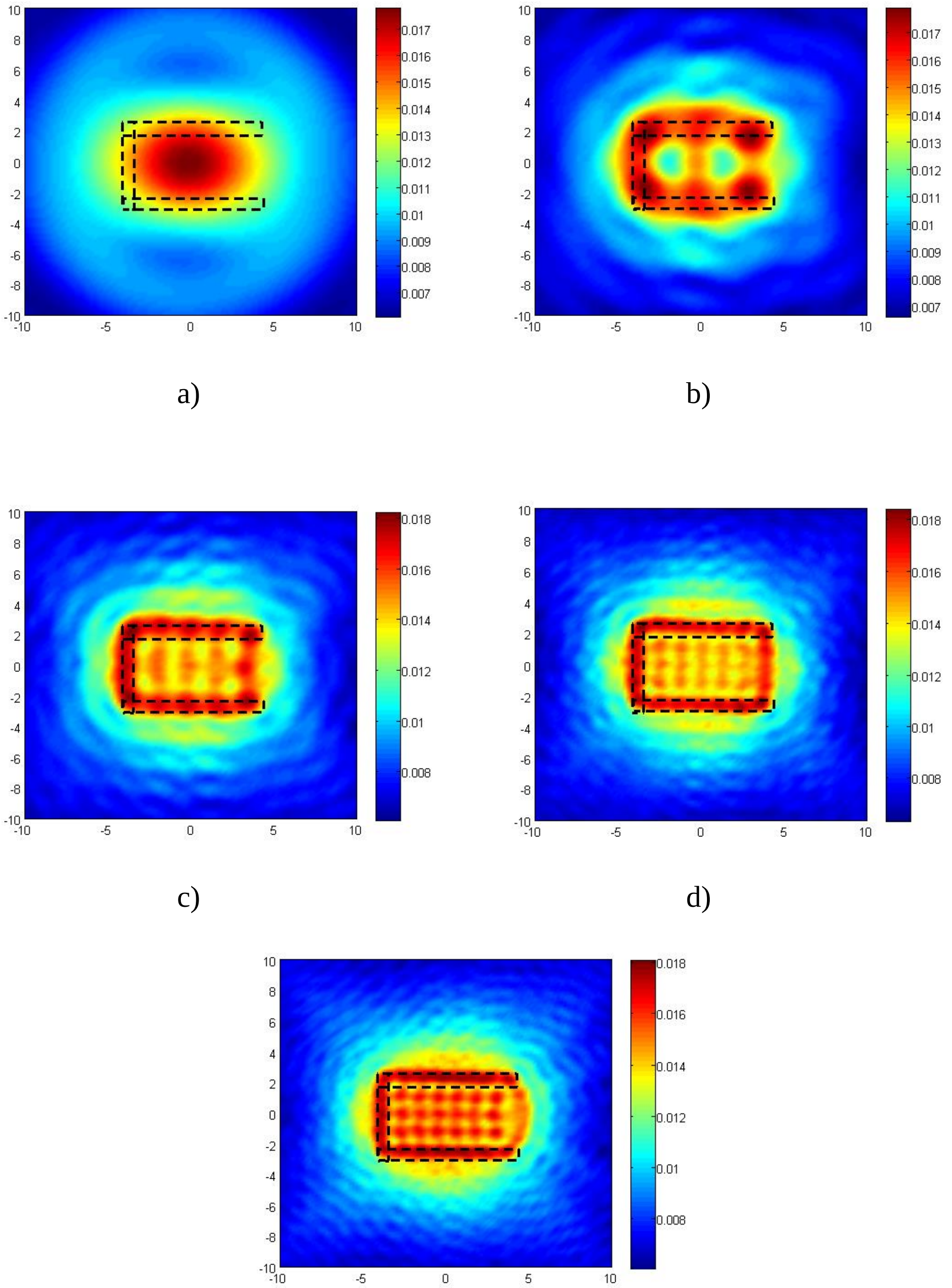

a) b)

c) d)

e)

Figure 4.14 Single frequency reconstructions of a centered, U-shaped conducting object excited with TM polarized incident field at a) 2 GHz, b) 6 GHz, c) 10 GHz, d) 14 GHz, e) 16 GHz

The discussed result now includes the multifrequency assessment of the method, which are given in Figure 4.15. According to this figure, we can say that combination of the higher frequencies are more accurate than the lower frequencies. In terms of resolution and quality, lower frequencies does not provide a property to the final result that higher frequencies cannot give. This result indicates that a single frequency quality assessment should be made before combining the frequencies together.

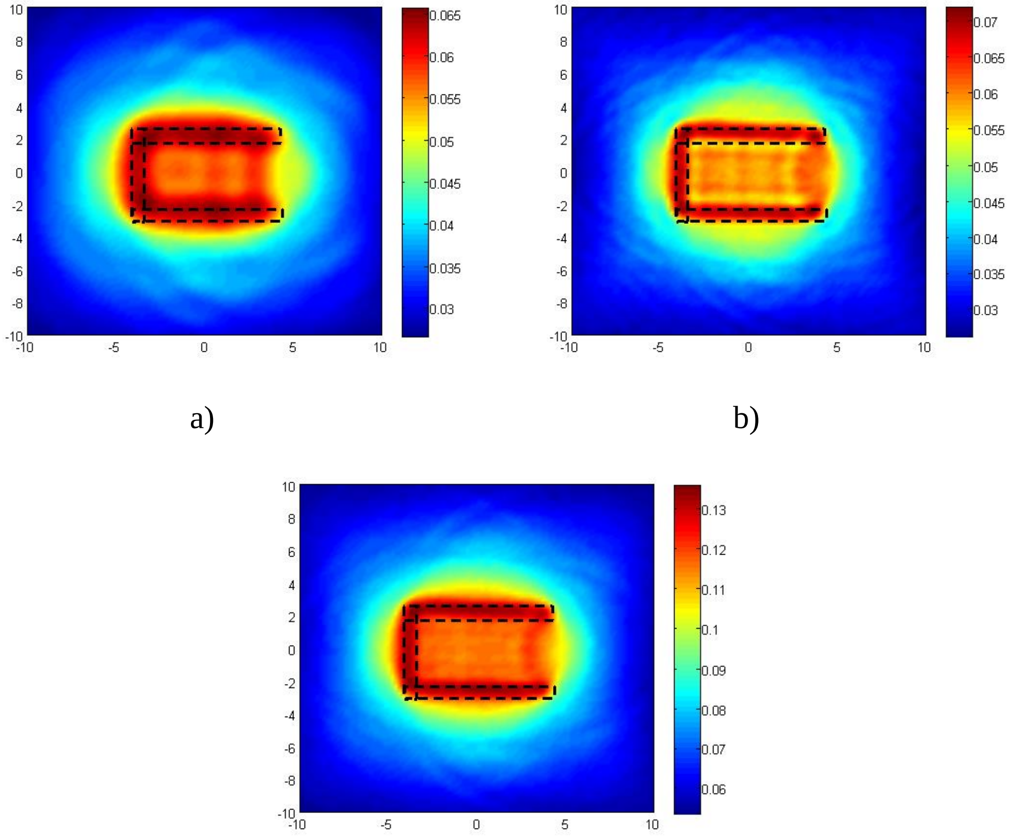

a) b)

c)

Figure 4.15 Multiple frequency reconstructions of a centered, U-shaped rectangular conducting object excited with TM polarized incident field between a) 2 and 8 GHz, b) 10 and 16 GHz, c) 2 and 16 GHz

We now continue with the qualitative method comparison of the U shaped metallic object. According to the Figure 4.16, it is possible to say that each of the methods produce a unique result. In SSM, the reconstruction has enough resolution and quality the determine the interedted object, but on the other hand, it produces a lot of noise around the scatterer that can make the results unreliable in some cases. In contrary, LSM produces relatively no noise, but while denoising, it may very well cause the object to disappear depending on the level of noise in the measurements. FM produces a scarcely better inversion compared to the other two, but it suffers from the same noise inside the scatterer as the SSM. This could be a sign that a combination of these methods may produce more satisfying results with appropriate weighting. In a future study, a multi-method scheme can be proposed along with the experimental verification.

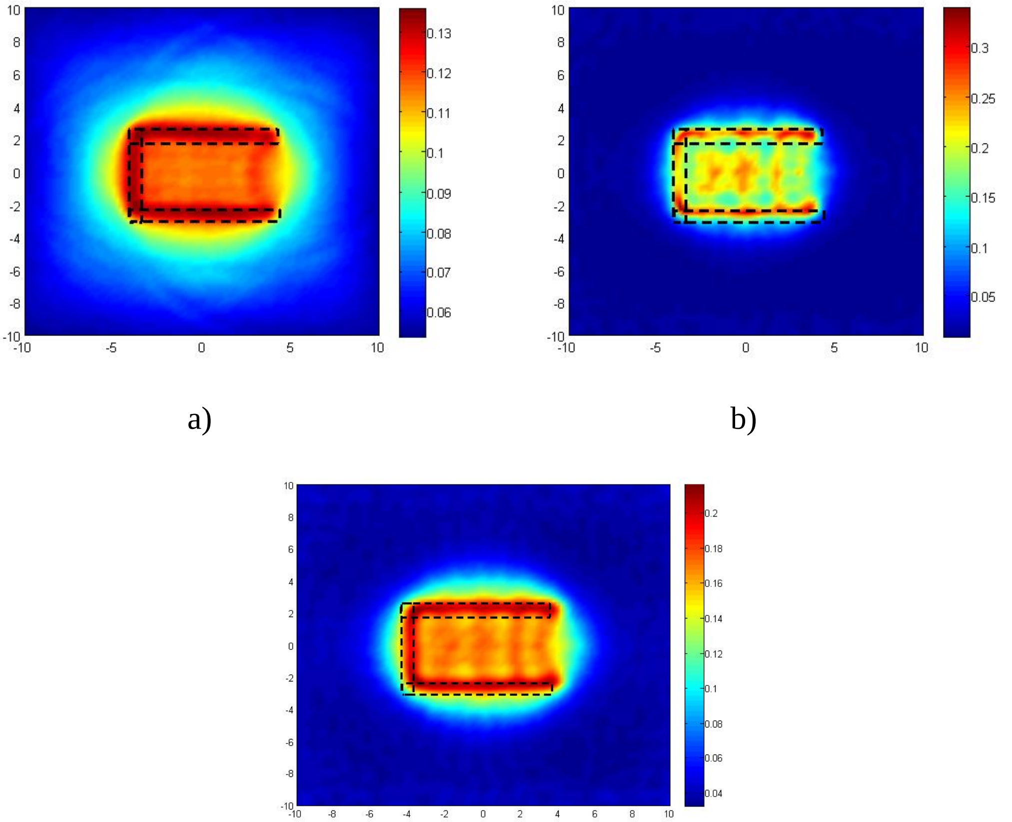

a)

b)

c)

Figure 4.16 Multiple frequency reconstructions of a centered, U-shaped conducting object excited with TM polarized incident field and measured between 2 and 16 GHz and solved using different qualitative methods a) SSM, b) LSM, c) FM

We now turn our attention to another data set which is measured under the same Fresnel setup, namely Opus 2 measurements. The related information can be found in [39]-[40]. This data set contains more complex scattering objects which gives us the possibility to test the capabilities and downfalls of the qualitative inverse scattering methods. Difference of this data set, other than complex scatterers is that it also contains more measurements, in terms of both transmitting and receiving points. All the measurements are made at 360 receiving points and 18 transmitting points which supposed to give more information on the measured objects. We begin with the measurement named ‘FoamDielExtTM’ which consists of a foam polyethylene cylinder ($\varepsilon_r = 1.30$) attached to relatively smaller dielectric cylindrical object as given in Figure 4.17. Foam polyethylene is centered in the rectangular coordinate system and the distance between the scatterers are 55.5 mm, respectively. Single frequency reconstructions at 2 GHz, 6 GHz and 10 GHz are given in Figure 4.18. Actual measurements are conducted between 2 and 10 GHz with 1 GHz interval, but we think that presenting 3 of these are enough to give the idea to the readers. According to the figure, the lower frequencies tend to represent the dielectric object better while diminishing the foam polyethylene, but as the frequency increases, the presence of the foam polyethylene becomes more and more clear. This gives a justification to combine the frequencies to obtain accurate reconstructions which we will discuss in the following figure. The comparison of the inversion methods with the multifrequency is given in Figure 4.19. This is the first case that the SSM produces more accurate inversion compared to the other methods. If we look at the results carefully, we observe that both LSM and FM cause a loss of information about the large Foam polyethylene cylinder while the SSM accomplishes to locate this object too. This is a promising result as it shows that SSM can be used in the reconstruction of the more complex situations.

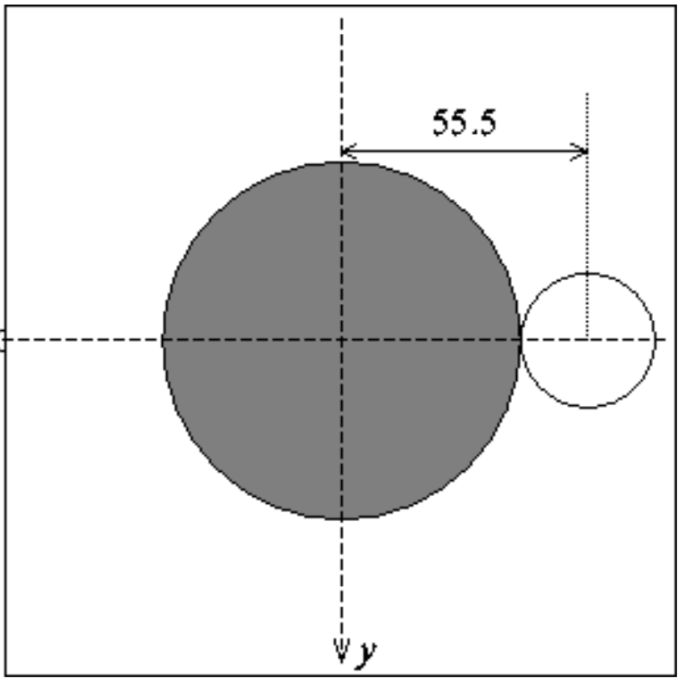

Figure 4.17 Visualization of 'FoamDielExtTM' measurement set of Fresnel Opus 2 experimental data that includes a dielectric cylinder located next to large foam polyethylene cylinder

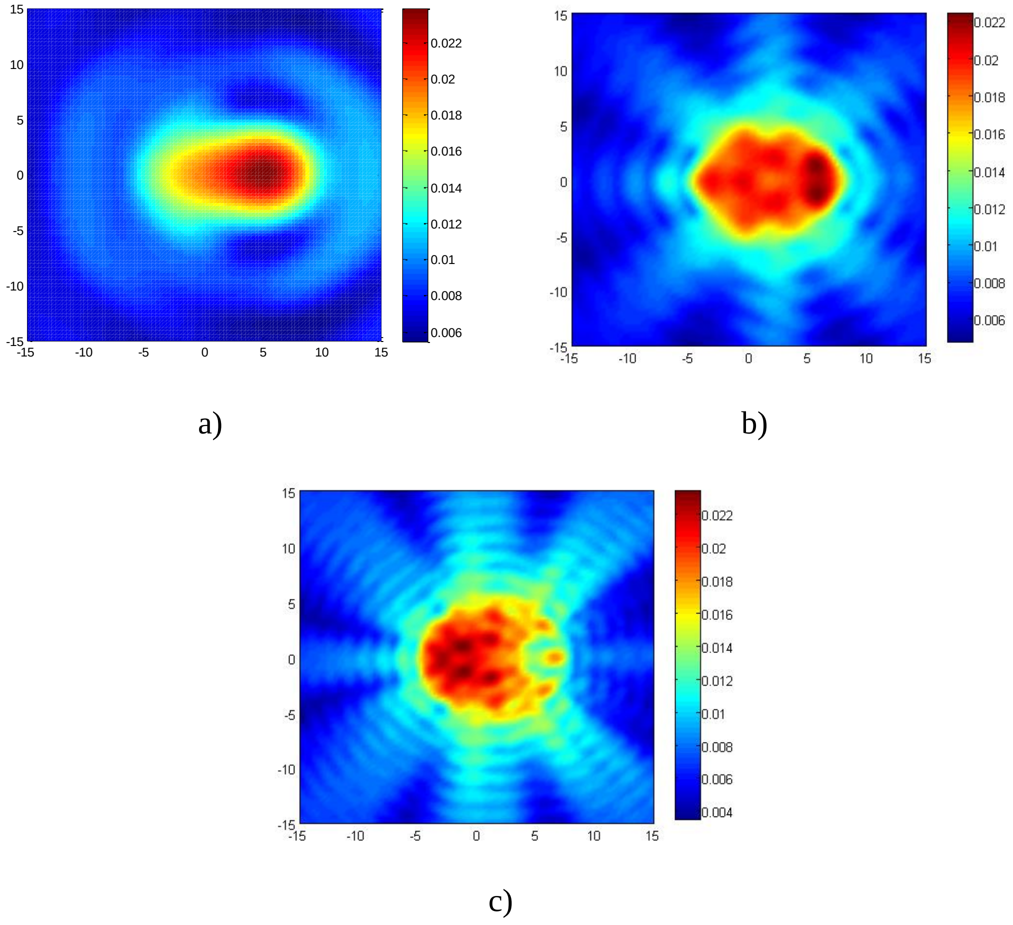

a)

b)

c)

Figure 4.18 Single frequency reconstructions of a centered cylindrical foam polyethylene and an off-centered external cylindrical dielectric object excited with TM polarized incident field at a) 2 GHz, b) 6 GHz, c) 10 GHz

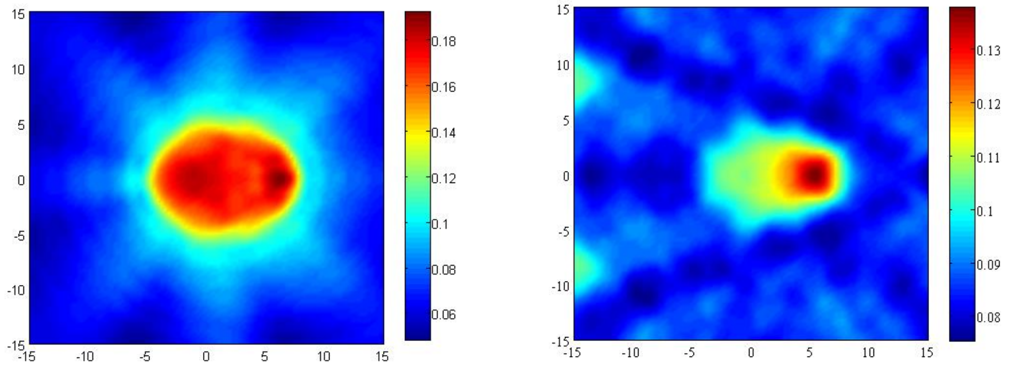

a)

b)

Figure 4.19 Multiple frequency reconstructions of a centered cylindrical foam polyethylene and an off-centered external cylindrical dielectric object excited with TM polarized incident field and measured between 2 and 16 GHz and solved using different qualitative methods a) SSM, b) LSM, c) FM

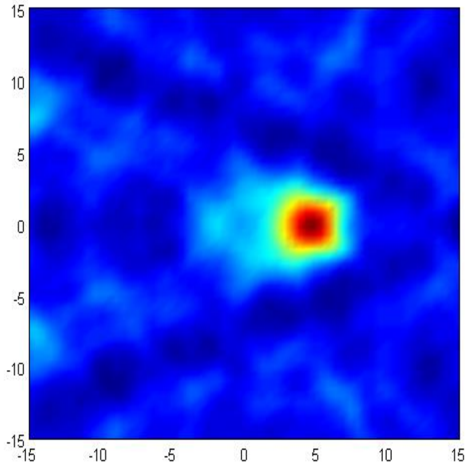

c)

Figure 4.19 (continuous) Multiple frequency reconstructions of a centered cylindrical foam polyethylene and an off-centered external cylindrical dielectric object excited with TM polarized incident field and measured between 2 and 16 GHz and solved using different qualitative methods a) SSM, b) LSM, c) FM

Following case is realized based on the measurement called ‘FoamDielIntTM’. Given in Figure 4.20 that, the scatterer consists of two cylindrical dielectric objects that the smaller one is placed inside the larger. SSM results obtained as the earlier setup is shown in Figure 4.21 Obviously, the quality of the reconstruction increases with the frequency. The scatterer inside can also be observed in the 10 GHz measurement as it is an interesting result in terms of a qualitative inversion method. This can be the result of the backprojection operator that the SSM uses, but a detailed study should be made to reveal the actual reason behind it. Since the purpose of this study is to determine the success of the algorithm for experimental data, we find it is unnecessary to dive into a deeper subject than required. But for more interested readers, in [53], a study is made to use SSM for the reconstruction of layered media in which the author claims that the algorithm can be used to determine the impedance of the boundary of the object, and iteratively of the object itself. This study is made only theoretically, and has not been tested neither through numerical simulation nor with the experimental setups so it stands as mathematical justifications that awaits experimental realization.

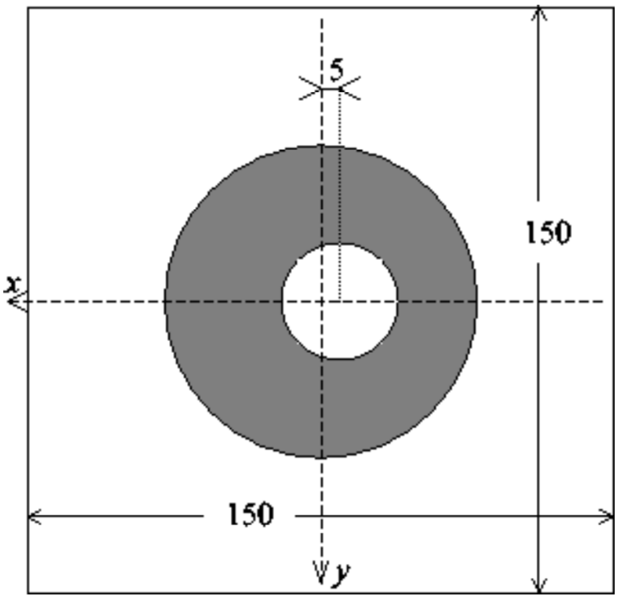

Figure 4.20 Visualization of ‘FoamDielIntTM’ measurement set of Fresnel Opus 2 experimental data that includes a dielectric cylinder located inside of a large foam polyethylene cylinder

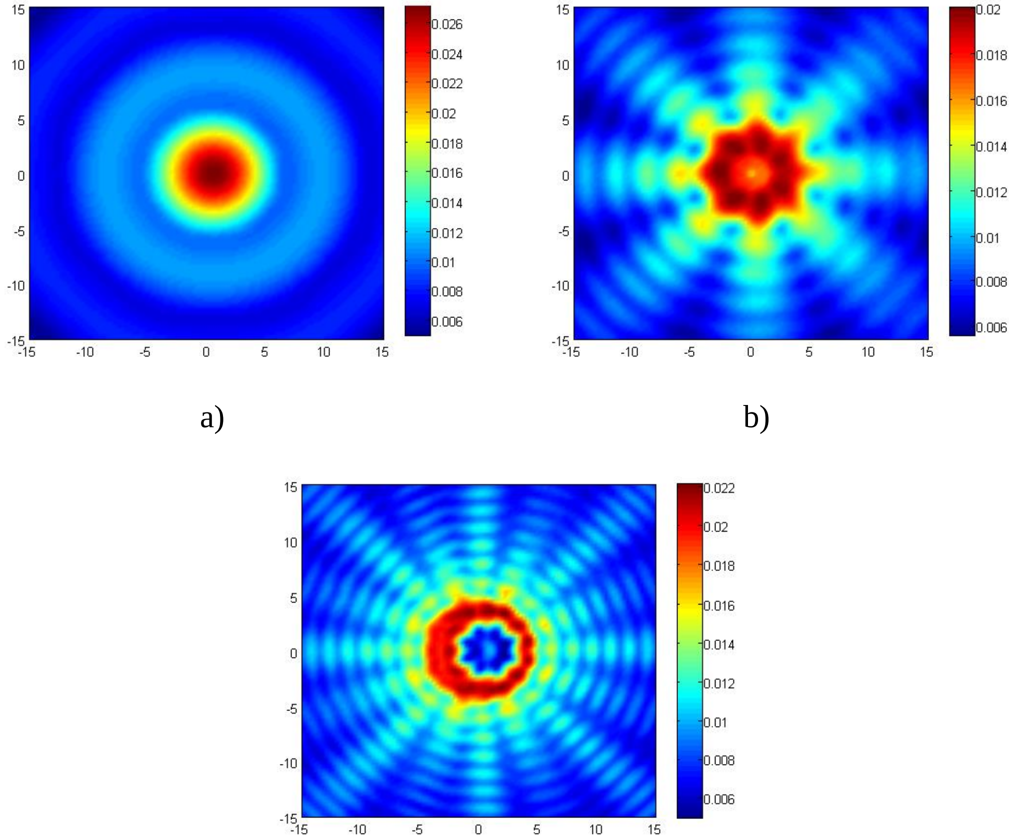

a)

b)

c)

Figure 4.21 Single frequency reconstructions of a centered foam polyethylene and an off-centered internal dielectric object excited with TM polarized incident field at a) 2 GHz, b) 6 GHz, c) 10 GHz

Second set of inversion of the same data set includes the realization of the SSM, LSM and FM with multifrequency. Reconstructions are given above in Figure 4.22 Same with the ‘FoamDielIntTM’ measurement, FM and LSM are failed to reconstruct the outer object while SSM is able to accomplish. SSM on the other hand has failed to differentiate the inner object from the outer one distinctively.

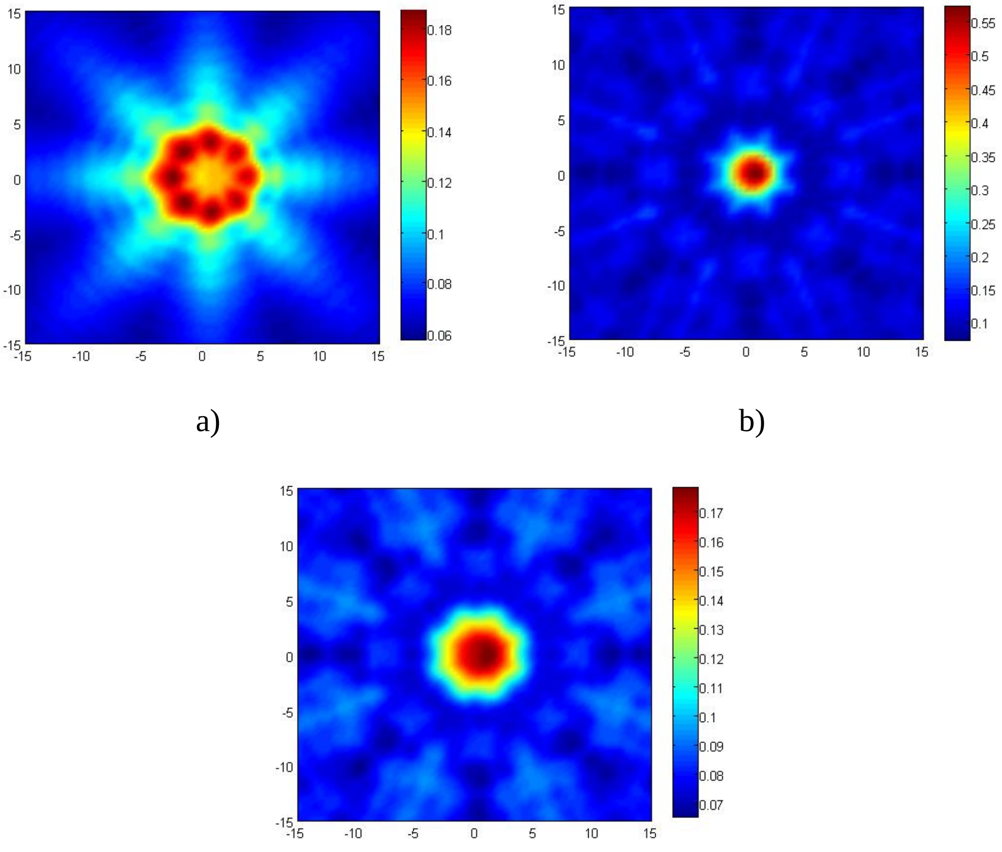

a) b)

c)

Figure 4.22 Multiple frequency reconstructions of a centered foam polyethylene and an off-centered internal dielectric object excited with TM polarized incident field and measured between 2 and 16 GHz and solved using different qualitative methods a) SSM, b) LSM, c) FM

We now continue with another set of measurement, this time, it includes a small metallic object placed next to a dielectric object as shown in Figure 4.23. Large dielectric object is centered to the coordinate system, and the distance between the center points of the objects are 54.25 mm. Single frequency results in Figure 4.24 shows that the presence of the metallic object becomes more vague as the frequency increases, which is exactly opposite with the dielectric object as it becomes more and more distinctive and dominant.

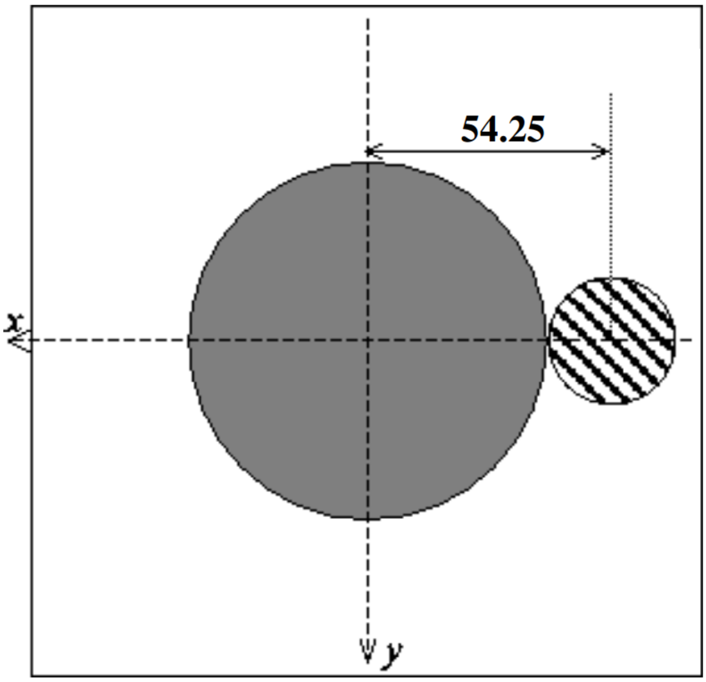

Figure 4.23 Visualization of 'FoamMetExtTM' measurement set of Fresnel Opus 2 experimental data that includes a metal cylinder located next to large foam polyethylene cylinder

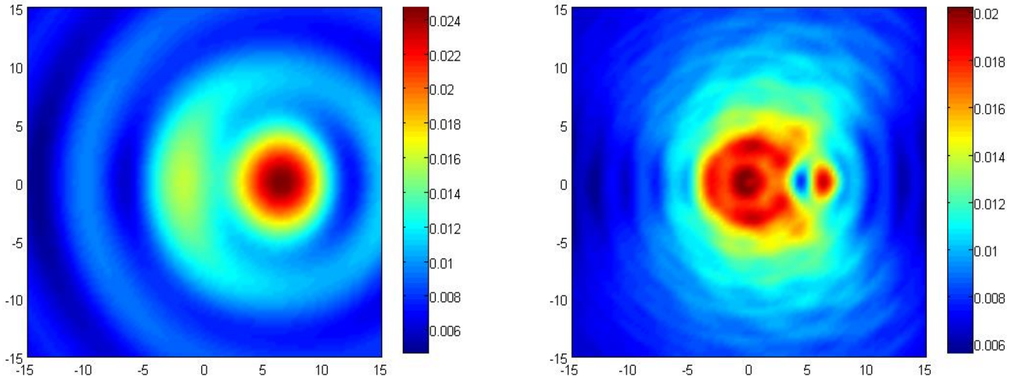

a) b)

Figure 4.24 Single frequency reconstructions of a centered foam polyethylene and an off-centered external metal object excited with TM polarized incident field at a) 2 GHz, b) 6 GHz, c) 10 GHz

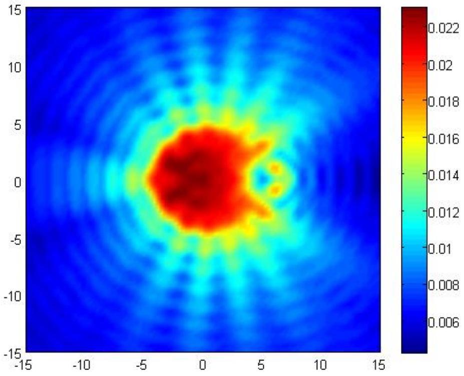

c)

Figure 4.24 (continuous) Single frequency reconstructions of a centered foam polyethylene and an off-centered external metal object excited with TM polarized incident field at a) 2 GHz, b) 6 GHz, c) 10 GHz

The multifrequency results of the different methods presents a different case this time as the FM result can be considered slightly more realistic when the noise of the SSM is also accounted for. Both the SSM and FM are accurately locate the objects but SSM contains significant noise around the scatterers similar to earlier inversions. LSM fails to both methods as only a trace of the entire dielectric object can be observed in the result as can be observed in Figure 4.25.

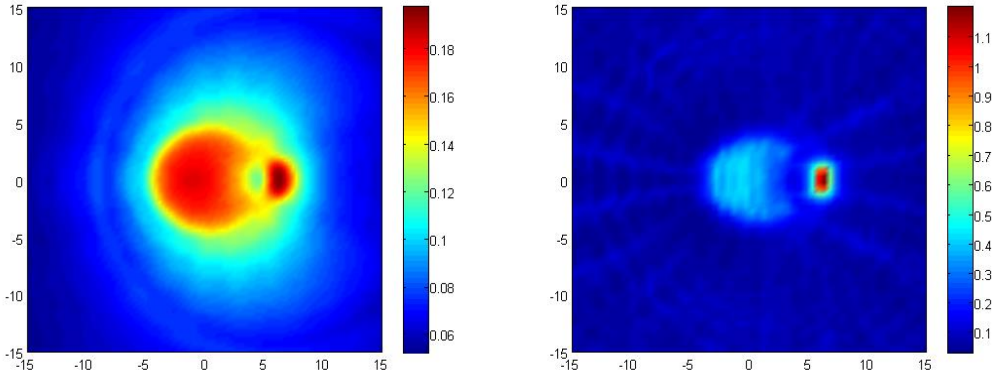

a) b)

Figure 4.25 Multiple frequency reconstructions of a centered foam polyethylene and an off-centered external metal object excited with TM polarized incident field and measured between 2 and 16 GHz and solved using different qualitative methods a) SSM, b) LSM, c) FM

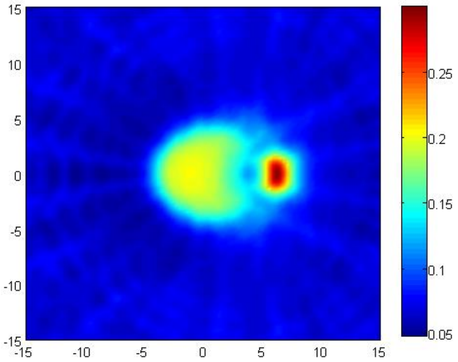

c)

Figure 4.25 (continuous) Multiple frequency reconstructions of a centered foam polyethylene and an off-centered external metal object excited with TM polarized incident field and measured between 2 and 16 GHz and solved using different qualitative methods a) SSM, b) LSM, c) FM

The last setup of the Fresnel database contains a combination of the earlier scatterers as it contains two small dielectric cylinders located inside and next to a larger dielectric scatterer, as shown in Figure 4.26. The inside scatterer is slightly off centered with 5 mm, and the outer cylinder has a distance of 55.5 mm from the center of the coordinate system. The same outcome can be inferred from the single frequency reconstructions with the earlier case, as given in Figure 4.27. On the contrary, the multifrequency results of the three methods given in Figure 4.28. shows inaccurate inversion of the entire object which all of them fail to locate the inner scatterer.

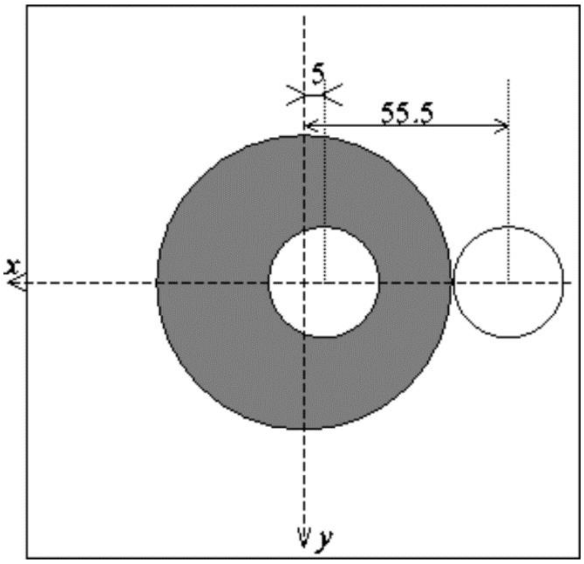

Figure 4.26 Visualization of ‘FoamTwinDielTM’ measurement set of Fresnel Opus 2 experimental data that contains two smaller dielectric objects one located inside of a larger cylindrical foam polyethylene, the other is placed next to foam

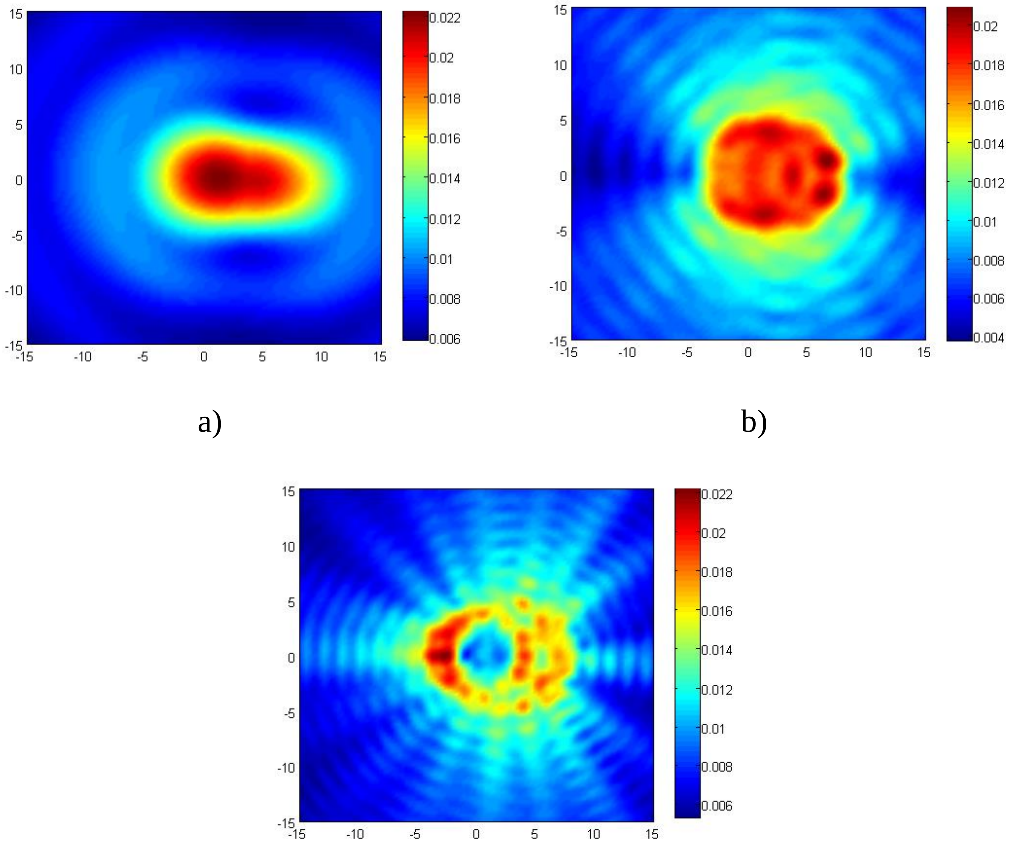

a) b)

c)

Figure 4.27 Single frequency reconstructions of a centered foam polyethylene, off-centered internal dielectric cylinder and an off-centered external dielectric cylinder object excited with TM polarized incident field at a) 2 GHz, b) 6 GHz, c) 10 GHz

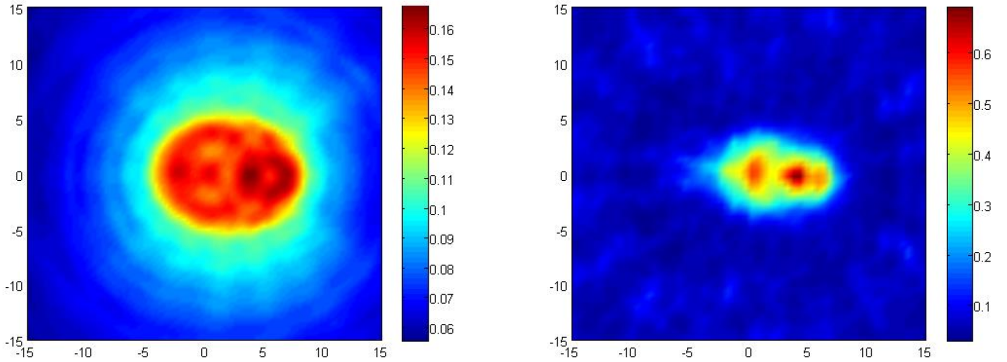

a) b)

Figure 4.28 Multiple frequency reconstructions of a centered foam polyethylene, off-centered internal dielectric cylinder and an off-centered external dielectric cylinder object excited with TM polarized incident field and measured between 2 and 16 GHz and solved using different qualitative methods a) SSM, b) LSM, c) FM

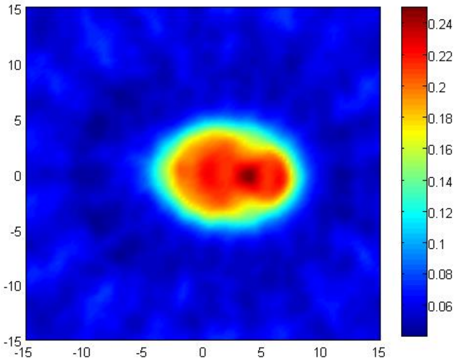

c)

Figure 4.28 (continuous) Multiple frequency reconstructions of a centered foam polyethylene, off-centered internal dielectric cylinder and an off-centered external dielectric cylinder object excited with TM polarized incident field and measured between 2 and 16 GHz and solved using different qualitative methods a) SSM, b) LSM, c) FM

This concludes our discussion on the results produced form the Fresnel database and the near-field (relatively far-field) electromagnetic measurements. In summary, we can say that the algorithm accurately converts the scattered field knowledge to the information of the shape and location of the source as tested against two different, known to be popular qualitative methods. In the following section, we will test our algorithm against the scattering parameter measurements which we will use in later studies if shown to be successful.

4.2 ITU Electromagnetics Research Group Database

Next, we will give some of the results we obtained using bistatic microwave imaging system for measuring S-parameters. In this setup, we used two horn antennas with operational frequencies are between 1-18GHz, a two port vector network analyzer, and rotational equipments to obtain measurements from different points. The antennas are located at a radius R = 85cm from the center and rotated in a circular domain with 15 degrees steps which adds up to 24 different points. All the measurements are made between 1-6GHz with 0.25GHz step size which means 21 different frequencies. The polarizations of the antennas are TM polarizations. The system can be seen in Figure 4.29.

Also, to reduce the unwanted coupling effect of the antennas, the measurements are not conducted where the antennas are too close to each other, more specifically, only 432 of the 576 possible values are used in inversion. The illustration of this is given in Figure 4.29.

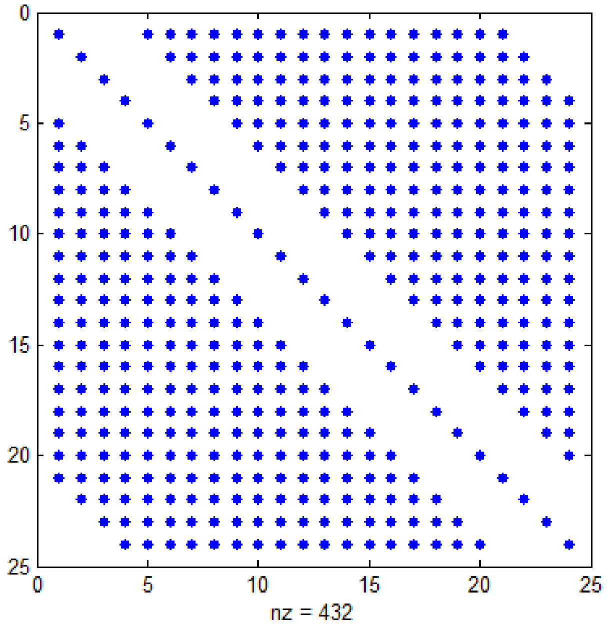

Figure 4.29 The nonzero elements of an S-parameter experimental data

Figure 4.30 Scattering Parameter Measurement System Setup

Before giving the total imaging results obtained for scattering parameter measurements, we should give the insight on the process of SSM used in the entire study. As it is delivered on a mathematical basis, SSM uses a collection of approximation domains to enclose the scattering objects and obtain a meaningful reconstruction. For this purpose, in two dimensional cases, generally smaller cylindrical approximation domains are merged to form a bigger approximation domain which contains the closure of all the scatterers inside of it. These cylidrical domains are rotated around the origin in this case and the backpropagation of the SSM given in (3.18) is solved outside of this domain. This step is repeated for all the rotations of the initial approximation domain and finally all the interested areas are computed in terms of SSM which is finalized by merging the numerical results together to form a reconstructed image which should supposedly produce accurate result in terms of locating the scattering objects. The zeroth approximation G_0 is formed to exclude the origin so that it would not cause a singularity at that point. Since the original formulation in (3.23) is done so that the source point of the G_0 is at the origin, if G_0 would contain the point 0 inside of it, this would actually cause a singularity at that point. A singularity is a bad news if a solution is to be obtained at that point and for this reason, it should be avoided in some way. By slightly shifting the domain in the desired way away from the center, we accomplish this goal and eliminate the singularity at the origin. Figure 4.31 shows the first case of the results obtained using single approximation domain. The scattering objects are two dielectrical cylindrical objects with $\varepsilon_r \cong 2$, their locations are denoted by thin dashed lines in the images. The approximation domains used are shown by thick dashed lines and differs in the images. The reconstructions are obtained for four approximation domains rotated 90° from each other in each repetition. The second case is two Perfectly Electric Conducting (PEC) objects off-centered as in the first case. Same setup is used to obtain the reconstructions and given in Figure 4.32. As it can be observed in both figures, complying with the earlier statements, the inside of the G is not solvable thus does not contain solution inside of it. Even though it is vague, we can see the traces of the scattering objects around of G which proposedly gives the accurate locations and shapes of these objects when merged. The final results of these objects are obtained for 100 rotations of the initial approximation domain G_0 as it is done for all of the measurements throughout the study. We have determined with a numerical analysis that 100 rotations are sufficient enough to obtain high resolution from the reconstructions while increasing this value to the level of 200 causes burden to computers in terms of memory and processing time. We will continue with the total reconstruction results of the scattering parameter measurements.

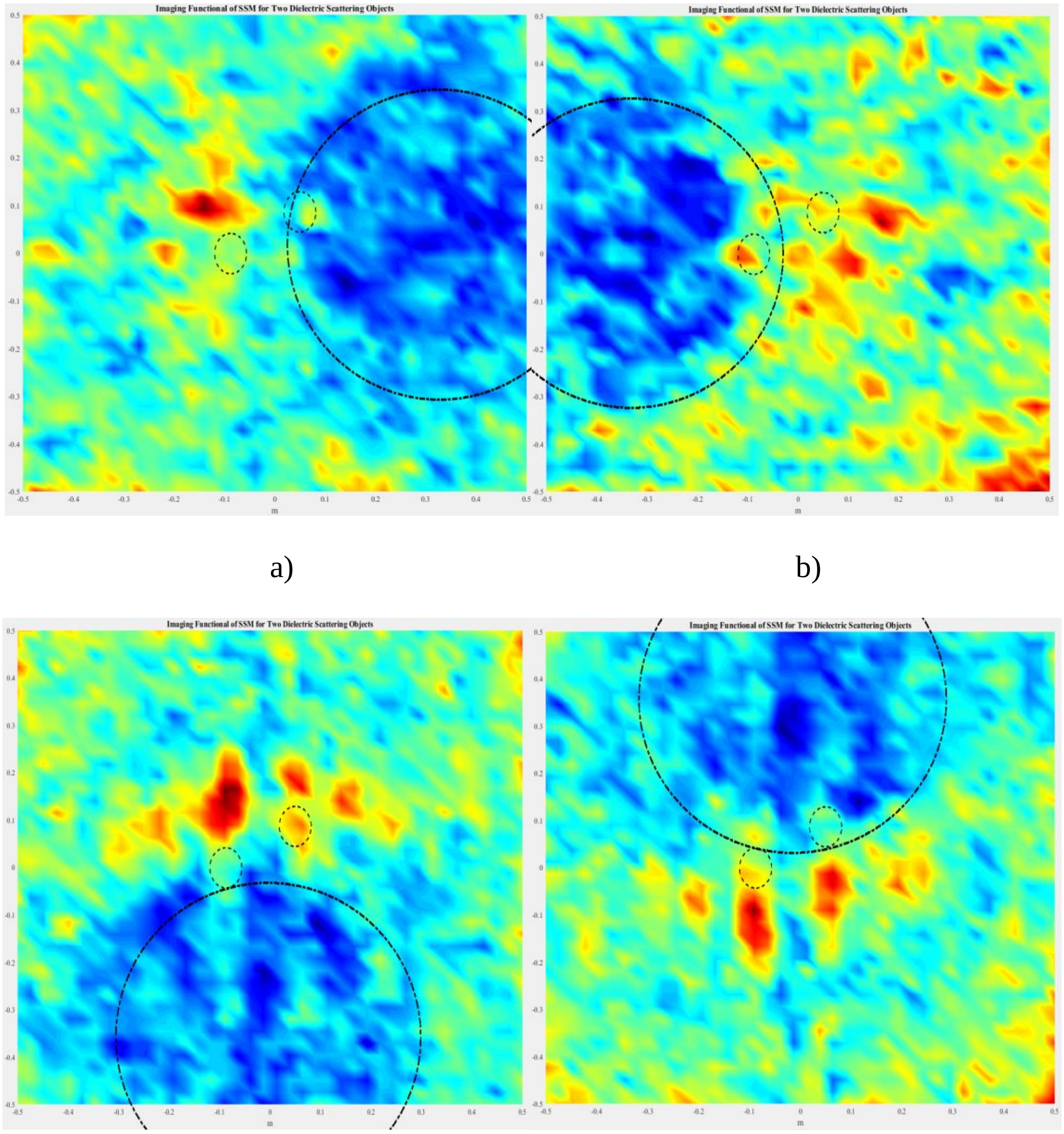

a) b)

c) d)

Figure 4.31 Imaging function I(z) of SSM for two dielectric scattering objects with R=0.85m under different approximation domains with radius 0.3m a) G(x)=0.3× (cosθ +1.05, sinθ), b) G(x)=0.3×(cosθ -1.05, sinθ), c) G(x)=0.3×(cosθ, sinθ +1.05), d) G(x)=0.3×(cosθ, sinθ -1.05).

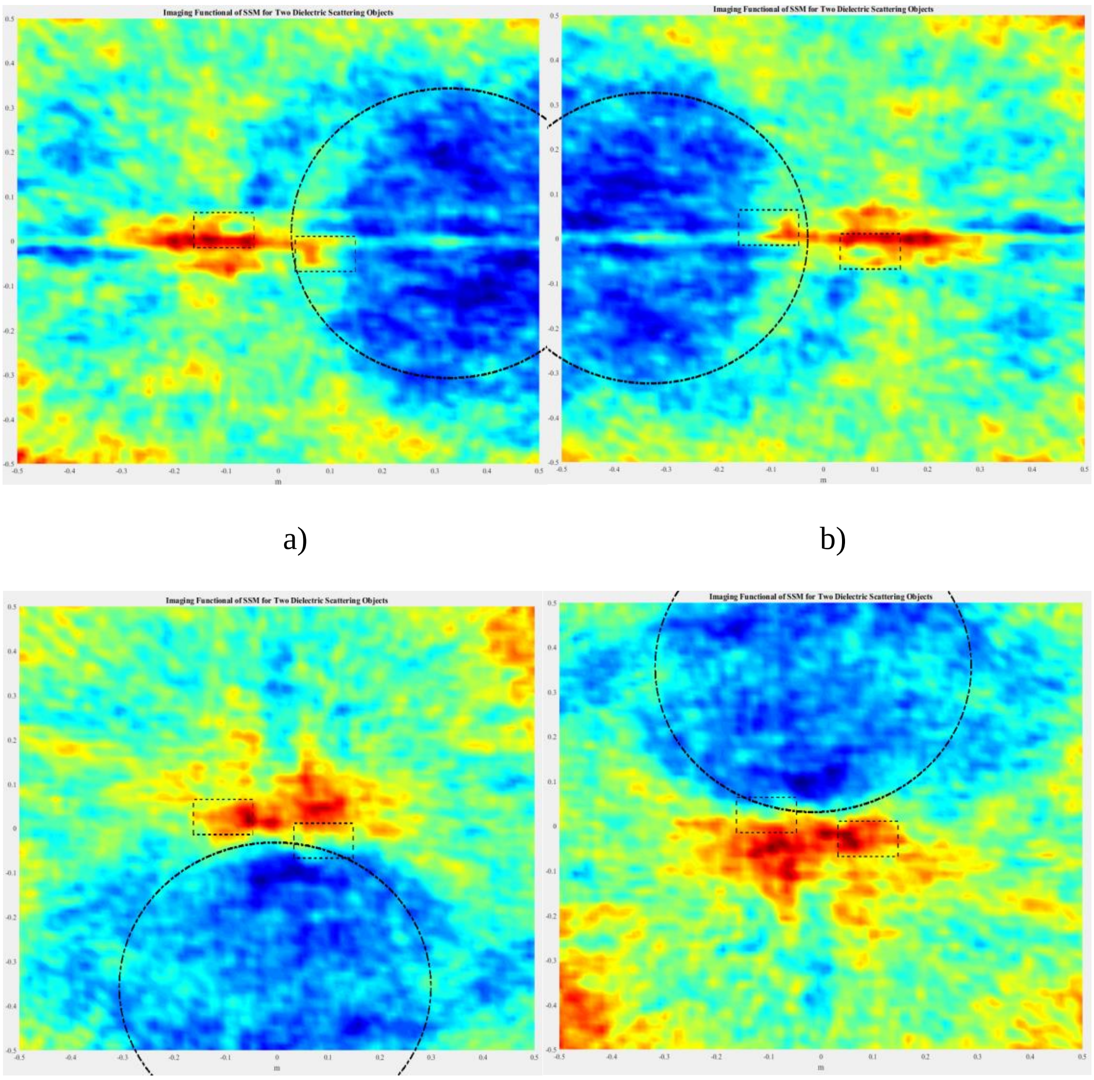

a) b)

c) d)

Figure 4.32 Imaging function I(z) of SSM for two PEC scattering objects with R=0.85m under different approximation domains with radius 0.3m, a) G(x)=0.3×(cosθ +1.05, sinθ), b) G(x)=0.3×(cosθ -1.05, sinθ), c) G(x)=0.3×(cosθ, sinθ +1.05), d) G(x)=0.3×(cosθ, sinθ -1.05).

The first setup involves the measurement of a centered conducting object, namely a rectangular PEC object which is hollow inside. The size of the object is given as (10,6) cm and the height is approximately 60 cm which we assume to be infinite since the reconstructions will be two dimensional. The thickness of the shell is sufficiently thick that no field can be induced inside of the object through an outer interference. Thus, we should consider this rectangular object as a solid block that contains no hollow parts in itself. Figure 4.33 shows the single frequency reconstructions of this centered object at different frequencies between 0.8 GHz and 4.8 GHz with 0.8 GHz intervals.

This collection of MATLAB figures shows clearly that as the frequency of the measurement increases, the sharpness of the image also increases. With efficient measurements, it is possible to get more detailed information on the scatterer. On the other hand, as we observe in this set of data, it is also possible to scatter all the valuable information away with noise.

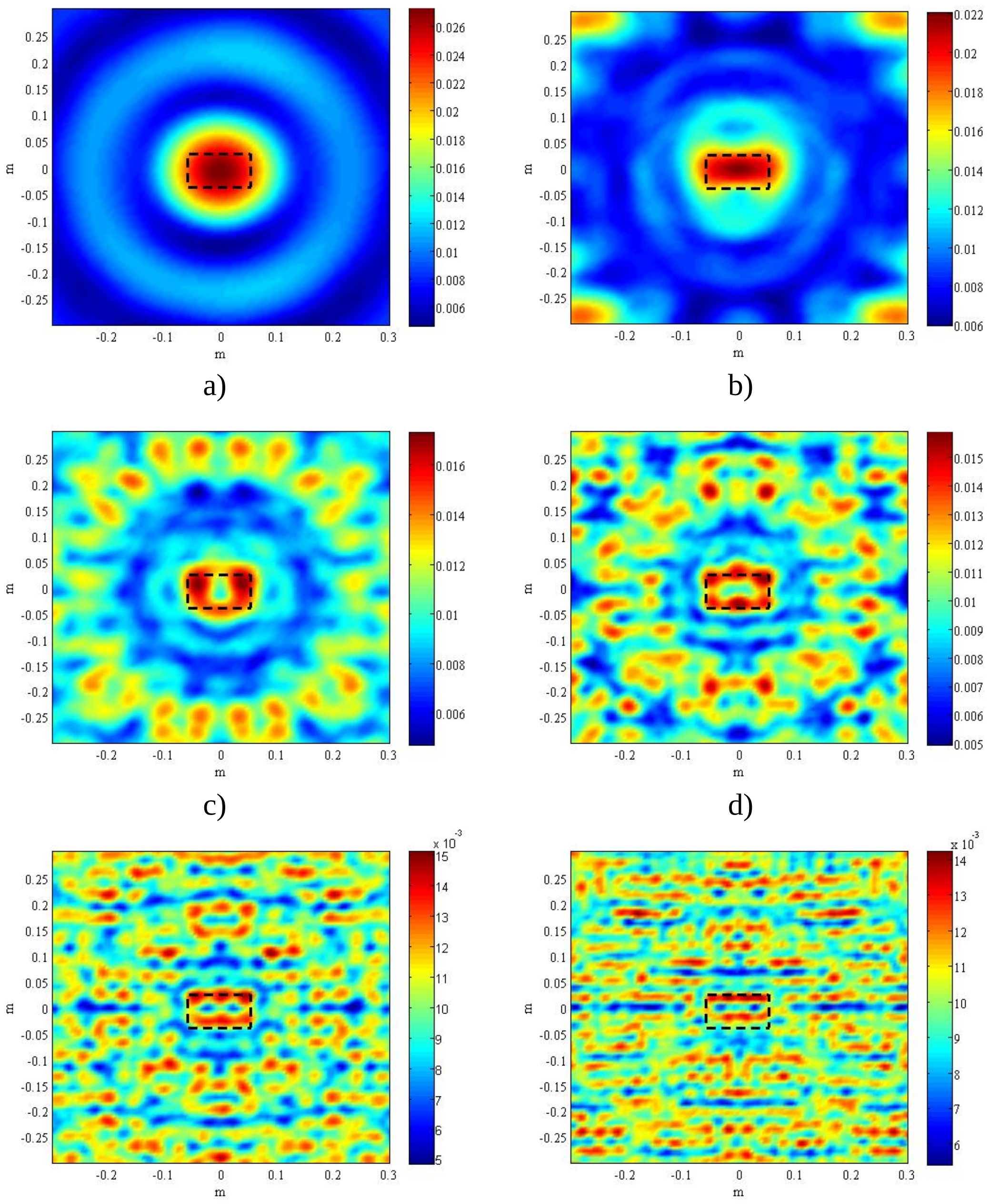

a) b)

c) d)

e) f)

Figure 4.33 Single frequency inversions of a centered PEC object at frequencies a) 0.8 GHz, b) 1.6 GHz, c) 2.4 GHz, d) 3.2 GHz, e) 4 GHz, f) 4.8 GHz.

Since the implementation of the multifrequency concept is fairly simple as it is proposed in the third section with three different methodology, we will apply this configuration also to the scattering parameter measurements. Figure 4.34 is the result of a series of reconstruction through the multifrequency scheme and the positive effects of the addition can be observed clearly. The detail of the increases with the number of added frequencies to the total result, as a cost, the noise in the image also becomes significant. To understand the effect of the frequency comprehensively, we should also compare the reconstruction in the higher frequencies and the lower frequencies.

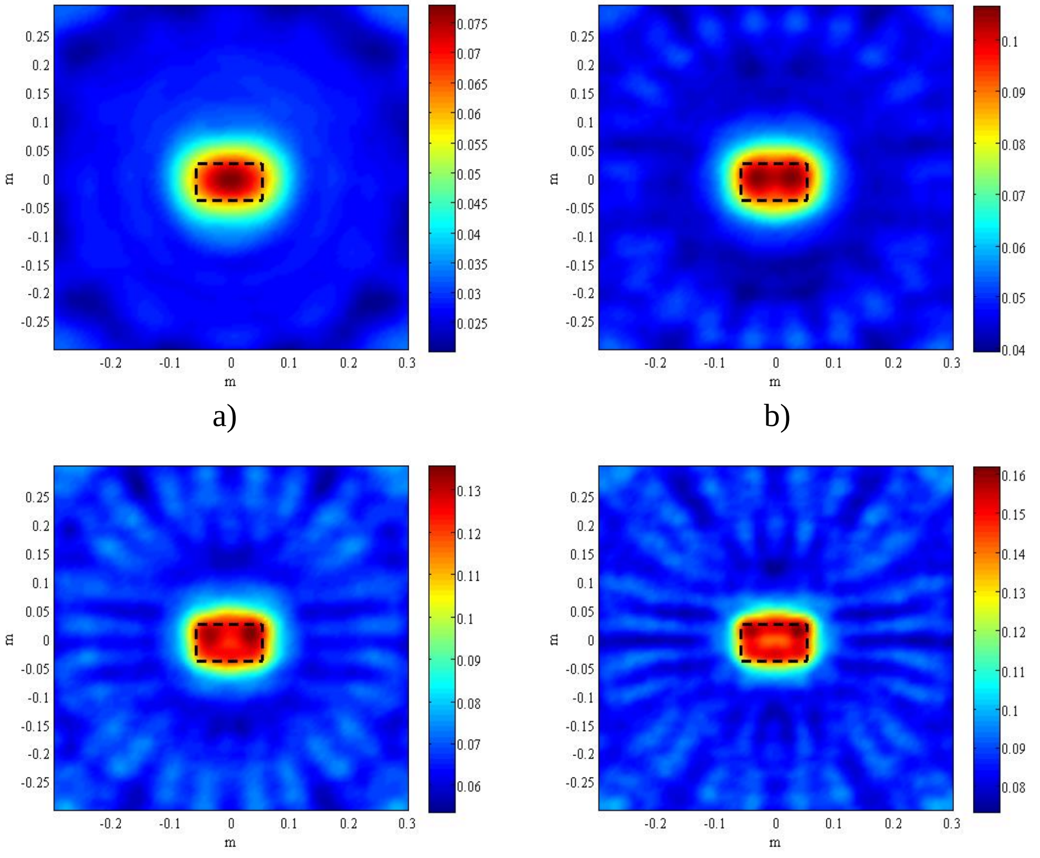

a) b)

c) d)

Figure 4.34 Multiple frequency inversions of a centered PEC object, between frequencies a) 0.8-1.6 GHz, b) 0.8-2.4 GHz, c) 0.8-3.2 GHz, d) 0.8-4 GHz, e) 0.8-5.2 GHz

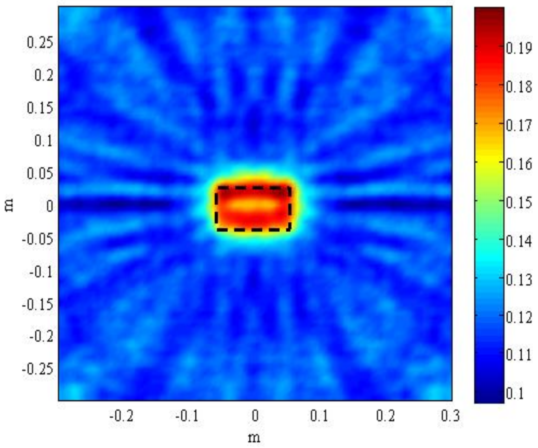

e)

Figure 4.34 (continuous) Multiple frequency inversions of a centered PEC object, between frequencies a) 0.8-1.6 GHz, b) 0.8-2.4 GHz, c) 0.8-3.2 GHz, d) 0.8-4 GHz, e) 0.8-5.2 GHz

Figure 4.35 shows such a result which consists of three different images obtained from variable frequencies. First image is the imaging functional obtained through the summation of the reconstructions at 0.8 GHz, 1.2 GHz and 1.6 GHz. Second image is obtained from the medium frequencies of the measurement which are 2.4 GHz, 2.8 GHz, 3.2 GHz, 3.6 GHz and 4 GHz. The last one on the other hand is a higher frequency reconstruction as it uses frequencies 4 GHz, 4.4 GHz, 4.8 GHz and 5.2 GHz to form the total result. It is clear as day that the higher frequencies are overwhelmed by the noise in the measurement as they can only provide small discrimination of the object from the background medium. Thus, it is justifiable to state that the higher frequencies does not provide positive effects to the outcome in this setup which is contradictory with the Fresnel data. A conclusion about the most effective frequencies for the method cannot be made since the effectiveness of the measurement does not only depend on the inversion method’s capability of using that frequency but the effectiveness of the measurement system at that frequency as well. And we observe that the high frequency results in this far-field setup are rather noisy compared to the Fresnel setup. We will provide one more comparison between high and low frequencies in the rest of the results section to verify the results discussed here.

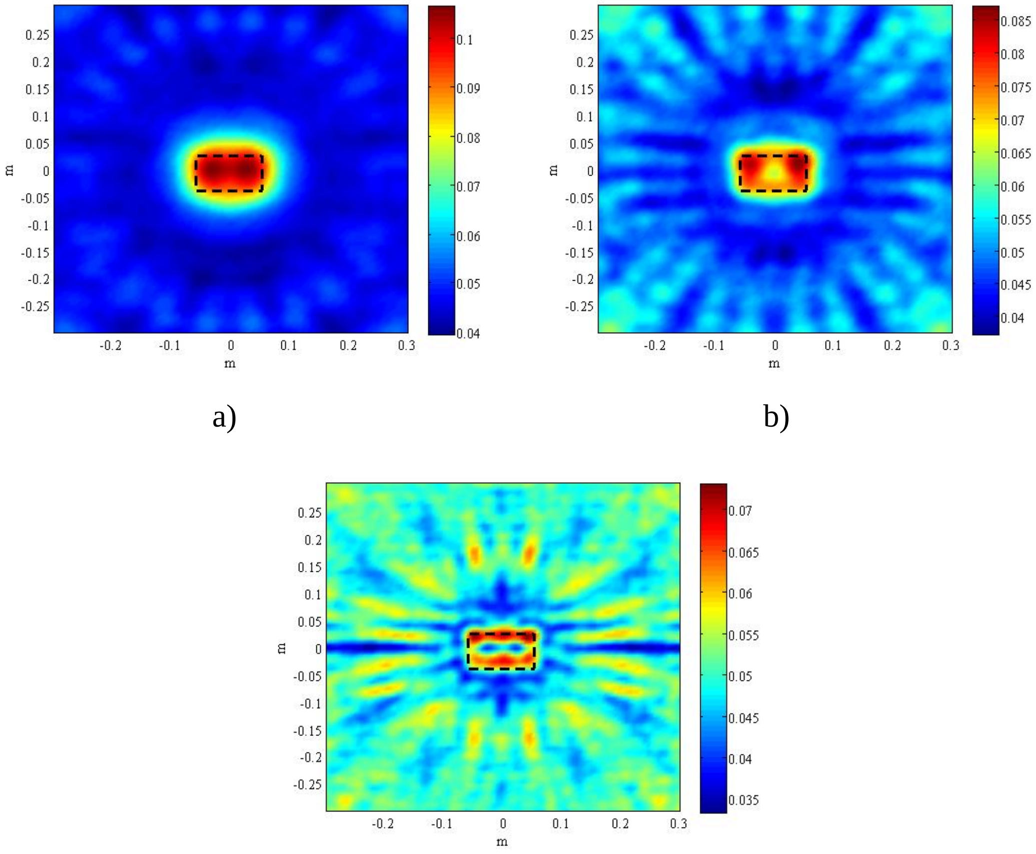

a) b)

c)

Figure 4.35 Comparison of higher and lower multiple frequency inversions of a centered PEC object between frequencies a) 0.8-1.6 GHz, b) 2.4-4 GHz, c) 4-5.2 GHz

Next discussion will be made on the proposed frequency merging techniques. Figure 4.36 shows the reconstructions obtained using these algorithms which are obtained by merging all the measured frequencies (between 0.8 GHz and 5.2 GHz) by the given methods. First image is the direct summation obtained without normalizing the original results. This result contains small error component compared to the others, but it also contains less information about the object as well. Second image is the normalized summation of frequencies, which obtains more noise along with more information. Third merging method is the weighted summation, which has lower performance in this case. This is caused by the conversion of the original result to a binary one through k-means algorithm as explained, which erroneously converts the noise in the image and then the normalization increases its level, which affects the total outcome.

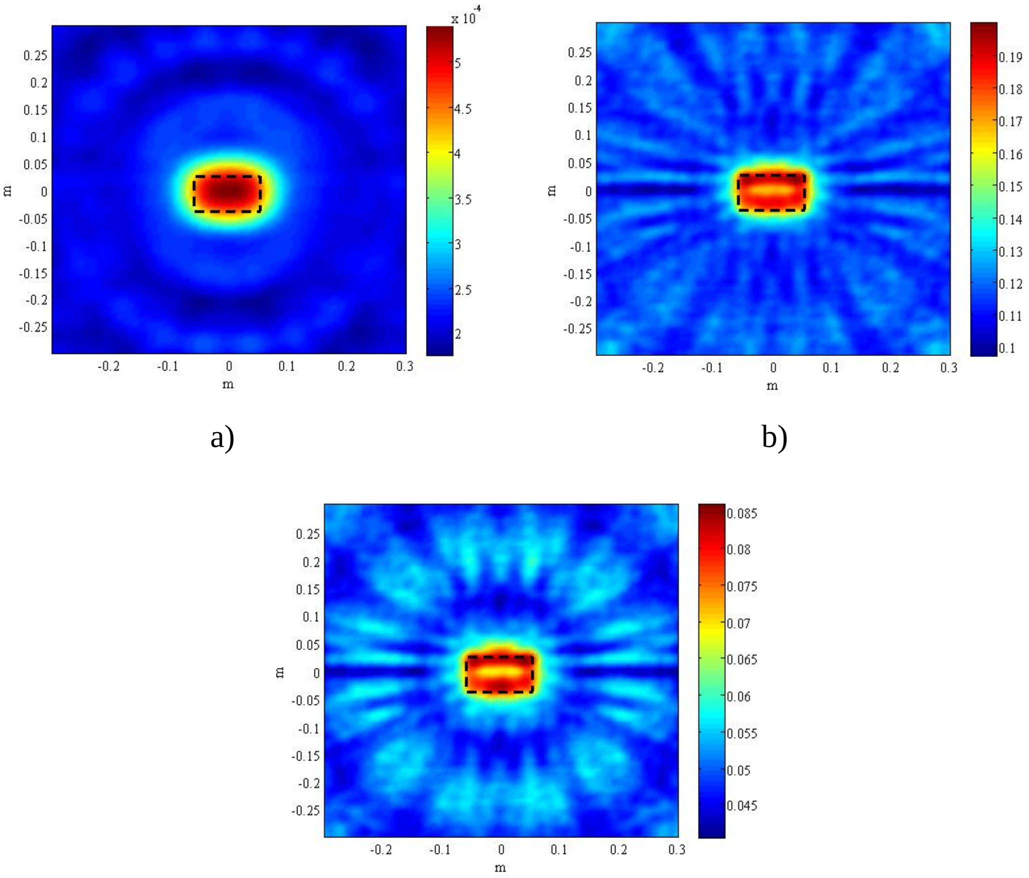

a) b)

c)

Figure 4.36 Comparison of different multifrequency merge approaches of a centered PEC object a) direct summation, b) normalized summation, c) weighted summation results obtained between 0.8 GHz and 5.2 GHz

The last inversions are made for the comparison of the qualitative methods as in the Fresnel data results and similarly, the results shows the same characteristics as the earlier cases in Figure 4.37. SSM contains the most information about the object and highest image error, and the LSM is the exact opposite. FM is more accurate as it contains information closer to SSM and error closer to LSM. But more interesting topic is how to apply a cut-off value to these images what would be the result. If the cut-off value for the object is chosen to be the points where the value of the reconstructed image is considerably higher (red in this coloring technique), it is obvious that SSM will overcome the other methods as the noise will cancel out. On the other hand, the result of SSM will be beaten if an intermediate value is selected as cut-off. The SSM will simply oversize the actual object and the details obtained will be destroyed.

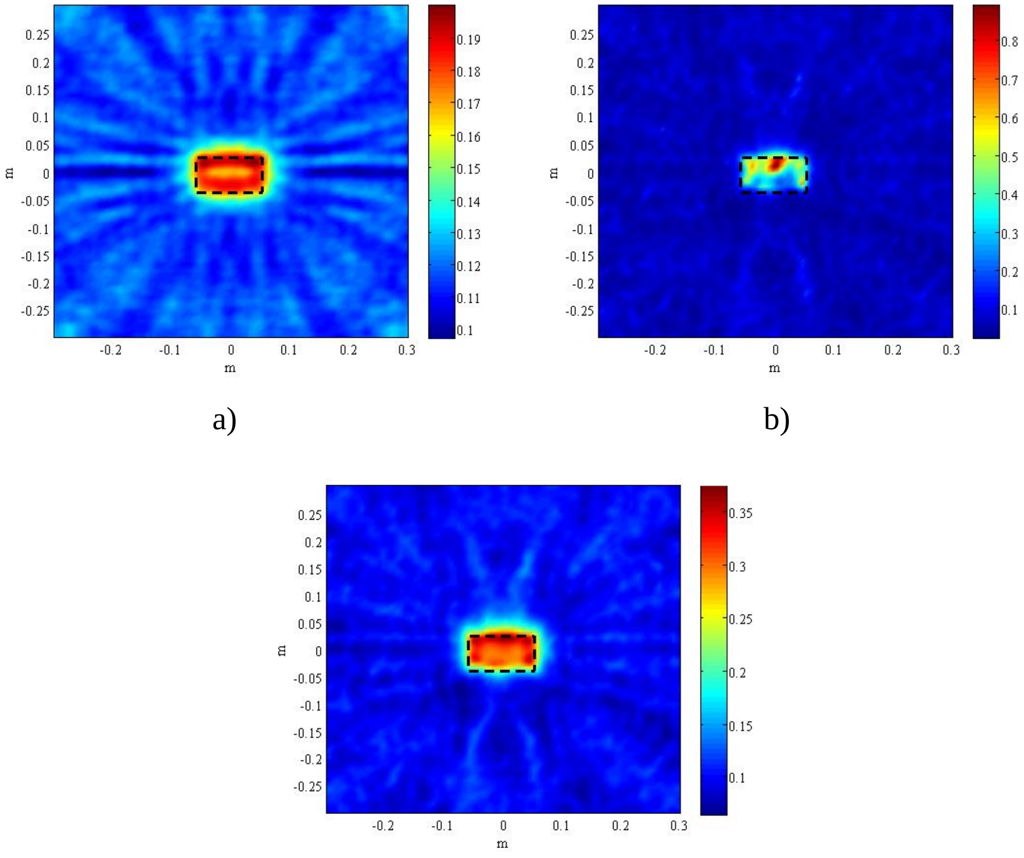

a)

b)

c)

Figure 4.37 Centered PEC object, reconstructed using multiple frequency scheme and compared in terms of qualitative microwave imaging methods a) SSM, b) LSM, c) FM

Since the accuracy of the method is tested and compared with the other methods, we now move on with the second scattering object configuration in the same measurement setup. This time, there are two dielectric cylinders which are both off-centered where the objects are located at (-10,0) cm and (5,10) cm with 6 cm radius, respectively. Measurements are made at 21 frequencies between 1 GHz and 6 GHz with a regular interval of 250 MHz. Figure 4.38 shows the single frequency reconstructions obtained through the inversion of data between 1 GHz and 6 GHz with 1 GHz intervals. The results obtained from higher frequencies 4, 5 and GHz are quite disturbing for the sake of this study as they do not contain a discriminative information about the scatterers whatsoever. Yet, there is an explanation about these results. Unlike PEC objects, dielectric objects absorbs some of the incident field and does not directly scatter all the field. Thus, the scattering from the dielectric objects will be smaller than the PEC objects. This, combined with the higher noise caused from this measurement setup, can be explosive in terms of the effectiveness and the quality of the results. Other than that, the images are as expected as they become sharper but erroneous as the frequency increases.

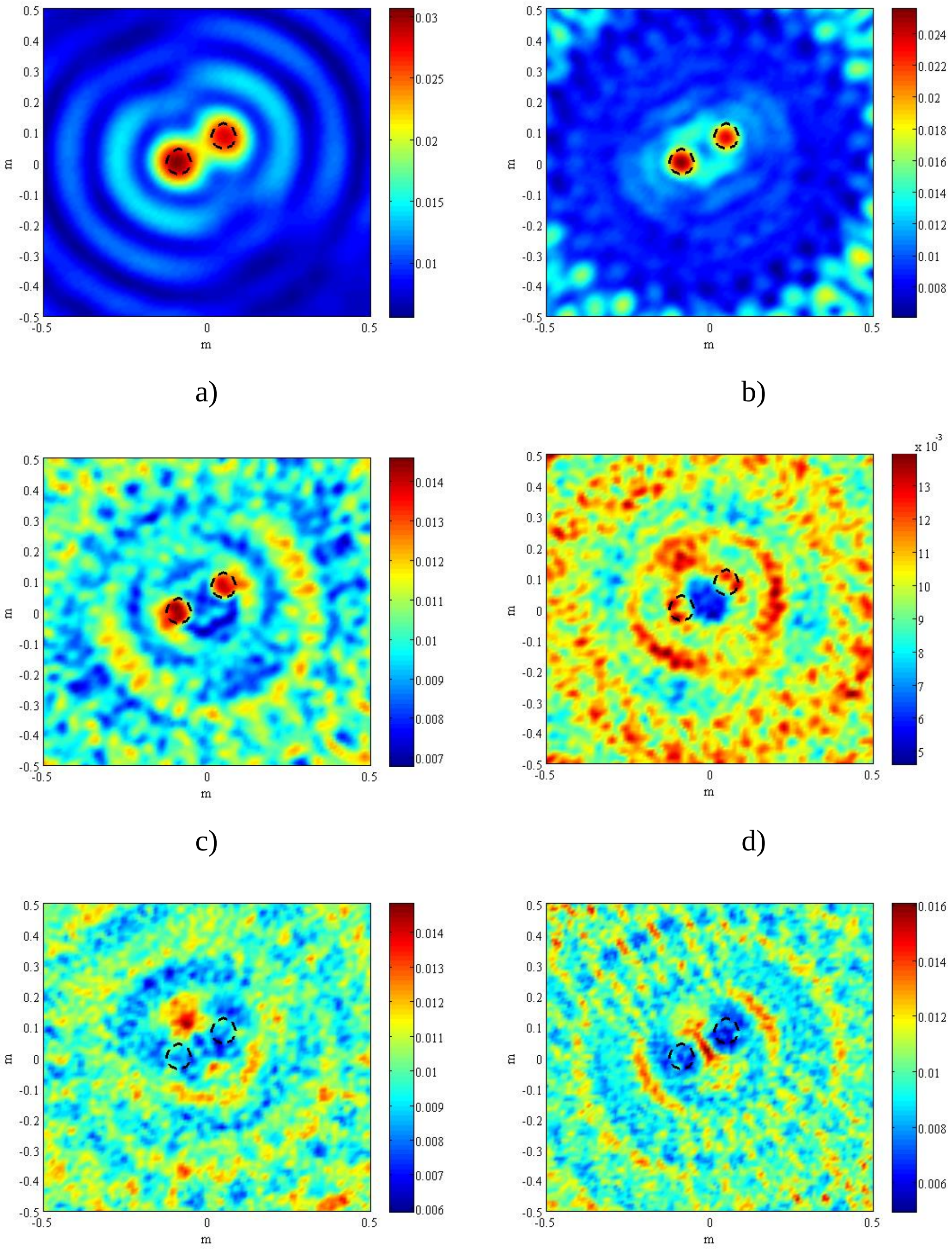

a) b)

c) d)

e) f)

Figure 4.38 Single frequency inversions of two off-centered cylindrical dielectric objects at frequencies a) 1 GHz, b) 2 GHz, c) 3 GHz, d) 4 GHz, e) 5 GHz, f) 6 GHz.

Multifrequency results obtained with normalized summation is provided in Figure 4.39. The multiscattering level is decreased between the objects as the frequency increases, which can be explained as the scattered field from one object and incident to another. The result is more erroneous with the increase of frequency as usual.

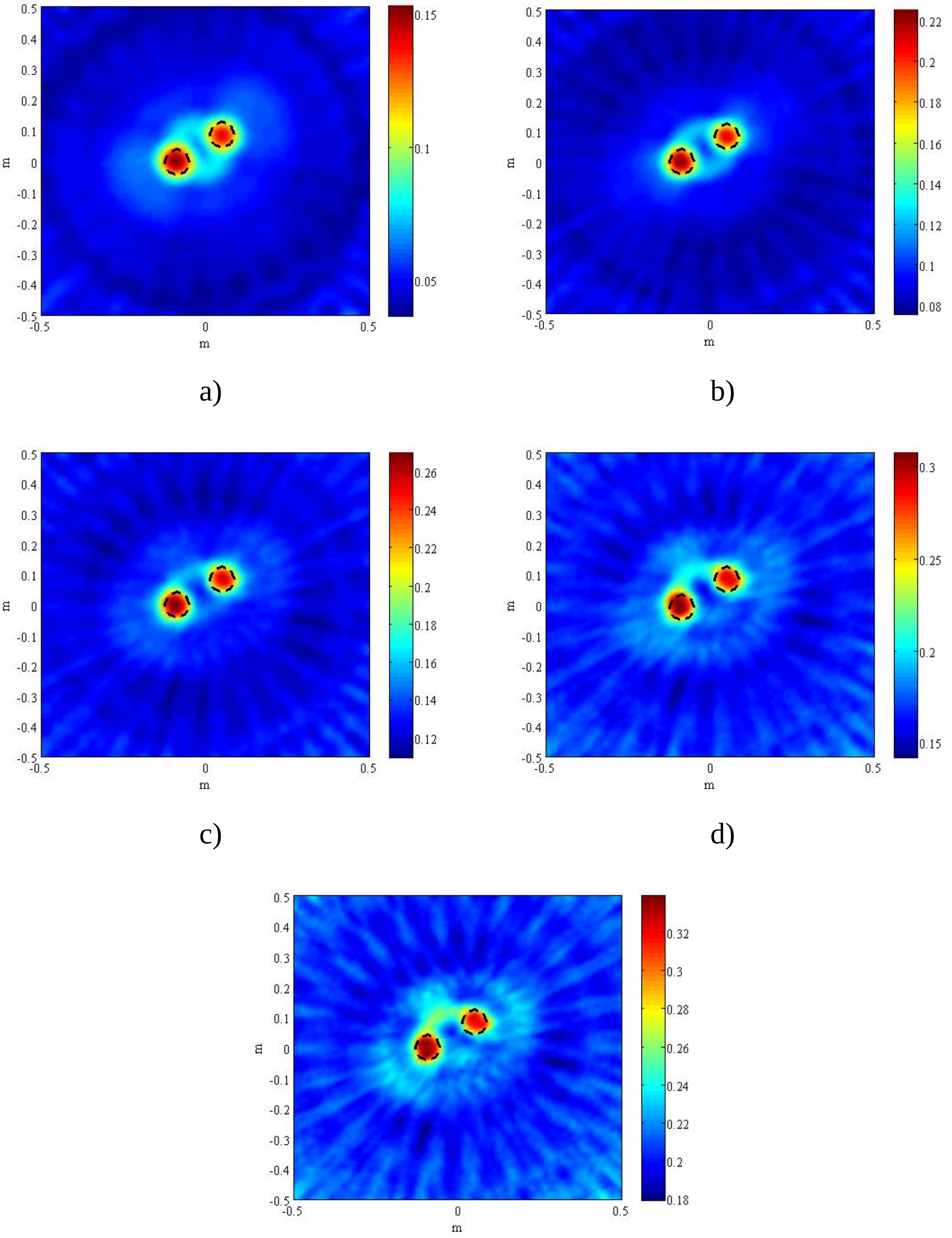

a)

b)

c)

d)

e)

Figure 4.39 Multiple frequency inversions of two off-centered dielectric objects between frequencies a) 1-2 GHz, b) 1-3 GHz, c) 1-4 GHz, d) 1-5 GHz, e) 1-6 GHz

We provide another high-low frequency comparison which is necessary to come to a conclusion. The results obtained from three frequency range is given below in Figure 4.40. First image shows the summation reconstructions between 1 GHz and 3 GHz, second gives the middle frequencies between 2 GHz and 4 GHz, and the third is obtained from the data between 4 GHz and 6 GHz. Similar, even more obvious that the results obtained from higher frequencies becomes completely invaluable with the level of noise contained in the measurement. In terms of reconstructing the object itself, 2 and 4 GHz range is the most successful, yet they contain a significant amount of noise which can effect the total outcome with a more complex medium from the current case.

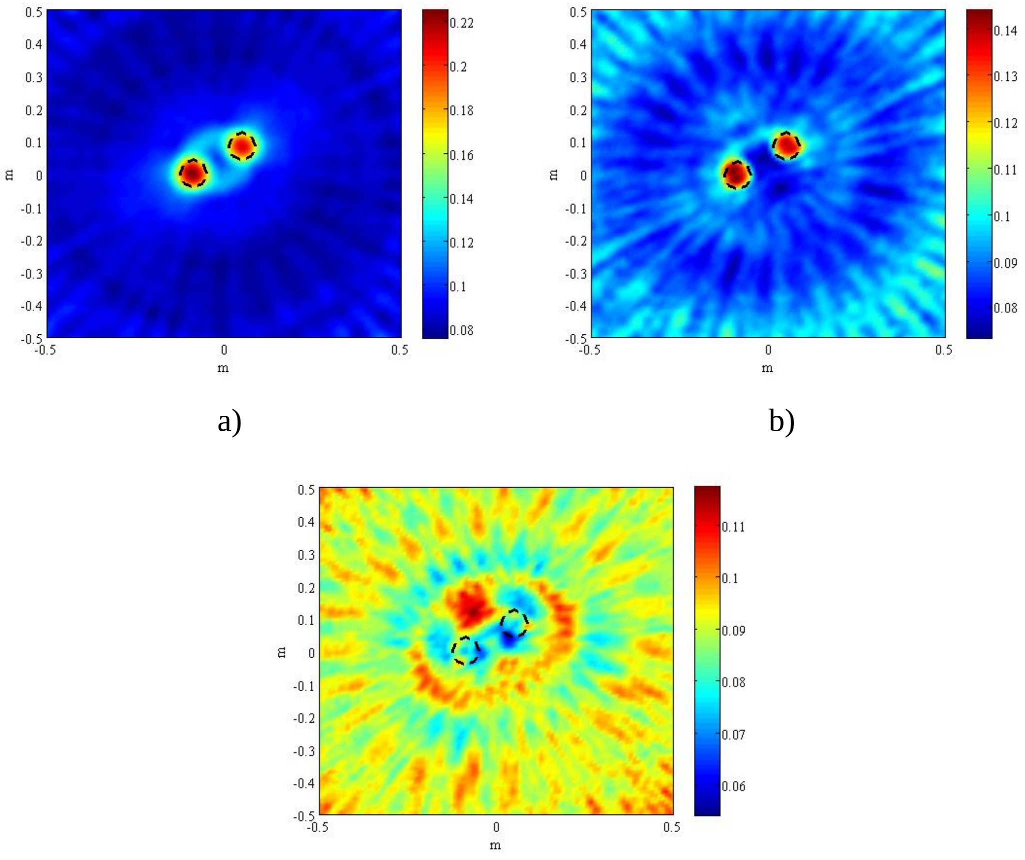

a) b)

c)

Figure 4.40 Comparison of higher and lower multiple frequency inversions of two off-centered cylindrical dielectric objects between frequencies a) 1-3 GHz, b) 2-4 GHz, c) 4-6 GHz

Multifrequency scheme comparison for this case is given in Figure 4.41. According to this result, similar outcome can be observed with the earlier case that the highest reconstruction quality can be achieved through direct summation, but the numerical outcome of the two normalization based summation method are more promising if a extension to these methods to suppress the outside noise can be proposed.

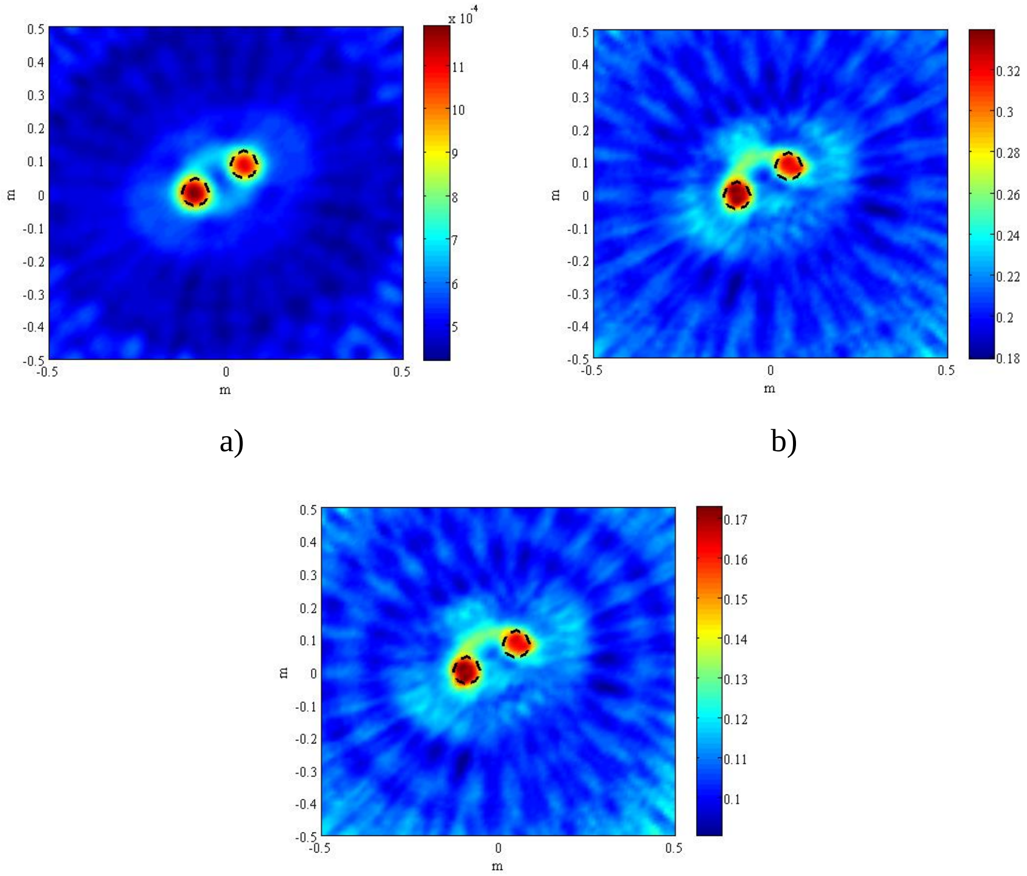

a) b)

c)

Figure 4.41 Comparison of different multifrequency merge approaches of two off-centered dielectric objects a) direct summation, b) normalized summation, c) weighted summation results obtained between 1 GHz and 6 GHz

We conclude the two dielectric cylindrical object case with the comparison of SSM, LSM and FM, as usual. The results for this purpose are obtained and given in Figure 4.42 below. The LSM diminishes the objects when suppressing noise to a size that the objects seen in the reconstructions are quite smaller than the actual ones. However, the interesting and unusual result is actually obtained from FM algorithm. The result contains a significant amount of noise (more than SSM) which decreases the quality of the result which is an occurance specific for this case. Most accurate result is obtained using SSM in this case which has substantial quality in terms of reconstructing the shape and location of the objects. With this comparison, we finish our discussion about the dielectric cylinder case. It is now appropriate to continue with the two off-centered PEC object case which should also be beneficial to our study, to observe the effects of the multiscattering between the scatterers.

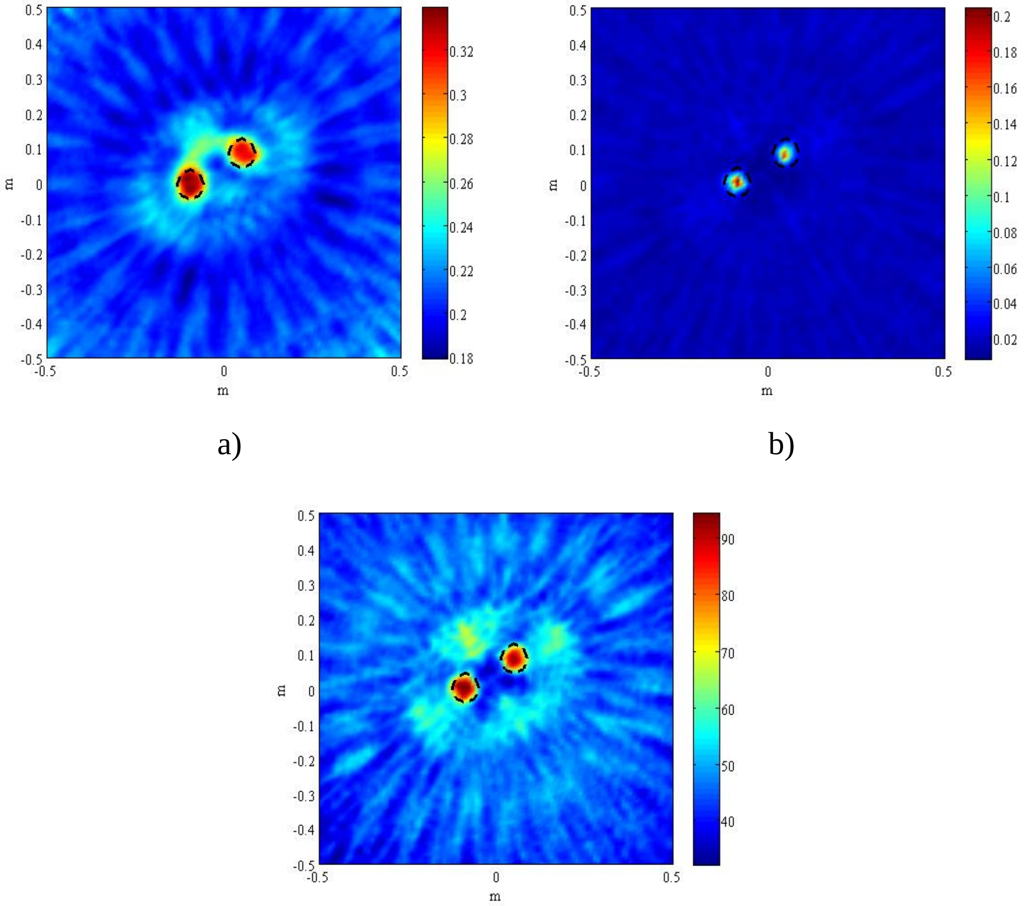

a) b)

c)

Figure 4.42 Two off-centered cylindrical dielectric objects, reconstructed using multiple frequency scheme and compared in terms of qualitative microwave imaging methods a) SSM, b) LSM, c) FM between frequencies 1 GHz and 6 GHz

The two PEC object case was introduced back then when we were trying to demonstrate the basic processes of SSM. Here, we will give a detailed discussion about this case along with the full measurement results in two dimensions. Figure 4.43 shows the single frequency reconstructions. The objects are located off-centered where their centers are at (-10,3) cm and (10,-3) cm, respectively. The long side of each object are measured to be 10 cm while the short sides are 6 cm. The actual places of the objects are shown with the dashed lines similar to earlier cases. According to the reconstructions, we can possibly say that since the objects are relatively large (10x6) cm, we obtain better resolution around 1-2 GHz, while the higher frequencies causes tremendous amount of distortion due to noise. The higher frequencies however, produces better results compared to dielectric cases because of the scattering properties of PEC objects. Since the incident field cannot be contained inside of PEC objects, considerably higher portion of the incident field will scatterer and collected by the receiving antennas which allows us to obtain more information. Even at the 5 GHz and 6 GHz, a trace of the scatterers can be observed in the images.

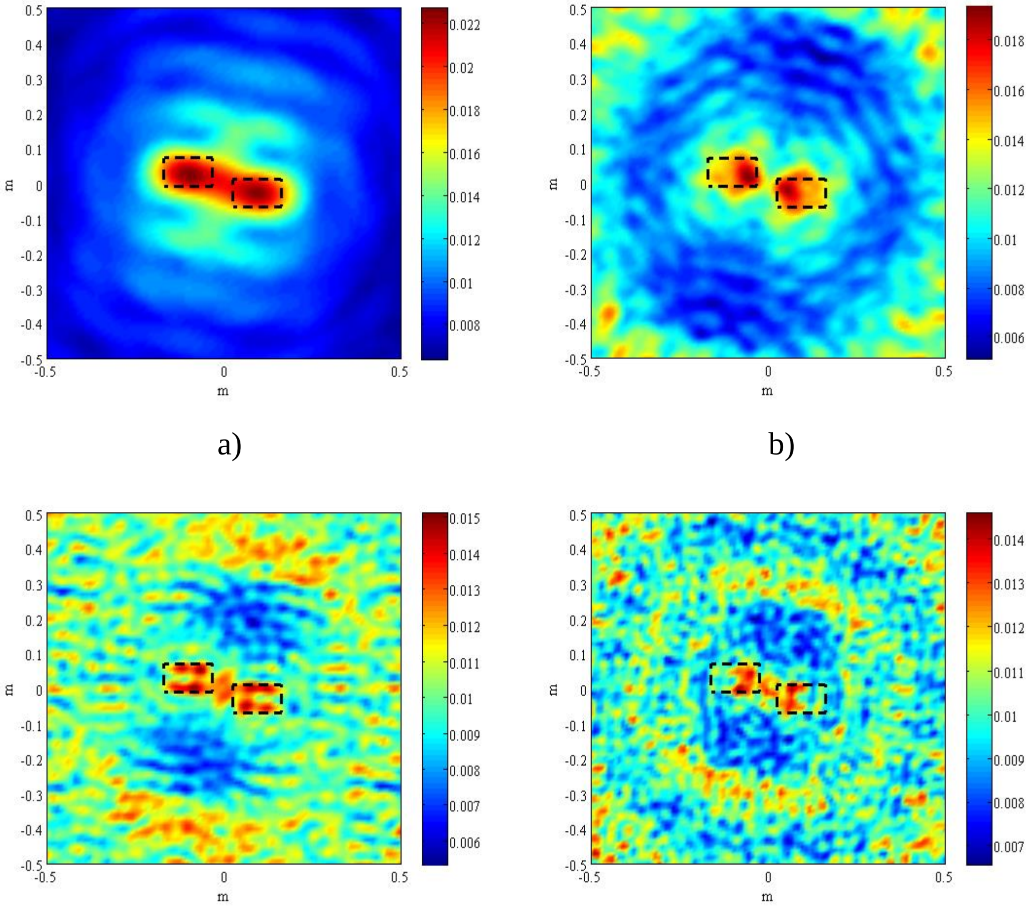

a) b)

c) d)

Figure 4.43 Single frequency inversions of two off-centered rectangular PEC objects at frequencies a) 1 GHz, b) 2 GHz, c) 3 GHz, d) 4 GHz, e) 5 GHz, f) 6 GHz

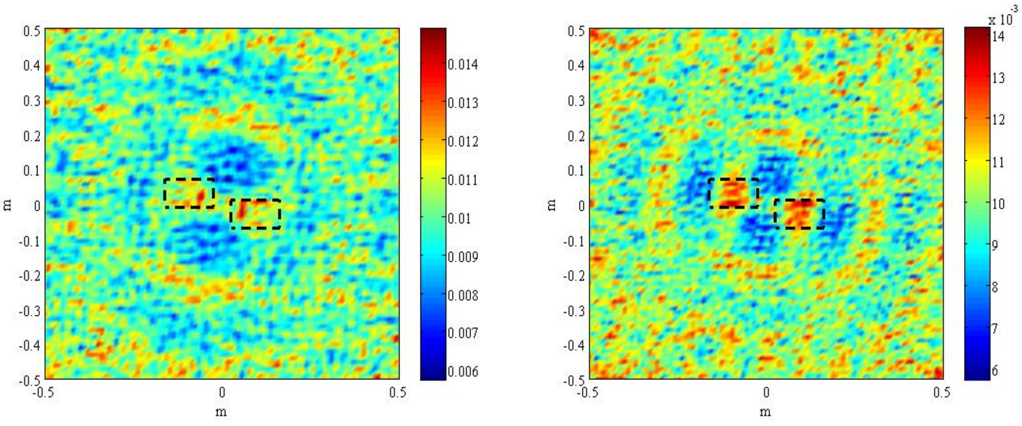

e) f)

Figure 4.43 (continuous) Single frequency inversions of two off-centered rectangular PEC objects at frequencies a) 1 GHz, b) 2 GHz, c) 3 GHz, d) 4 GHz, e) 5 GHz, f) 6 GHz

Multifrequency results are formed in the same frequencies with the two dielectric scatterer setup and given in Figure 4.44. With an accurate cut-off value, the summation of frequencies between 1 and 3 GHz tend to produce the most proper outcome. As in the earlier cases, the increase in frequency sharpens the image and adds more detail to the reconstructed object.

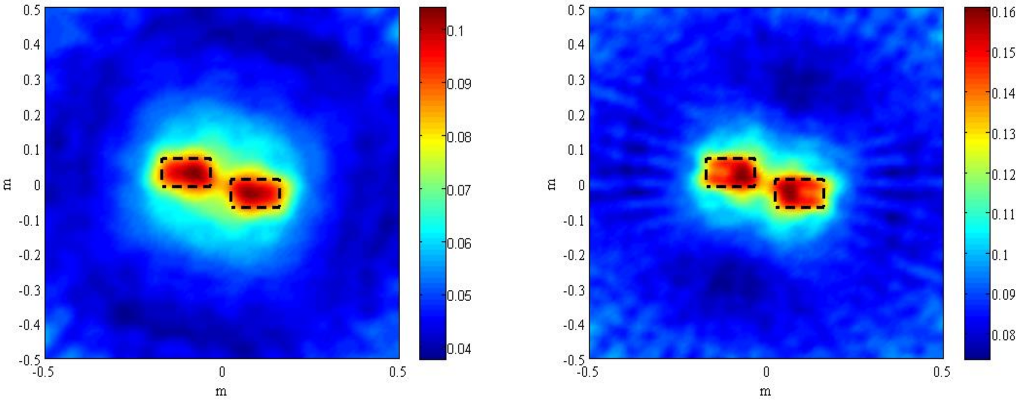

a) b)

Figure 4.44 Multiple frequency inversions of two off-centered rectangular metallic objects between frequencies a) 1-2 GHz, b) 1-3 GHz, c) 1-4 GHz, d) 1-5 GHz, e) 1-6 GHz GHz

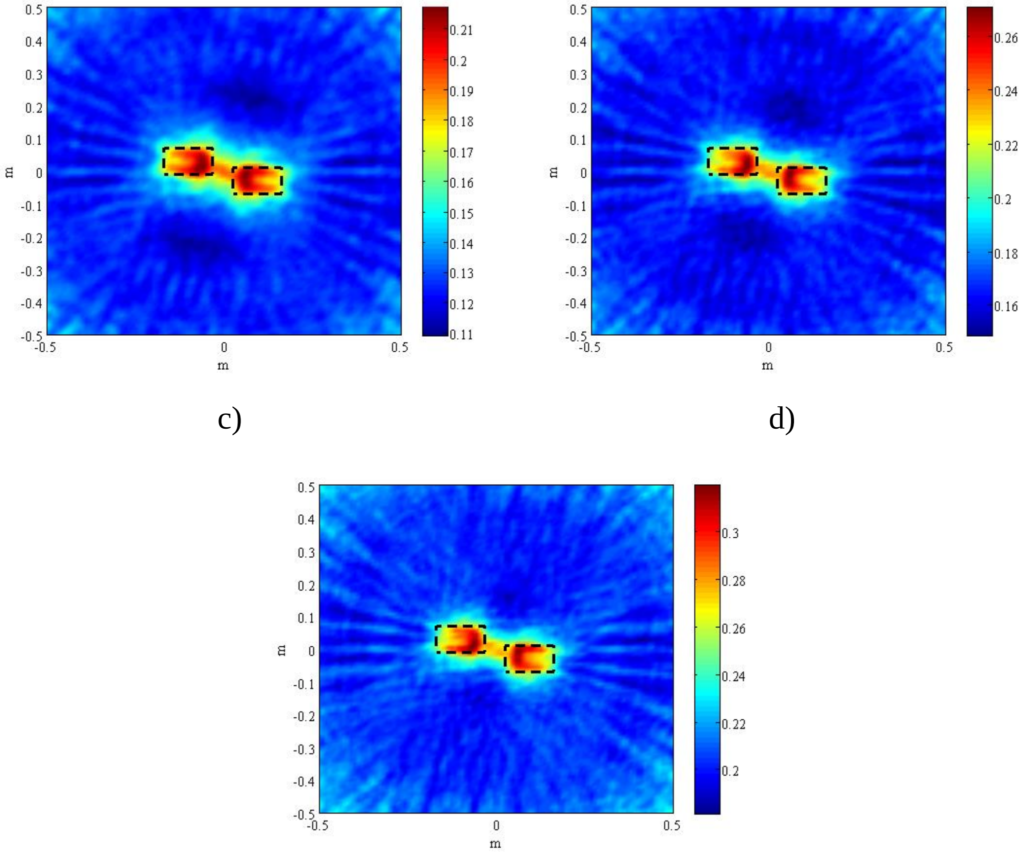

c) d)

e)

Figure 4.44 (continuous) Multiple frequency inversions of two off-centered rectangular metallic objects between frequencies a) 1-2 GHz, b) 1-3 GHz, c) 1-4 GHz, d) 1-5 GHz, e) 1-6 GHz GHz

The comparison of summation methods and qualitative inversion methods are provided in Figure 4.45 and Figure 4.46, respectively. For this case, the most robust merging algorithm is the direct summation as it resembles the result obtained from the merging of frequencies between 1 and 3 GHz in normalized summation. As for the comparison of LSM, FM and SSM, in terms of detail about the scattering objects, FM has the edge, while the LSM leads as usual in terms of suppressing the noise. SSM however needs a denoising or a cut-off process to compete with other methods. With these deductions, we can continue with a new case where we try to separate an inner object inside another using SSM which we have failed to do so in Opus 2 measurements of the Fresnel setup.

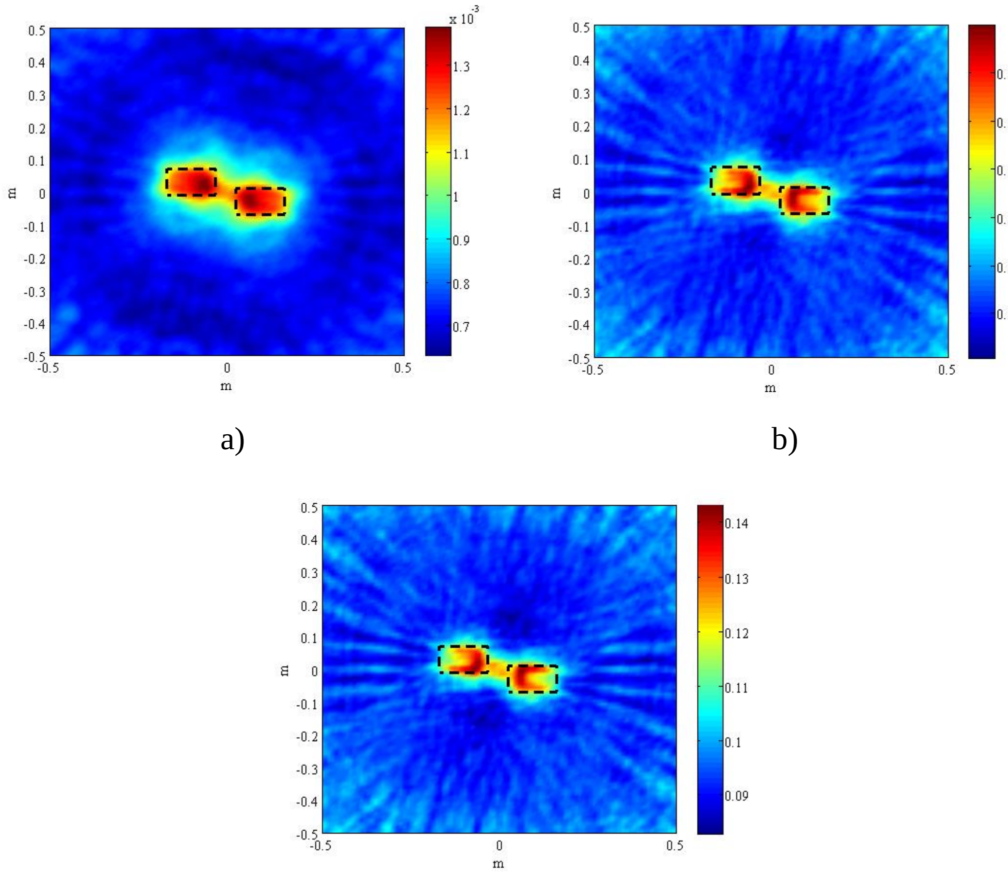

a) b)

c)

Figure 4.45 Comparison of different multifrequency merge approaches of two off-centered rectangular metallic objects a) direct summation, b) normalized summation, c) weighted summation results obtained between 1 GHz and 6 GHz

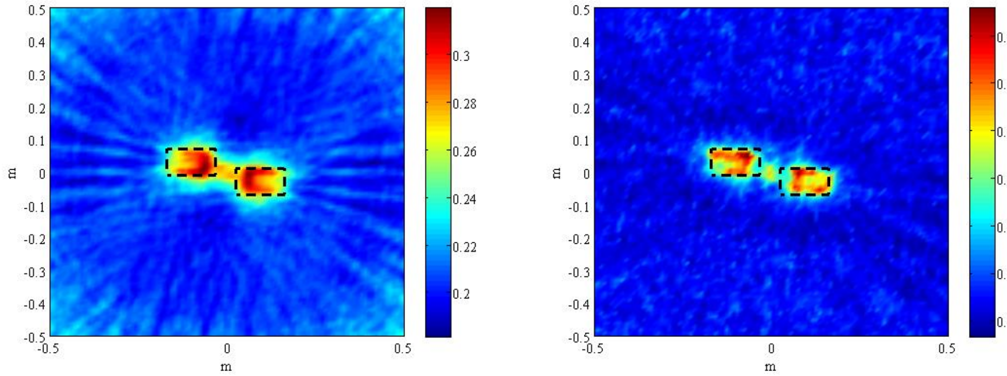

a) b)

Figure 4.46 Two off-centered rectangular PEC objects, reconstructed using multiple frequency scheme and compared in terms of qualitative microwave imaging methods a) SSM, b) LSM, c) FM between frequencies 1 GHz and 6 GHz

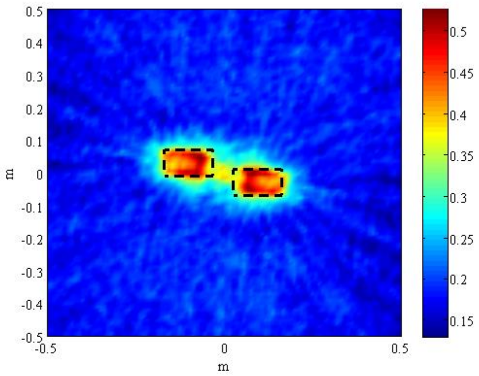

c)

Figure 4.46 (continuous) Two off-centered rectangular PEC objects, reconstructed using multiple frequency scheme and compared in terms of qualitative microwave imaging methods a) SSM, b) LSM, c) FM between frequencies 1 GHz and 6 GHz

There are two setups left to tend, but before that, it is beneficiary to mention that all the experiments that are discussed until now are actually contain only simple objects with no inhomogeneity is included inside, except for the opus 2 measurements in which the methods have failed to locate the inner inhomogeneity. However, an extension is proposed in [55] to tackle such problems which involves in solving the Green's function for the outer object and then extracting the result from the original measurement. The proposed method is tested for LSM and FM in the given study where the both methods have managed to produce satisfying reconstructions of the inner discontinuity. In this part, we will test the same approach with the SSM in our standard course and give the results unadulterated as before.

To increase the quality of the outcome through higher signal power and more penetration, a different setup is implemented. This time, two cavity-backed Vivaldi antenna [56] are used as transmitter and receiver, that are located approximately 17 cm away from the center, which may be considered as near-field compared to the other measurements where the antennas are located 85 cm away from the center. Figure 4.47 shows a visualization of the new setup. The object of interest is a balloon filled with either air or water, which is buried inside of a bowl with soil stuffing. The measurements are made at 12 transmitter and 12 receiver points for the air filled object and 24 transmitter and 24 receiver points for the water filled one. Bistatic setup is used to cover all the points in a fast pace. 41 frequencies are used to enhance the resolution. An illustration of the experimental data is given in Figure 4.48.

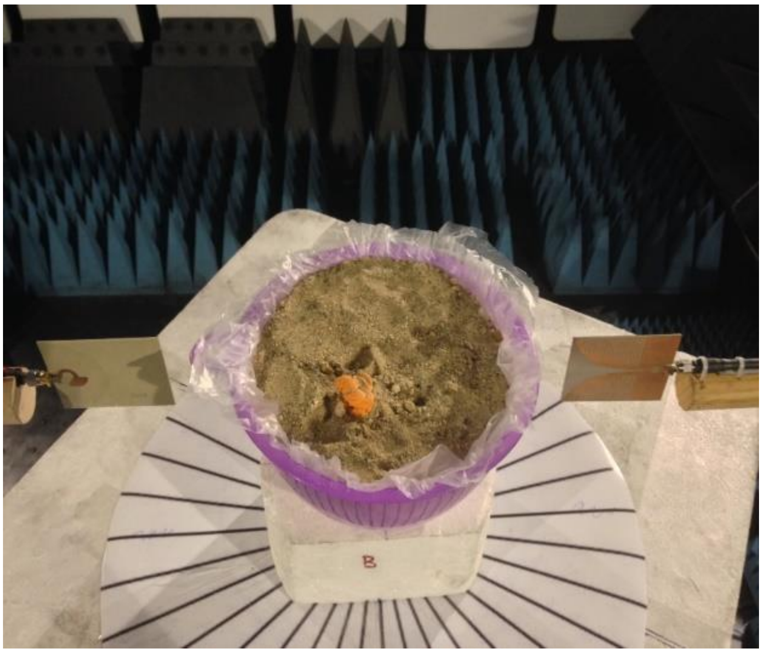

Figure 4.47 Buried object measurement setup for SSM.

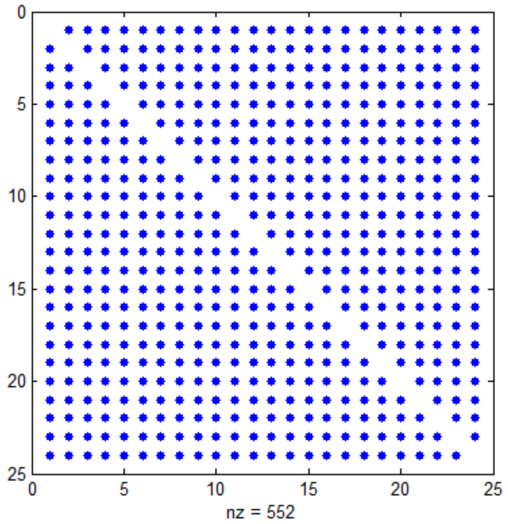

Figure 4.48 Nonzero elements of an exemplary measurement data

First discussion is about the air-filled object contained inside the bowl. First, measurements of the bowl filled with soil is made, then the interested scattering object is placed inside the bowl with center at (7,0) cm and the same measurements are repeated. 12 points can be considered as miniscule as these type of qualitative methods are generally implemented algorithmically with more than 100 far-field angles in most of the numerical studies. However, as it can be observed in Figure 4.49, the results of the tended setup is quite satisfactory even in single frequency reconstructions. It is shown that the extraction of the background object (bowl) from the entire setup can be used to locate the inner object as the study suggests. The performance of the antenna reduces with increase of the frequency as given in [43], along with the quality of the reconstruction. Results at 2, 3, 4, 5 and 6 GHz are solely gives the location and shape of the balloon and the background is eliminated. As the frequency increases however, the original object diminishes while the nonexistent objects appear in the figures.

To overcome the inferiority of the higher frequencies in terms of noise, we will use multifrequency approach once again. In Figure 4.50, four particular result are given. 11 frequencies between 2 GHz and 3 GHz reconstructions are merged into a single image given in Figure 4.50(a). Extending the range to 4 GHz, 21 frequencies are used to obtain the result in Figure 4.50(b). Similarly, 31 frequencies between 2 GHz and 5 GHz are summed up into Figure 4.50(c) and 41 frequencies with 2 GHz lower and 6 GHz higher limit added to form up Figure 4.50(d), respectively.

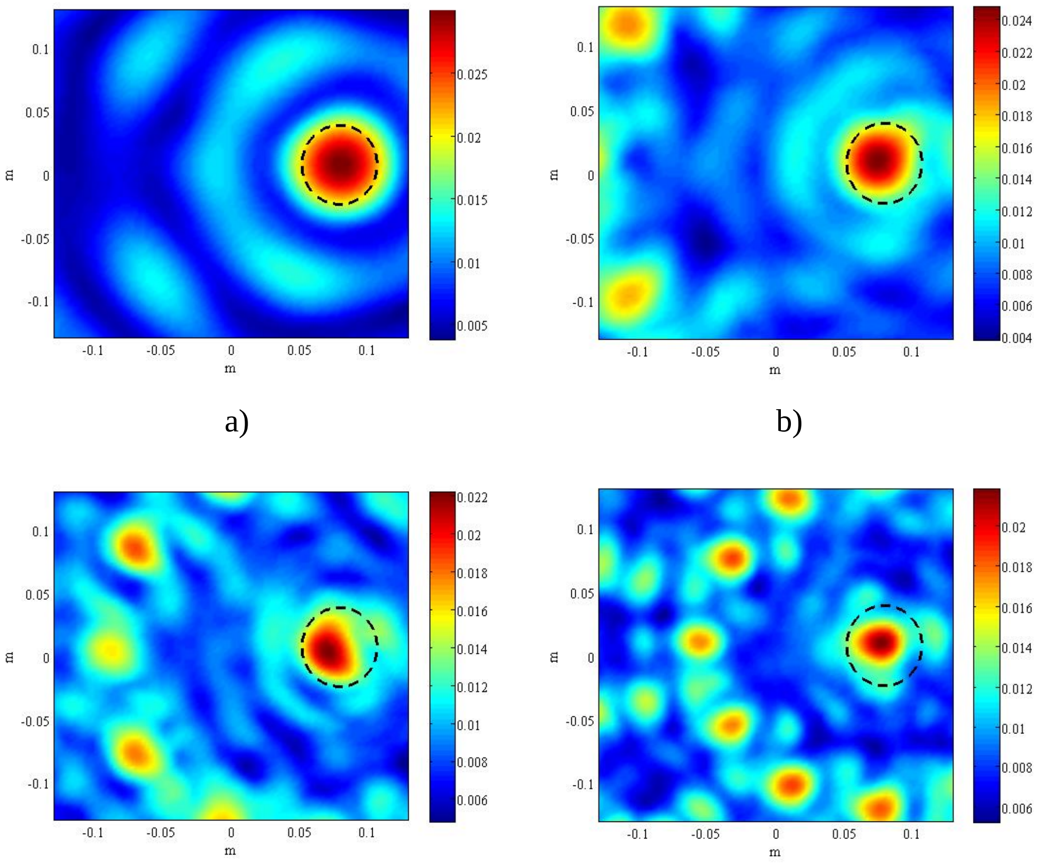

a) b)

c) d)

Figure 4.49 Single frequency inversion results of an air-filled balloon inside soil, at frequencies a) 2 GHz, b) 3 GHz, c) 4 GHz, d) 5 GHz, e) 6 GHz

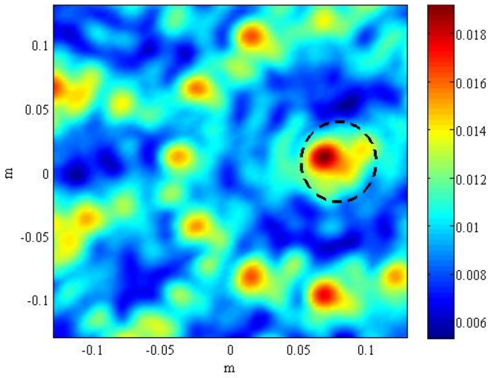

e)

Figure 4.49 (continuous) Single frequency inversion results of an air-filled balloon inside soil, at frequencies a) 2 GHz, b) 3 GHz, c) 4 GHz, d) 5 GHz, e) 6 GHz

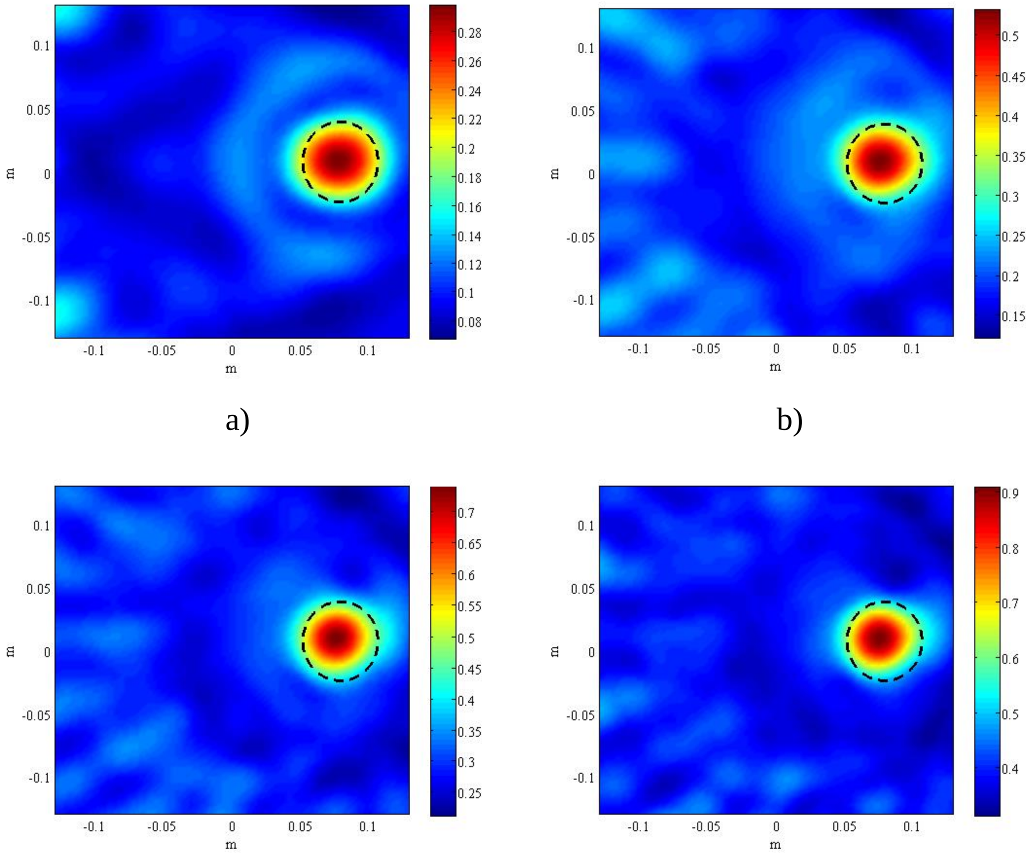

a) b)

c) d)

Figure 4.50 Multiple frequency inversion results of an air-filled balloon inside soil, between frequencies a) 2-3 GHz, b) 2-4 GHz, c) 2-5 GHz, d) 2-6 GHz

All the combinations seems to form similar results as the lower frequencies are more dominant in value. The result in Figure 4.50(a) seems to be the most appropriate choice with a convenient cut-off value since it complies more with the original shape compared to other images.

The comparison of merging algorithms are given in Figure 4.51. The direct summation has the edge compared to the other two, while normalized summation and weighted summation methods have equivalent performance on this case. SSM, LSM and FM results are also compared and shown in Figure 4.52. Performance of the SSM is marginally better than FM and LSM since it is closer to the original object. LSM has the inferior result in this case. With these outcome, we justify the methodology in the given study and also effectiveness of the SSM in both scattering parameter and near-filed measurements.

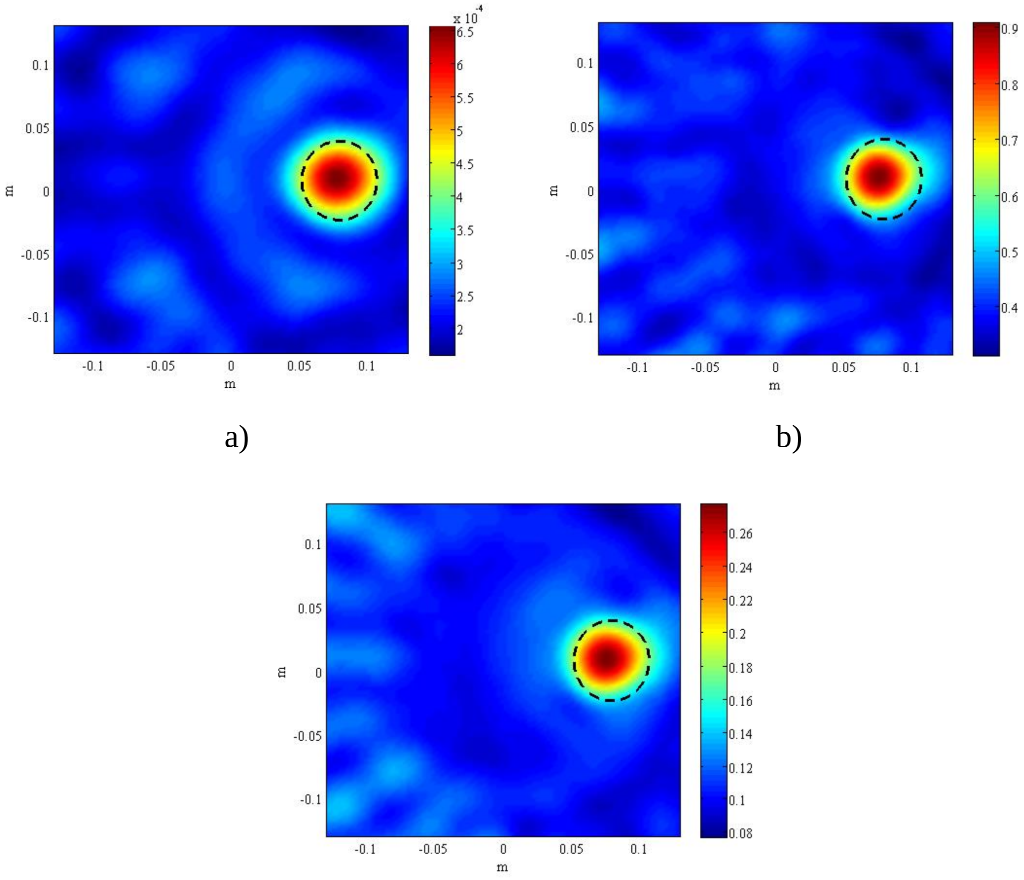

a) b)

c)

Figure 4.51 Multiple frequency inversion results of an air-filled balloon inside soil, comparison of different multifrequency merge approaches a) direct summation, b) normalized summation, c) weighted summation

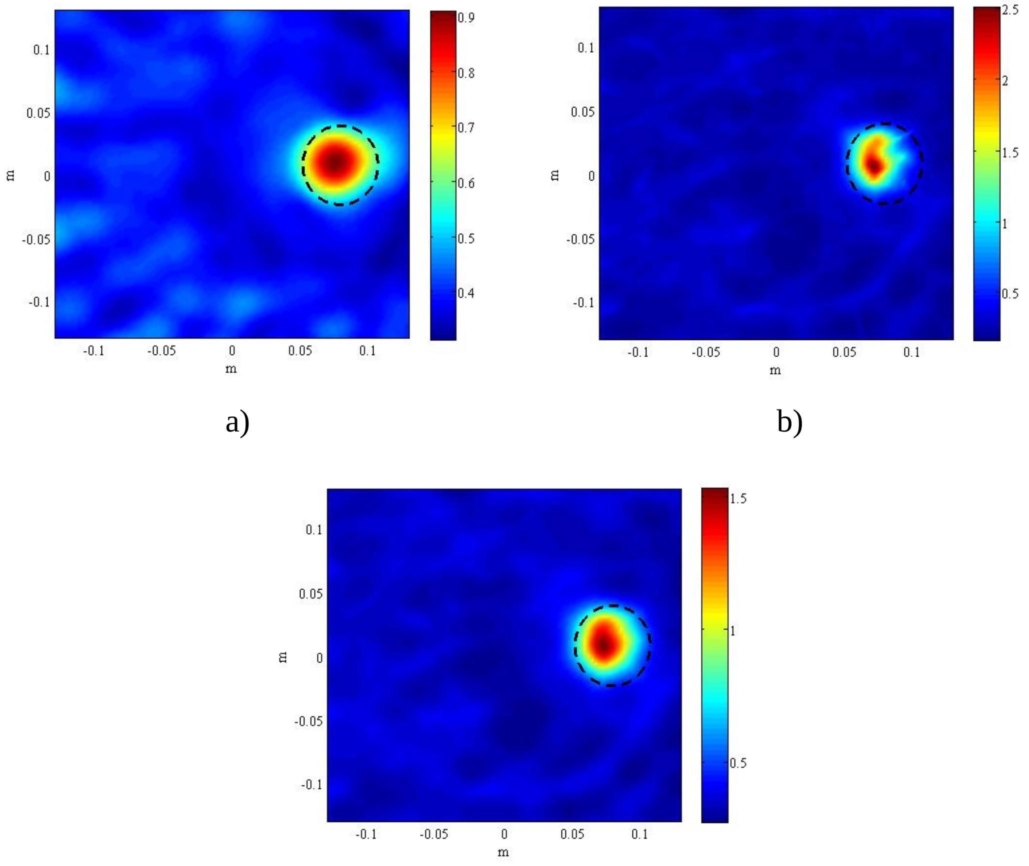

a) b)

c)

Figure 4.52 Off-centered air-filled balloon buried in soil, reconstructed using multiple frequency scheme, compared in terms of qualitative microwave imaging methods a) SSM, b) LSM, c) FM between frequencies 2 GHz and 6 GHz

The final case of the entire thesis is the water filled balloon buried inside a bowl full of soil. Same method is used to eliminate the background objects as it is proven to be successful in earlier cases. The water occupies more space compared to air in the latter setup, with a similar oval shape having (4,6) cm dimensions with a center of (8,0) cm. All the single frequencies show some composure where the most promising is the 3 GHz by a small margin according to the Figure 4.53. One thing to mention is that all the reconstructions contain significant amount of noise which may very well cause the method to be useless in more complex cases where the inhomogeneity is not limited to single discontinuities.

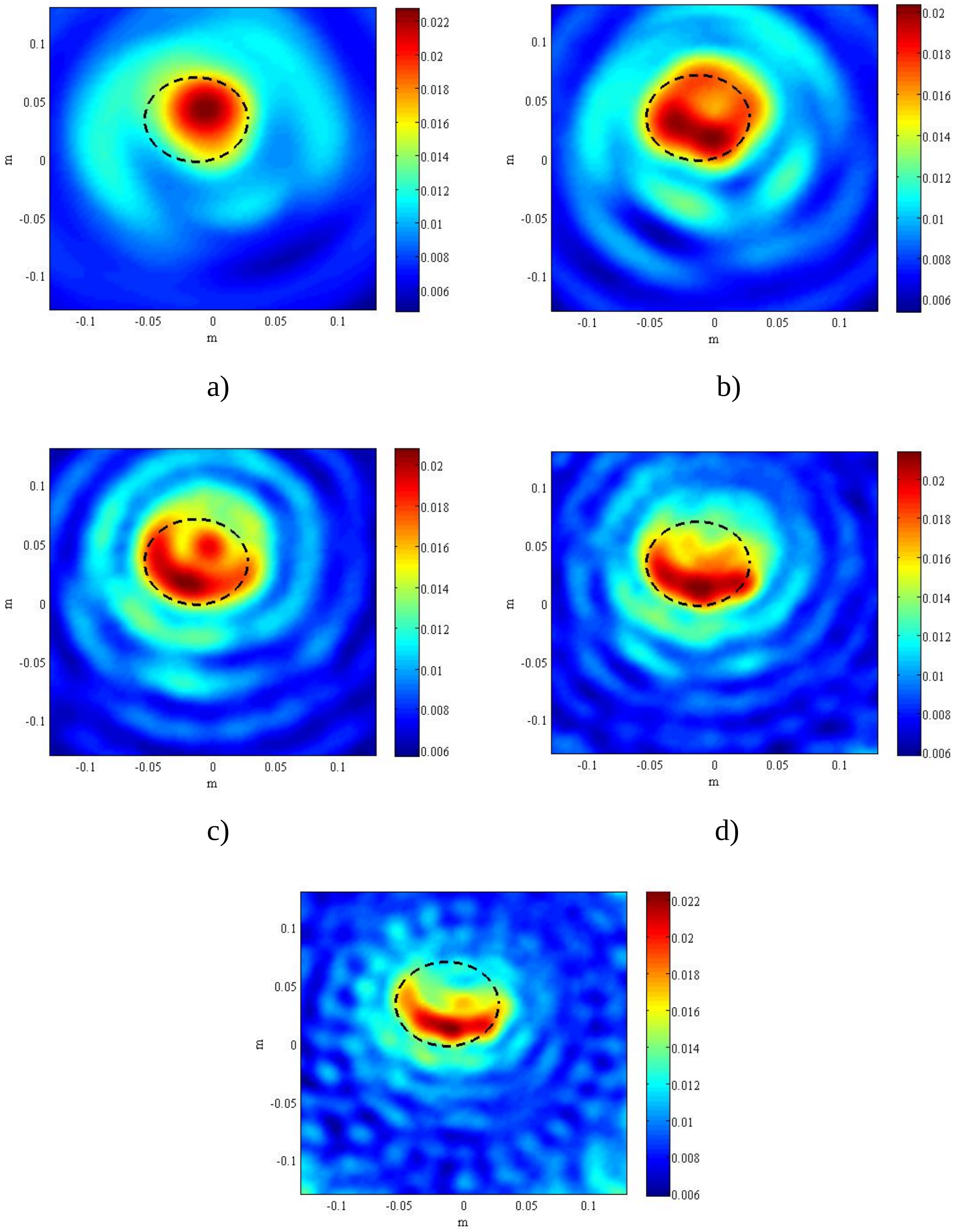

a)

b)

c)

d)

e)

Figure 4.53 Single frequency inversion results of a water-filled balloon buried in soil, at frequencies a) 2 GHz, b) 3 GHz, c) 4 GHz, d) 5 GHz, e) 6 GHz

The continuance of the setup is provided with the multifrequency results given in Figure 4.54. The summations are made between 2 GHz and 3 GHz in (a), 2 GHz and 4 GHz in (b), 2 GHz and 5 GHz in (c) and 2 GHz and 6 GHz in (d). The most definite result is obtained from the (b) as it yields more information on the object compared to the other images. The addition of the higher frequencies on the other hand barely makes a difference after a point. The interesting point in this case is that the noise in the images are reduced as the higher frequencies are added to the inversion which is not the general situation.

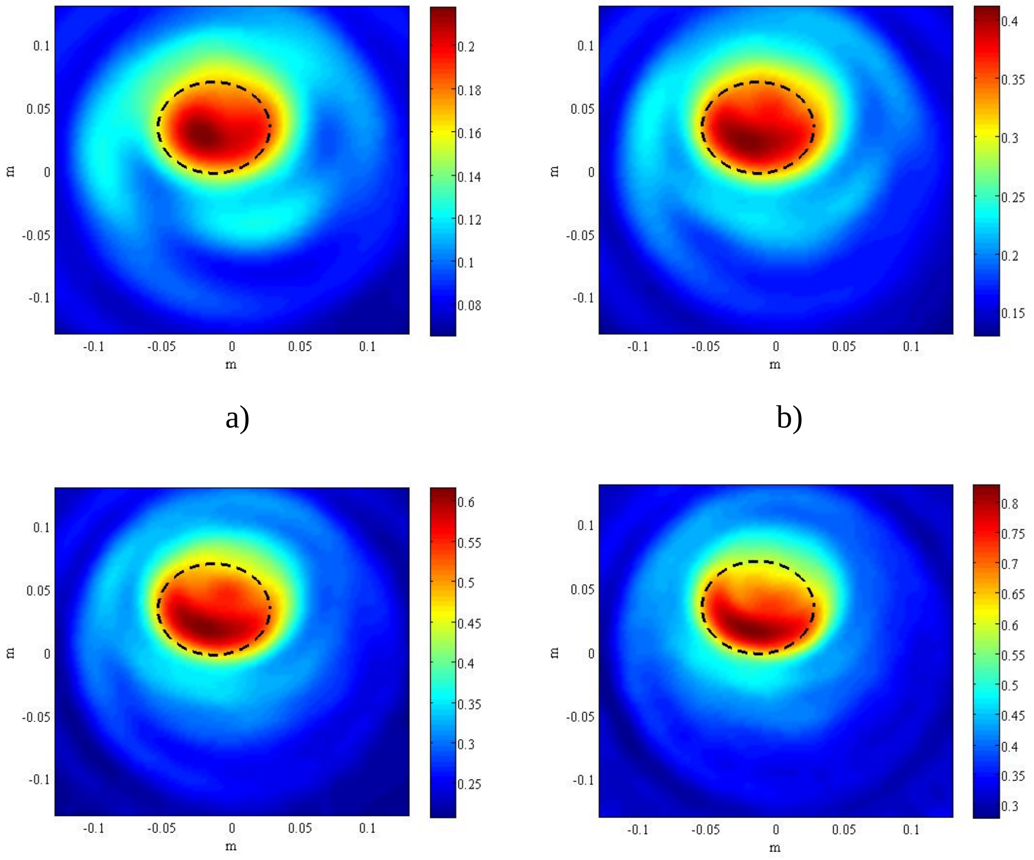

a) b)

c) d)

Figure 4.54 Multiple frequency inversion results of a water-filled balloon buried in soil, between frequencies a) 2-3 GHz, b) 2-4 GHz, c) 2-5 GHz, d) 2-6 GHz

The comparison of the frequency combination algorithms are not visually provided in this case as they produced the same outcome with the air filled object and no additional comment can made. Also, the results of the different methods comes out exactly as expected and explained in the latter case, so it is unnecessary to give the same comments entirely. Since we have covered all the necessary quality issues that the method needs to be investigated about, we can now continue with other performance issues such as the resource consumption of the method and duration of the algorithm compared to similar methods.

4.3 Time and Performance

The simplicity of these qualitative methods comes from their uncomplicated implementation. Even though the mathematical explanation is burdensome, once understood, the method can be implemented and optimized through brief pieces of computer code with availability of troubleshooting. Also, the code converts the experimental data into a reconstructed image with a faster pace than quantitative methods such that it takes only few seconds. In contrary, quantitative methods takes several minutes at best to solve the problem assuming that the measurement contains smaller error and algorithm converges after more limited amount of iterations. For example, SSM solves the two dielectric scattering case with 100x100 discretization of the investigation domain for 21 frequencies in approximately 3 seconds, while CSI solves the same setup for only one frequency in 2 minutes, which shows tremendous difference in terms of time-span of the algorithms. Of course, we do not argue that whether SSM can produce more accurate results than CSI in most cases and yields the actual electrical parameters of the scattering objects, but we simply mention that SSM can be a successful initiation to CSI or an other algorithm to reduce the computing time.

4.4 Practical Application of This Study

In this thesis, the necessary steps for constructing a microwave imaging scheme is discussed. These steps include the use of a complex yet fast algorithm to solve the measurement results and a strong and robust measurement system to perform accurate measurements and to obtain accurate reconstructions. For this purpose, such an inverse scattering algorithm is proposed and realized for different cases with two extensions and the results are shown and discussed in this section. According to these results, it is possible to deduct the different features of each experimental setup that is presented. In first setup it is possible to observe the better quality of higher frequency while in the second setup it can be inferred as otherwise. Cause of this is most likely the effectiveness of the used antennas at those frequencies as they differ in each setup. While a discrimination can be made in terms of frequency, the multifrequency approach is generally successful especially for the scattering parameter measurements. Also, the scattering parameter approach seems to be accurate as verified through various results.

5. CONCLUSIONS AND FUTURE WORK

In this study, an inverse scattering algorithm is formulated, implemented and tested for various situations and compared with similar methods that exists which are popular in their area. It can be observed that SSM generates fairly satisfying results on both against the real measurements obtained in electric fields and scattering parameter measurements obtained from the experimental structure that is constructed in our laboratory environment. In terms of its place in the qualitative inverse scattering methods, SSM is head-to-head with other methods, according to the comparative results given in the latter section. Performance wise, SSM produces results in seconds as the other qualitative methods and much faster than quantitative ones which may take hours to produce the same results depending on the case, which concurs with our intuitions. We have also made additions to the initial configuration of the method. One of our additions to originally provided method is adding a multifrequency scheme to optimize the outcome of the method which is proven to be useful. Even though it is a simple addition to the method, it produces a significant increase to the performance of the method. This addition is implemented to other methods as well and proven to be useful generally. Another and perhaps the most important one is that we have shown that it is possible to generate viable results with this method through different types of data other than the far-field pattern experimentally. It is possible to apply this situation to other methods as given in the cases of LSM and FM.

In a future work, we will search for a way to outcome the inhomogeneity problem through the given iterative methodology designed for SSM. Also, we will try to enhance our reconstructions and mathematical justifications to vectoral three dimensional electromagnetic inverse scattering problem.

REFERENCES

[1] Brown, R. W., Cheng, Y. C. N., Haacke, E. M., Thompson, M. R., & Venkatesan, R. (2014). *Magnetic resonance imaging: physical principles and sequence design*. John Wiley & Sons.

[2] Forman, S. D., Cohen, J. D., Fitzgerald, M., Eddy, W. F., Mintun, M. A., & Noll, D. C. (1995). Improved assessment of significant activation in functional magnetic resonance imaging (fMRI): use of a cluster-size threshold. *Magnetic Resonance in medicine*, *33*(5), 636-647.

[3] Devaney, A. J. (1982). A filtered backpropagation algorithm for diffraction tomography. *Ultrasonic imaging*, *4*(4), 336-350.

[4] Natterer, F. (1986). *The mathematics of computerized tomography* (Vol. 32). Siam.

[5] Herman, G. T. (2009). *Fundamentals of computerized tomography: image reconstruction from projections*. Springer Science & Business Media.

[6] Townsend, D. W., Valk, P. E., & Maisey, M. N. (2005). *Positron emission tomography*. Springer-Verlag London Limited.

[7] Chugani, H. T., Phelps, M. E., & Mazziotta, J. C. (1987). Positron emission tomography study of human brain functional development. *Annals of neurology*, *22*(4), 487-497.

[8] Van Den Berg, P. M., & Kleinman, R. E. (1997). A contrast source inversion method. *Inverse problems*, *13*(6), 1607.

[9] Van den Berg, P. M., Van Broekhoven, A. L., & Abubakar, A. (1999). Extended contrast source inversion. *Inverse problems*, *15*(5), 1325.

[10] Abubakar, A., Hu, W., Van Den Berg, P. M., & Habashy, T. M. (2008). A finite-difference contrast source inversion method. *Inverse Problems*, *24*(6), 065004.

[11] Joachimowicz, N., Pichot, C., & Hugonin, J. P. (1991). Inverse scattering: an iterative numerical method for electromagnetic imaging. *Antennas and Propagation, IEEE Transactions on*, *39*(12), 1742-1753.

[12] Kress, R. (2003). Newton's method for inverse obstacle scattering meets the method of least squares. *Inverse Problems*, *19*(6), S91.

[13] Devaney, A. J. (1982). Inversion formula for inverse scattering within the Born approximation. *Optics Letters*, *7*(3), 111-112.

[14] Moghaddam, M., & Chew, W. C. (1993). Study of some practical issues in inversion with the Born iterative method using time-domain data. *Antennas and Propagation, IEEE Transactions on*, *41*(2), 177-184.

[15] Chew, W. C., & Wang, Y. M. (1990). Reconstruction of two-dimensional permittivity distribution using the distorted Born iterative method. *Medical Imaging, IEEE Transactions on*, *9*(2), 218-225.

[16] Hadamard, J. (1902). *Sur les problèmes aux dérivées partielles et leur signification physique.* Princeton University Bulletin. pp. 49–52.

[17] Golub, G. H., & Reinsch, C. (1970). Singular value decomposition and least squares solutions. *Numerische mathematik*, *14*(5), 403-420.

[18] Tikhonov, A. N., & Arsenin, V. I. (1977). *Solutions of ill-posed problems*. Vh Winston.

[19] Golub, G. H., Hansen, P. C., & O'Leary, D. P. (1999). Tikhonov regularization and total least squares. *SIAM Journal on Matrix Analysis and Applications*,*21*(1), 185-194.

[20] Seber, G. A., & Lee, A. J. (2012). *Linear regression analysis* (Vol. 936). John Wiley & Sons.

[21] Lawson, C. L., & Hanson, R. J. (1974). *Solving least squares problems* (Vol. 161). Englewood Cliffs, NJ: Prentice-hall.

[22] Colton, D., Haddar, H., & Piana, M. (2003). The linear sampling method in inverse electromagnetic scattering theory. *Inverse problems*, *19*(6), S105.

[23] Cakoni, F., & Colton, D. (2003). On the mathematical basis of the linear sampling method. *Georgian Mathematical Journal*, *10*(3), 411-425.

[24] Colton, D., & Kirsch, A. (1996). A simple method for solving inverse scattering problems in the resonance region. *Inverse problems*, *12*(4), 383.

[25] Colton, D., Piana, M., & Potthast, R. (1997). A simple method using Morozov's discrepancy principle for solving inverse scattering problems.*Inverse Problems*, *13*(6), 1477.

[26] Kirsch, A., & Grinberg, N. (2008). *The factorization method for inverse problems* (Vol. 36, pp. xiv+-201). Oxford: Oxford University Press.

[27] Kirsch, A. (1998). Characterization of the shape of a scattering obstacle using the spectral data of the far field operator. *Inverse problems*, *14*(6), 1489.

[28] Chen, J., Chen, Z., & Huang, G. (2013). Reverse time migration for extended obstacles: electromagnetic waves. *Inverse Problems*, *29*(8), 085006.

[29] Luke, D. R., & Potthast, R. (2003). The No Response Test---A Sampling Method for Inverse Scattering Problems. *SIAM Journal on Applied Mathematics*, *63*(4), 1292-1312.

[30] Nakamura, G., Potthast, R., & Sini, M. (2006). Unification of the probe and singular sources methods for the inverse boundary value problem by the no-response test. *Communications in Partial Differential Equations*, *31*(10), 1505-1528.

[31] Ikehata, M. (2000). The probe method and its applications. *CHAPMAN AND HALL CRC RESEARCH NOTES IN MATHEMATICS*, 57-68.

[32] Erhard, K., & Potthast, R. (2006). A numerical study of the probe method.*SIAM Journal on Scientific Computing*, *28*(5), 1597-1612.

[33] Potthast, R. (1998). A point source method for inverse acoustic and electromagnetic obstacle scattering problems. *IMA Journal of Applied Mathematics*, *61*(2), 119-140.

[34] Hassen, M. B., Erhard, K., & Potthast, R. (2006). The point-source method for 3D reconstructions for the Helmholtz and Maxwell equations. *Inverse Problems*, *22*(1), 331.

[35] Potthast, R. (2001). *Point sources and multipoles in inverse scattering theory*. CRC Press.

[36] Potthast, R. (2000). Stability estimates and reconstructions in inverse acoustic scattering using singular sources. *Journal of computational and applied mathematics*, *114*(2), 247-274.

[37] Potthast, R., & Stratis, I. (2005). The singular sources method for an inverse transmission problem. *Computing*, *75*(2-3), 237-255.

[38] Potthast, R. (2006). A survey on sampling and probe methods for inverse problems. *Inverse Problems*, *22*(2), R1.

[39] W. C. Chew, *Waves and Fields in Inhomogeneous Media*. New York: IEEE, 1995.

[40] C. A. Balanis, *Advanced Engineering Electromagnetics*. New York: Wiley, 1989, pp. 178–182.

[41] M. Pastorino, *Microwave imaging*. Hoboken N.J.: John Wiley, 2010.

[42] Beckmann, P., & Spizzichino, A. (1987). The scattering of electromagnetic waves from rough surfaces. *Norwood, MA, Artech House, Inc., 1987, 511 p.*

[43] Sarvas, J. (1987). Basic mathematical and electromagnetic concepts of the biomagnetic inverse problem. *Physics in medicine and biology*, *32*(1), 11.

[44] Tarantola, A. (2005). *Inverse problem theory and methods for model parameter estimation*. siam.

[45] Scherzer, O. (1993). The use of Morozov's discrepancy principle for Tikhonov regularization for solving nonlinear ill-posed problems. *Computing*,*51*(1), 45-60.

[46] Luke, D. R., & Potthast, (2003). R. Image processing for limited aperture inverse acoustic obstacle scattering. *Pacific Institute for the Mathematical Sciences Preprint (PIMS-03-12), Download: http://www. pims. math. ca/publications/preprints*.

[47] Haynes, M., & Moghaddam, M. (2012). Vector green's function for S-parameter measurements of the electromagnetic volume integral equation.*Antennas and Propagation, IEEE Transactions on*, *60*(3), 1400-1413.

[48] Haynes, M., Clarkson, S., & Moghaddam, M. (2012). Electromagnetic inverse scattering algorithm and experiment using absolute source characterization. *Antennas and Propagation, IEEE Transactions on*, *60*(4), 1854-1867.

[49] Haynes, M., & Moghaddam, M. (2011). Multipole and S-parameter antenna and propagation model. *Antennas and Propagation, IEEE Transactions on*,*59*(1), 225-235.

[50] Geffrin, J. M., & Sabouroux, P. (2009). Continuing with the Fresnel database: experimental setup and improvements in 3D scattering measurements.*Inverse Problems*, *25*(2), 024001.

[51] Geffrin, J. M., Sabouroux, P., & Eyraud, C. (2005). Free space experimental scattering database continuation: experimental set-up and measurement precision. *inverse Problems*, *21*(6), S117.

[52] Geffrin, J. M., Sabouroux, P., & Eyraud, C. (2005). Free space experimental scattering database continuation: experimental set-up and measurement precision. *inverse Problems*, *21*(6), S117.

[53] Potthast, R. (2004). A new non-iterative singular sources method for the reconstruction of piecewise constant media. *Numerische Mathematik*, *98*(4), 703-730.

[54] Akinci, M. N., Caglayan, T., Özgür, S., Alkasi, U., Abbak, M., & Çayören, M. (2015). Experimental Assessment of Linear Sampling and Factorization Methods for Microwave Imaging of Concealed Targets. *International Journal of Antennas and Propagation*, *501*, 504059.

[55] Akinci, M. N., Caglayan, T., Ozgur, S., Alkasi, U., Ahmadzay, H., Abbak, M., ... & Akduman, I. (2015). Qualitative microwave imaging with scattering parameters measurements. *Microwave Theory and Techniques, IEEE Transactions on*, *63*(9), 2730- 2740.

[56] Abbak, M., Çayören, M., & Akduman, I. (2014). Microwave breast phantom measurements with a cavity-backed Vivaldi antenna. *IET Microwaves, Antennas & Propagation*, *8*(13), 1127.

CURRICULUM VITAE

Name Surname : **Tuğhan ÇAĞLAYAN**

Place and Date of Birth : **Gazipaşa/12.08.1992**

E-Mail : **caglayant@itu.edu.tr**

EDUCATION :

- **B.Sc.** : 2014, Istanbul Technical University, Electrical and Electronics Faculty, Electronics and Communications Engineering

PROFESSIONAL EXPERIENCE AND REWARDS:

- 2014-2015 TUBITAK Research Engineer at Project 113E977
- 2015-2016 Research Assistant at Istanbul Technical University
- 2016-present Network Engineer at Garanti Technology

PUBLICATIONS, PRESENTATIONS AND PATENTS ON THE THESIS:

- T. Caglayan, M. Cayoren “Electromagnetic Imaging With Singular Sources Method: Preliminary Experimental Results”, AES 2016 Conference. (accepted)

OTHER PUBLICATIONS, PRESENTATIONS AND PATENTS:

- M. N. Akıncı, T. Çaglayan, S. Özgür, U. Alkaşı, H. Ahmadzay, M. Abbak, M. Çayören and İ. Akduman, “Qualitative Microwave Imaging with Scattering Parameters Measurements”, IEEE Trans. on Microwave Theory and Techniques, Vol. 63 , No. 9, 2015.
- M. N. Akıncı, T. Çaglayan, S. Özgür, U. Alkaşı, M. Abbak, and M. Çayören, “Experimental Assessment of Linear Sampling and Factorization Methods for Microwave Imaging of Concealed Targets”, International Journal of Antennas and Propagation, 504059, 2015.